Boundary conditions for the Boltzmann equation from gas-surface interaction kinetic models

Kazuo Aoki, Vincent Giovangigli, Shingo Kosuge

Boundary conditions for the Boltzmann equation from gas-surface interaction kinetic models

Kazuo Aoki,[1] Vincent Giovangigli,[2] and Shingo Kosuge[3]
[1]*Department of Mathematics, National Cheng Kung University, Tainan 70101, Taiwan*
[2]*CMAP, Centre National de la Recherche Scientifique, École Polytechnique, 91128 Palaiseau Cedex, France*
[3]*Institute for Liberal Arts and Sciences, Kyoto University, Kyoto 606-8501, Japan*

(Received 24 June 2022; accepted 30 August 2022; published 27 September 2022)

Boundary conditions for the Boltzmann equation are investigated on the basis of a kinetic model for gas-surface interactions. The model takes into account gas and physisorbed molecules interacting with a surface potential and colliding with phonons. The potential field is generated by fixed crystal molecules, and the interaction with phonons represents the fluctuating part of the surface. The interaction layer is assumed to be thinner than the mean free path of the gas and physisorbed molecules, and the phonons are assumed to be at equilibrium. The asymptotic kinetic equation for the inner physisorbate layer is derived and used to investigate gas distribution boundary conditions. To be more specific, a model of the boundary condition for the Boltzmann equation is derived on the basis of an approximate iterative solution of the kinetic equation for the physisorbate layer, and the quality of the model is assessed by detailed numerical simulations, which also clarify the behavior of the molecules in the layer.

DOI: 10.1103/PhysRevE.106.035306

I. INTRODUCTION

Empirically derived Maxwell boundary conditions have traditionally been used at solid walls for Boltzmann equations. The flux of reflected gas molecules (or particles) at the wall is then specified as a linear combination between specular reflection and diffuse reflection of the incident flux [1]. More general boundary conditions for kinetic equations involve scattering kernels relating the incident and reflected molecular fluxes at the surface [1–6]. A main disadvantage of these boundary conditions, however, is that they are mathematical in nature, derived empirically, and not related to physical quantities like atom characteristics, crystal characteristics, or interaction potentials [1]. A more physical approach is to obtain information about the reflected molecules by the use of molecular dynamics (MD) simulations [7–10]. However, it is not easy in general to construct handy models of gas-solid interaction on the basis of the results of MD simulations.

An alternative physical approach is to use *kinetic equations* that describe gas molecules subject to a potential field generated by fixed crystal molecules and colliding with phonons describing the fluctuating part of the surface potential [11–19]. A kinetic equation for volume or surface phonons may also be introduced [11,20–22], but it may otherwise be assumed that phonons are at equilibrium [12,13]. We investigate in this paper gas distribution functions in the neighborhood of a crystal surface on the basis of a kinetic framework similar to that used in [11–18]. The phonons are assumed to be at equilibrium for the sake of simplicity.

The kinetic equation governing the distribution function near the crystal is rescaled by assuming that the adsorbate layer is thin in comparison with the mean free path and that the phonon-molecule collision dynamics is fast with respect to molecular collisions. This implies in particular that the characteristic time of transit through the layer is shorter than the gas mean free time for collisions. In contrast, previous work by two of the present authors was associated with fluid type scalings and reactive crystal surfaces [23–26].

The rescaled inner structure of the physisorbate is analyzed, and the zeroth-order equation, which involves the interaction potential and the phonon collision operator, is obtained. The equation forms a half-space problem that has a different structure from traditional half-space problems relevant to Knudsen layers [27–29]. More specifically, its solution is determined by specifying the velocity distribution for the molecules toward the surface at infinity. Therefore, the velocity distribution of the outgoing molecules at infinity is determined by that of the incident molecules there. This means that the solution of the half-space problem for the physisorbate layer provides the boundary condition for the Boltzmann equation that holds outside the layer.

We first propose an iteration scheme for the half-space problem for the physisorbate layer and construct a model of the boundary condition for the Boltzmann equation on the basis of the first iteration. The model has the form of the Maxwell boundary condition with a velocity-dependent accommodation coefficient. Then, we carry out an accurate numerical analysis of the problem, assuming some explicit forms of the interaction potential as well as the phonon characteristic time, in order to observe the resulting velocity distribution of the outgoing molecules at infinity determined in response to a given velocity distribution of the incoming molecules there. The numerical result validates the model based on the first iteration and also reveals singular properties of the half-space problem for the physisorbate layer.

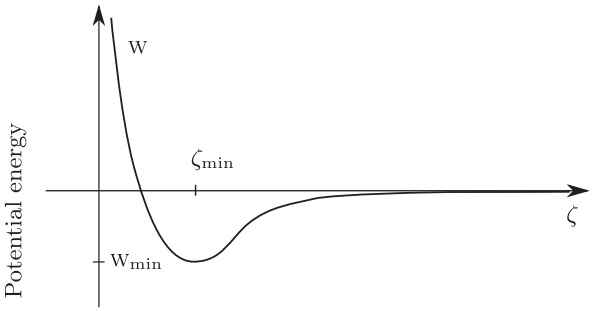

FIG. 1. Typical surface interaction potential W as a function of ζ.

The paper is organized as follows. A kinetic model for gas-surface interaction is proposed in Sec. II, and the kinetic equation for the inner physisorbate layer is derived by appropriate scaling (kinetic scaling) in Sec. III. In Sec. IV, it is shown that the boundary condition for the Boltzmann equation is related to the solution of the half-space problem for the inner physisorbate layer. An approximate solution for the half-space problem and the resulting model of the boundary condition for the Boltzmann equation are obtained in Sec. V. Then, the same half-space problem is solved numerically for the purpose of validating the model boundary condition in Sec. VI and clarifying the behavior of the solution in Sec. VII. Finally, Sec. VIII is devoted to concluding remarks.

II. A GAS-SURFACE INTERACTION KINETIC MODEL

The kinetic equation modeling a gas interacting with a crystal surface is presented in this section [11–18].

A. Interaction potential and Maxwellians

We consider a single monatomic gas interacting with a crystal surface assumed to be planar and located at $z = 0$ with the spatial coordinates written as $\boldsymbol{x} = (x, y, z)$. The base vector $\boldsymbol{e}_z$ is in the normal direction and oriented toward the gas, and the tangential coordinates read $\boldsymbol{x}_\parallel = (x, y)$ with $\boldsymbol{x} = (\boldsymbol{x}_\parallel, z)$. We denote by W the interaction potential between *fixed* crystal molecules and physisorbed or gas molecules. The interaction potential W is assumed to only depend on the normal coordinate z for the sake of simplicity and is written in the form

$$\mathrm{W}(z) = \mathrm{W}_{\mathrm{s}}(z/\delta) = \mathrm{W}_{\mathrm{s}}(\zeta), \tag{1}$$

where δ is a characteristic range of the surface potential and $\zeta = z/\delta$ denotes the rescaled normal coordinate, which is dimensionless. The rescaled potential W_{s} is such that

$$\lim_{\zeta\to 0} \mathrm{W}_{\mathrm{s}}(\zeta) = +\infty, \quad \lim_{\zeta\to+\infty} \mathrm{W}_{\mathrm{s}}(\zeta) = 0, \tag{2}$$

and usually involves an attractive zone and a repulsing zone as Lennard-Jones (LJ) potentials integrated over all crystal molecules, as illustrated in Fig. 1. In the repulsive zone $(0, \zeta_{\min})$, where $\zeta_{\min} > 0$, the potential W decreases from $+\infty$ to $\mathrm{W}_{\min} = \mathrm{W}_{\mathrm{s}}(\zeta_{\min}) < 0$ and in the attractive zone $(\zeta_{\min}, +\infty)$ the potential W increases from $\mathrm{W}_{\min}$ up to zero.

The wall Maxwellian distribution is given by

$$\mathrm{M}(\boldsymbol{c}) = \Big(\frac{m}{2\pi k_{\mathrm{B}} T_{\mathrm{w}}}\Big)^{3/2} \exp\Big(-\frac{m|\boldsymbol{c}|^2}{2k_{\mathrm{B}} T_{\mathrm{w}}}\Big), \tag{3}$$

where m denotes the gas molecular mass, k_{B} denotes the Boltzmann constant, $\boldsymbol{c}$ denotes the physisorbed or gas molecular velocity, and T_{w} denotes the wall temperature. We also denote by c_z the normal velocity and by $\boldsymbol{c}_\parallel = (c_x, c_y)$ the tangential velocity so that $\boldsymbol{c} = (\boldsymbol{c}_\parallel, c_z)$. The wall temperature T_{w} is assumed to be constant and uniform.

The modified Maxwellian distribution is defined as

$$\begin{aligned}\mathrm{m} &= \mathrm{M}\exp\Big(-\frac{\mathrm{W}}{k_{\mathrm{B}} T_{\mathrm{w}}}\Big)\\ &= \Big(\frac{m}{2\pi k_{\mathrm{B}} T_{\mathrm{w}}}\Big)^{3/2} \exp\Big(-\frac{m|\boldsymbol{c}|^2}{2k_{\mathrm{B}} T_{\mathrm{w}}} - \frac{\mathrm{W}}{k_{\mathrm{B}} T_{\mathrm{w}}}\Big).\end{aligned} \tag{4}$$

B. Kinetic equation

The monatomic gas is assumed to be governed by the Boltzmann equation [11,12,14]

$$\frac{\partial f}{\partial t} + \boldsymbol{c}\cdot\frac{\partial f}{\partial \boldsymbol{x}} - \frac{1}{m}\frac{\partial \mathrm{W}}{\partial \boldsymbol{x}}\cdot\frac{\partial f}{\partial \boldsymbol{c}} = J(f, f) + J_{\mathrm{ph}}(f), \tag{5}$$

where $f(t, \boldsymbol{x}, \boldsymbol{c})$ denotes the velocity distribution function of physisorbed or gas molecules, $J(f, f)$ denotes the gas-gas collision operator, and $J_{\mathrm{ph}}(f)$ denotes the gas-phonon collision operator.

The gas-gas collision operator $J(f, f)$ is in the traditional form [30–33]

$$J(f, f) = \int [f(\boldsymbol{c}')f(\boldsymbol{c}'_*) - f(\boldsymbol{c})f(\boldsymbol{c}_*)]\mathsf{W}\, d\boldsymbol{c}_* d\boldsymbol{c}' d\boldsymbol{c}'_*, \tag{6}$$

where in a direct collision $\boldsymbol{c}_*$ denotes the velocity of the collision partner, $\boldsymbol{c}'$ and $\boldsymbol{c}'_*$ denote the velocities after collision, W denotes the transition probability for gas-gas collisions, and the dependence on $(t, \boldsymbol{x})$ has been left implicit. Only binary collisions are considered and the transition probability W satisfies the reciprocity relation $\mathsf{W}(\boldsymbol{c}, \boldsymbol{c}_*, \boldsymbol{c}', \boldsymbol{c}'_*) = \mathsf{W}(\boldsymbol{c}', \boldsymbol{c}'_*, \boldsymbol{c}, \boldsymbol{c}_*)$ associated with microreversibility. The collision term J may equivalently be written in terms of collision cross sections [1,30–34]. The collisional invariants of the operator J are associated with molecular number $\psi^1 = 1$, momentum $\psi^{1+\nu} = mc_\nu$, $\nu \in \{1, 2, 3\}$, as well as energy $\psi^5 = \frac{1}{2}m|\boldsymbol{c}|^2 + \mathrm{W}$.

The phonon collision operator $J_{\mathrm{ph}}(f)$ is in the form

$$J_{\mathrm{ph}}(f) = \int \Big(\frac{f(\boldsymbol{c}')}{\mathrm{m}(\boldsymbol{c}')} - \frac{f(\boldsymbol{c})}{\mathrm{m}(\boldsymbol{c})}\Big)\mathsf{W}_{\mathrm{ph}} d\boldsymbol{c}', \tag{7}$$

where W_{ph} denotes the transition probability. This operator is derived in Appendix A under the assumption that the phonons are at equilibrium [11,12]. The transition probability W_{ph} satisfies the reciprocity relation $\mathsf{W}_{\mathrm{ph}}(\boldsymbol{c}, \boldsymbol{c}') = \mathsf{W}_{\mathrm{ph}}(\boldsymbol{c}', \boldsymbol{c})$ and is nonzero only in the neighborhood of the surface. The collision term J_{ph} may further be simplified as $-(f - n\mathrm{M})/\tau_{\mathrm{ph}}$ where $n = \int f d\boldsymbol{c}$ denotes the local number density and τ_{ph} denotes a relaxation time independent of $\boldsymbol{c}$ [12]. The momentum and energy are not conserved by J_{ph}, since they may be given to phonons, and J_{ph} only conserves the number of gas molecules with the invariant $\psi^1 = 1$.

From the definition of the modified Maxwellian distribution and the properties of collision operators, it is obtained that

$$\frac{\partial \mathrm{m}}{\partial t} = 0, \quad \boldsymbol{c} \cdot \frac{\partial \mathrm{m}}{\partial \boldsymbol{x}} - \frac{1}{m}\frac{\partial \mathrm{w}}{\partial \boldsymbol{x}} \cdot \frac{\partial \mathrm{m}}{\partial \boldsymbol{c}} = 0,$$
$$J(\mathrm{m},\, \mathrm{m}) = 0, \quad J_{\mathrm{ph}}(\mathrm{m}) = 0. \tag{8}$$

The modified Maxwellian distribution m thus appears as a *natural solution* of isothermal thin layer kinetic equations in a potential field with phonon interactions or equivalently as a natural steady solution of the corresponding kinetic equation. Decomposing the second equation in Eq. (8) into the parallel and normal directions with respect to the surface, we may also write

$$\frac{\partial \mathrm{m}}{\partial \boldsymbol{x}_{\parallel}} = 0, \quad c_z \frac{\partial \mathrm{m}}{\partial z} - \frac{1}{m}\frac{d\mathrm{w}}{dz}\frac{\partial \mathrm{m}}{\partial c_z} = 0. \tag{9}$$

Since the phonon collision operator J_{ph} vanishes far from the surface as well as the potential w, we may let $z \to \infty$ in Eq. (5) in order to obtain the kinetic equation in the gas phase

$$\frac{\partial f_{\mathrm{g}}}{\partial t} + \boldsymbol{c} \cdot \frac{\partial f_{\mathrm{g}}}{\partial \boldsymbol{x}} = J(f_{\mathrm{g}},\, f_{\mathrm{g}}), \tag{10}$$

where $f_{\mathrm{g}}(t, \boldsymbol{x}, \boldsymbol{c})$ denotes the distribution function of gas molecules. This kinetic equation (10) is the standard Boltzmann equation for a monatomic gas and there is thus a sole kinetic framework describing both gas and physisorbed molecules. The gas equation is thus recovered far from the surface and the distribution f must converge to f_{g} far from the surface. The macroscopic conservation equations in the gas are further obtained by taking moments of Eq. (10) with the inner product

$$\langle \xi(\boldsymbol{c}),\, \zeta(\boldsymbol{c}) \rangle = \int \xi(\boldsymbol{c})\zeta(\boldsymbol{c})\, d\boldsymbol{c},$$

where $\xi(\boldsymbol{c})$ and $\zeta(\boldsymbol{c})$ are arbitrary functions of $\boldsymbol{c}$. The macroscopic properties naturally associated with the gas read $\langle f_{\mathrm{g}},\, \psi^1 \rangle = n_{\mathrm{g}}$, $\langle f_{\mathrm{g}},\, \psi_{\mathrm{g}}^{1+\nu} \rangle = \rho_{\mathrm{g}} v_{\mathrm{g}\,\nu}$, and $\langle f_{\mathrm{g}},\, \psi^5 \rangle = \frac{1}{2}\rho_{\mathrm{g}}|\boldsymbol{v}_{\mathrm{g}}|^2 + \mathcal{E}_{\mathrm{g}}$ where n_{g} denotes the gas number density, $\rho_{\mathrm{g}} = n_{\mathrm{g}} m$ denotes the gas mass density, $\boldsymbol{v}_{\mathrm{g}}$ denotes the gas mass average fluid velocity, $v_{\mathrm{g}\nu}$ denotes the component in the direction ν of $\boldsymbol{v}_{\mathrm{g}}$, and $\mathcal{E}_{\mathrm{g}} = n_{\mathrm{g}}(\frac{3}{2}k_{\mathrm{B}}T_{\mathrm{g}} + \mathrm{w})$ denotes the internal energy per unit volume, where T_{g} is the gas temperature.

C. Surface kinetic entropy

The kinetic entropies compatible with the phonon collision operators J_{ph} are slightly different from the traditional expressions. The origin of this modification is that phonons are supposed to be at equilibrium and the collision term J_{ph} has been simplified accordingly. Since phonons are interacting with gas molecules, there should still be a phonon entropy increase associated with this interaction. Such an increase of phonon entropy having been discarded, the corresponding terms are missing in the total entropy production and modified entropies have to be introduced [35,36]. These modifications are generally no longer required when phonons' kinetic equations are taken into account [21,22].

The kinetic entropy per unit volume associated with the physisorbed or gas molecules is defined by

$$\mathcal{S}^{\mathrm{kin}} = -k_{\mathrm{B}} \int f[\log(f/\mathrm{m}) - 1]\, d\boldsymbol{c}. \tag{11}$$

Multiplying the Boltzmann equation (5) by $\log(f/\mathrm{m})$, using Eq. (8), and integrating with respect to $\boldsymbol{c}$, we obtain a balance equation for $\mathcal{S}^{\mathrm{kin}}$ in the form

$$\frac{\partial \mathcal{S}^{\mathrm{kin}}}{\partial t} + \frac{\partial}{\partial \boldsymbol{x}} \cdot \boldsymbol{\mathcal{F}}^{\mathrm{kin}} = \mathfrak{v}^{\mathrm{kin}}, \tag{12}$$

where $\boldsymbol{\mathcal{F}}^{\mathrm{kin}}$ is the kinetic entropy flux

$$\boldsymbol{\mathcal{F}}^{\mathrm{kin}} = -k_{\mathrm{B}} \int \boldsymbol{c} f[\log(f/\mathrm{m}) - 1]\, d\boldsymbol{c},$$

and $\mathfrak{v}^{\mathrm{kin}}$ the kinetic entropy source term. The entropy source term $\mathfrak{v}^{\mathrm{kin}}$ may be split as $\mathfrak{v}^{\mathrm{kin}} = \mathfrak{v}^{\mathrm{kin}}_{\mathrm{co}} + \mathfrak{v}^{\mathrm{kin}}_{\mathrm{ph}}$ where

$$\mathfrak{v}^{\mathrm{kin}}_{\mathrm{co}} = -k_{\mathrm{B}} \int J(f,\, f) \log(f/\mathrm{m})\, d\boldsymbol{c}, \tag{13}$$

$$\mathfrak{v}^{\mathrm{kin}}_{\mathrm{ph}} = -k_{\mathrm{B}} \int J_{\mathrm{ph}}(f) \log(f/\mathrm{m})\, d\boldsymbol{c}. \tag{14}$$

Noting that $\log(\mathrm{m})$ is a collisional invariant of J and may be eliminated from Eq. (13), and using standard arguments from kinetic theory, it is obtained that

$$\mathfrak{v}^{\mathrm{kin}}_{\mathrm{co}} = \frac{k_{\mathrm{B}}}{4} \int \Upsilon(f(\boldsymbol{c})f(\boldsymbol{c}_*),\, f(\boldsymbol{c}')f(\boldsymbol{c}'_*))\, \mathsf{W}\, d\boldsymbol{c}\, d\boldsymbol{c}_* d\boldsymbol{c}' d\boldsymbol{c}'_*, \tag{15}$$

where Υ denotes the non-negative function $\Upsilon(x,\, y) = (x - y)(\log x - \log y)$. Similarly, it is obtained that

$$\mathfrak{v}^{\mathrm{kin}}_{\mathrm{ph}} = \frac{k_{\mathrm{B}}}{2} \int \Upsilon(f(\boldsymbol{c})/\mathrm{m}(\boldsymbol{c}),\, f(\boldsymbol{c}')/\mathrm{m}(\boldsymbol{c}'))\mathsf{W}_{\mathrm{ph}}\, d\boldsymbol{c}\, d\boldsymbol{c}'. \tag{16}$$

Since the function Υ only takes non-negative values, both $\mathfrak{v}^{\mathrm{kin}}_{\mathrm{co}}$ and $\mathfrak{v}^{\mathrm{kin}}_{\mathrm{ph}}$ are non-negative as well as $\mathfrak{v}^{\mathrm{kin}} = \mathfrak{v}^{\mathrm{kin}}_{\mathrm{co}} + \mathfrak{v}^{\mathrm{kin}}_{\mathrm{ph}}$. The Boltzmann equation (5) is therefore compatible with the Boltzmann H theorem and leads to a dissipative structure at the molecular level.

III. INNER LAYER KINETIC EQUATION

In order to investigate the interaction layer and kinetic boundary conditions, a *kinetic* scaling is introduced and the inner layer kinetic equation is obtained.

A. Kinetic scaling

We introduce characteristic quantities that are marked with the $\star$ superscript. We denote by $n^\star$ the characteristic number density and by $\tau^\star_{\mathrm{fr}}$ the characteristic mean free time. We denote by $v^\star = (k_{\mathrm{B}}T_{\mathrm{w}}/m)^{1/2}$ the characteristic thermal speed, by $f^\star = n^\star/v^{\star 3}$ the characteristic molecular velocity distribution, by $\lambda^\star = \tau^\star_{\mathrm{fr}} v^\star$ the mean free path, by $\mathsf{W}^\star = 1/(n^\star \tau^\star_{\mathrm{fr}} v^{\star 6})$ the characteristic transition probability, and by $\mathrm{w}^\star = m v^{\star 2}$ the characteristic potential. We also introduce the characteristic time for phonon interaction $\tau^\star_{\mathrm{ph}}$ that is easily related to the characteristic transition probability $\mathsf{W}^\star_{\mathrm{ph}}$ with $1/\tau^\star_{\mathrm{ph}} = \mathsf{W}^\star_{\mathrm{ph}} v^{\star 6}$. We recall that δ, which appeared in Sec. II A, is the characteristic length of the range of the surface potential, that

is, the distance normal to the surface where w is significant, so that the corresponding characteristic time of transit through the layer is given by $\tau_{\mathrm{la}}^\star = \delta/v^\star$.

With these characteristic quantities, we introduce the dimensionless quantities $\hat{t}, \hat{\boldsymbol{x}}, \hat{\boldsymbol{c}}, \hat{f}, \hat{f}_{\mathrm{g}}, \hat{\mathrm{w}}, \hat{\mathrm{m}}, \hat{\mathsf{W}}$, and $\hat{\mathsf{W}}_{\mathrm{ph}}$, which correspond to $t, \boldsymbol{x}, \boldsymbol{c}, f, f_{\mathrm{g}}, \mathrm{w}, \mathrm{m}, \mathsf{W}$, and W_{ph}, respectively, by the following relations:

$$\begin{aligned} &\hat{t} = t/\tau_{\mathrm{fr}}^\star, \quad \hat{\boldsymbol{x}} = \boldsymbol{x}/\lambda^\star, \quad \hat{\boldsymbol{c}} = \boldsymbol{c}/v^\star, \quad \hat{f} = f\, v^{\star 3}/n^\star, \\ &\hat{f}_{\mathrm{g}} = f_{\mathrm{g}}\, v^{\star 3}/n^\star, \quad \hat{\mathrm{m}} = \mathrm{m} v^{\star 3}, \quad \hat{\mathsf{W}} = \mathsf{W}/\mathsf{W}^\star, \\ &\hat{\mathsf{W}}_{\mathrm{ph}} = \mathsf{W}_{\mathrm{ph}}/\mathsf{W}_{\mathrm{ph}}^\star, \quad \hat{\mathrm{w}}(\zeta) = \mathrm{w}(z)/\mathrm{w}^\star = \mathrm{w}_{\mathrm{s}}(\zeta)/mv^{\star 2}, \end{aligned} \tag{17}$$

where the arguments of $\hat{\mathrm{w}}$, w, and w_{s} are shown explicitly for clarity. Substituting Eq. (17) into Eq. (5) and dividing the resulting equation by $n^\star/\tau_{\mathrm{fr}}^\star v^{\star 3}$, we obtain the rescaled dimensionless kinetic equation. In this process, we note that ζ appearing in Eq. (2) is expressed as $\zeta = z/\delta = (\lambda^\star/\delta)(z/\lambda^\star) = (1/\epsilon)(z/\tau_{\mathrm{fr}}^\star v^\star)$, where $\epsilon = \delta/\lambda^\star$, so that $d\mathrm{w}/dz = (mv^\star/\tau_{\mathrm{fr}}^\star)(1/\epsilon)(d\hat{\mathrm{w}}/d\zeta)$ holds.

The rescaled kinetic equation involves the dimensionless parameters

$$\epsilon_{\mathrm{ph}} = \frac{\tau_{\mathrm{ph}}^\star}{\tau_{\mathrm{fr}}^\star}, \quad \epsilon = \frac{\delta}{\lambda^\star} = \frac{\tau_{\mathrm{la}}^\star}{\tau_{\mathrm{fr}}^\star}. \tag{18}$$

The characteristic times and lengths at the solid-gas interface are generally such that $\tau_{\mathrm{ph}}^\star \leqslant \tau_{\mathrm{fr}}^\star$ and $\delta \leqslant \lambda^\star$ so that $\epsilon \leqslant 1$ and $\epsilon_{\mathrm{ph}} \leqslant 1$ [12]. Our aim in this paper is to derive *kinetic* boundary conditions and it is thus assumed that $\epsilon \ll 1$ so that $\delta \ll \lambda^\star$ and the adsorbate layer is a *thin layer*. Equivalently we have $\tau_{\mathrm{la}}^\star \ll \tau_{\mathrm{fr}}^\star$ and the characteristic time of transit through the adsorbate layer $\tau_{\mathrm{la}}^\star$ is shorter than the mean free time $\tau_{\mathrm{fr}}^\star$. It is further assumed that the characteristic time for phonon-molecule collisions $\tau_{\mathrm{ph}}^\star$ is of the same order as the transit time $\tau_{\mathrm{la}}^\star$ and we may write

$$\epsilon_{\mathrm{ph}} = \epsilon \ll 1. \tag{19}$$

This corresponds to a fast phonon-molecule dynamics $\tau_{\mathrm{ph}}^\star = \tau_{\mathrm{la}}^\star \ll \tau_{\mathrm{fr}}^\star$ and may be seen as the *simplest kinetic scaling* of the adsorbate layer model. It differs from the *fluid scalings* used in previous work concerned with fluid type boundary conditions [23–26].

In summary, under the assumption (19), the resulting rescaled dimensionless equation reads

$$\frac{\partial \hat{f}}{\partial \hat{t}} + \hat{\boldsymbol{c}}_\parallel \cdot \frac{\partial \hat{f}}{\partial \hat{\boldsymbol{x}}_\parallel} + \hat{c}_z \frac{\partial \hat{f}}{\partial \hat{z}} - \frac{1}{\epsilon}\frac{d\hat{\mathrm{w}}}{d\zeta}\frac{\partial \hat{f}}{\partial \hat{c}_z} = \frac{1}{\epsilon}\hat{J}_{\mathrm{ph}}(\hat{f}) + \hat{J}(\hat{f},\, \hat{f}), \tag{20}$$

where $\hat{\boldsymbol{c}}_\parallel = (\hat{c}_x,\, \hat{c}_y), \hat{\boldsymbol{x}}_\parallel = (\hat{x},\, \hat{y})$, and

$$\hat{J}(\hat{f},\, \hat{f}) = \int \big[\hat{f}(\hat{\boldsymbol{c}}')\hat{f}(\hat{\boldsymbol{c}}'_*) - \hat{f}(\hat{\boldsymbol{c}})\hat{f}(\hat{\boldsymbol{c}}_*)\big]\hat{\mathsf{W}}\, d\hat{\boldsymbol{c}}_* d\hat{\boldsymbol{c}}' d\hat{\boldsymbol{c}}'_*, \tag{21a}$$

$$\hat{J}_{\mathrm{ph}}(\hat{f}) = \int \Big(\frac{\hat{f}(\hat{\boldsymbol{c}}')}{\hat{\mathrm{m}}(\hat{\boldsymbol{c}}')} - \frac{\hat{f}(\hat{\boldsymbol{c}})}{\hat{\mathrm{m}}(\hat{\boldsymbol{c}})}\Big)\hat{\mathsf{W}}_{\mathrm{ph}} d\hat{\boldsymbol{c}}', \tag{21b}$$

$$\hat{\mathrm{m}} = (2\pi)^{-3/2}\exp(-|\hat{\boldsymbol{c}}|^2/2 - \hat{\mathrm{w}}). \tag{21c}$$

Here, we naturally assume that J_{ph} also has a length scale δ and $\hat{J}_{\mathrm{ph}}$ vanishes as $\zeta \to \infty$. Then, taking the limit $\zeta \to \infty$ of Eq. (20), we recover the dimensionless version of the Boltzmann equation Eq. (10) in the gas phase, i.e.,

$$\frac{\partial \hat{f}_{\mathrm{g}}}{\partial \hat{t}} + \hat{\boldsymbol{c}} \cdot \frac{\partial \hat{f}_{\mathrm{g}}}{\partial \hat{\boldsymbol{x}}} = \hat{J}(\hat{f}_{\mathrm{g}},\, \hat{f}_{\mathrm{g}}). \tag{22}$$

B. Inner layer

The surface interaction potential w depends on the adsorbate layer coordinate

$$\zeta = \hat{z}/\epsilon, \tag{23}$$

and the problem appears as multiscale, since it involves the normal coordinate $\hat{z} = z/\lambda^\star$ as well as the inner layer coordinate ζ. In order to investigate the adsorbate layer, we denote the solution in the layer by f and assume the form

$$\mathsf{f} = \hat{f}_{\mathrm{g}}(\hat{t},\, \hat{\boldsymbol{x}}_\parallel,\, \hat{z},\, \hat{\boldsymbol{c}}) + \mathsf{f}_{\mathrm{LC}}(\hat{t},\, \hat{\boldsymbol{x}}_\parallel,\, \zeta,\, \hat{\boldsymbol{c}}_\parallel,\, \hat{c}_z), \tag{24}$$

where $\hat{f}_{\mathrm{g}}$ is the solution of Eq. (22), that is, the solution outside the adsorbate layer, and f_{LC} is the *corrector* inside the layer that is assumed to vanish as $\zeta \to \infty$. We note that $\hat{f}_{\mathrm{g}}$ and thus Eq. (22) have been extended to $\hat{z} = 0$ in Eq. (24). If we take into account the fact that the inner layer distribution f is a function of $\hat{t}$, $\hat{\boldsymbol{x}}_\parallel$, ζ, $\hat{\boldsymbol{c}}_\parallel$, and $\hat{c}_z$, we have the following equation for f by rescaling Eq. (20):

$$\frac{\partial \mathsf{f}}{\partial \hat{t}} + \hat{\boldsymbol{c}}_\parallel \cdot \frac{\partial \mathsf{f}}{\partial \hat{\boldsymbol{x}}_\parallel} + \frac{1}{\epsilon}\hat{c}_z\frac{\partial \mathsf{f}}{\partial \zeta} - \frac{1}{\epsilon}\frac{d\hat{\mathrm{w}}}{d\zeta}\frac{\partial \mathsf{f}}{\partial \hat{c}_z} = \frac{1}{\epsilon}\hat{J}_{\mathrm{ph}}(\mathsf{f}) + \hat{J}(\mathsf{f},\, \mathsf{f}). \tag{25}$$

Equation (25) suggests that f be expanded as $\mathsf{f} = \mathsf{f}^{\langle 0\rangle} + O(\epsilon)$. Accordingly, the outer solution $\hat{f}_{\mathrm{g}}$ and the layer corrector f_{LC} are also expressed as $\hat{f}_{\mathrm{g}} = \hat{f}_{\mathrm{g}}^{\langle 0\rangle} + O(\epsilon)$ and $\mathsf{f}_{\mathrm{LC}} = \mathsf{f}_{\mathrm{LC}}^{\langle 0\rangle} + O(\epsilon)$, where the $O(\epsilon)$ term in the latter should vanish as $\zeta \to \infty$. It is obvious that $\hat{f}_{\mathrm{g}}^{\langle 0\rangle}$ is also governed by the Boltzmann equation (22). In the following, we consider only the zeroth order in ϵ, so that these forms are sufficient. From Eq. (25), the equation for the zeroth order is obtained as

$$\hat{c}_z\frac{\partial \mathsf{f}^{\langle 0\rangle}}{\partial \zeta} - \frac{d\hat{\mathrm{w}}}{d\zeta}\frac{\partial \mathsf{f}^{\langle 0\rangle}}{\partial \hat{c}_z} = \hat{J}_{\mathrm{ph}}(\mathsf{f}^{\langle 0\rangle}). \tag{26}$$

On the other hand, Eq. (24) may be written as

$$\begin{aligned} \mathsf{f}^{\langle 0\rangle}(\hat{t},\, \hat{\boldsymbol{x}}_\parallel,\, \zeta,\, \hat{\boldsymbol{c}}_\parallel,\, \hat{c}_z) &= \hat{f}_{\mathrm{g}}^{\langle 0\rangle}(\hat{t},\, \hat{\boldsymbol{x}}_\parallel,\, \epsilon\zeta,\, \hat{\boldsymbol{c}}_\parallel,\, \hat{c}_z) \\ &\quad + \mathsf{f}_{\mathrm{LC}}^{\langle 0\rangle}(\hat{t},\, \hat{\boldsymbol{x}}_\parallel,\, \zeta,\, \hat{\boldsymbol{c}}_\parallel,\, \hat{c}_z) + O(\epsilon). \end{aligned} \tag{27}$$

Now, we let $\zeta = 1/\sqrt{\epsilon}$ in Eq. (27) and take the limit as $\epsilon \to 0$ recalling that $\mathsf{f}_{\mathrm{LC}}^{\langle 0\rangle}$ vanishes as $\zeta \to \infty$. Then, we have

$$\mathsf{f}^{\langle 0\rangle}(\hat{t},\, \hat{\boldsymbol{x}}_\parallel,\, \infty,\, \hat{\boldsymbol{c}}_\parallel,\, \hat{c}_z) = \hat{f}_{\mathrm{g}}^{\langle 0\rangle}(\hat{t},\, \hat{\boldsymbol{x}}_\parallel,\, 0,\, \hat{\boldsymbol{c}}_\parallel,\, \hat{c}_z). \tag{28}$$

This provides the connection condition between the inner physisorbate layer and the outer gas domain.

C. Simplified phonon collision operator

It is assumed in the following that the phonon collision operator is in the relaxation form

$$J_{\mathrm{ph}}(f) = -\frac{1}{\tau_{\mathrm{ph}}}(f - n\mathrm{M}), \tag{29}$$

where M is the wall Maxwellian given by Eq. (3), n is the molecular number density defined by

$$n = \int f \, d\boldsymbol{c},$$

and $\tau_{\rm ph}$ is the phonon relaxation time, which is positive, dependent on z, and independent of the molecular velocity $\boldsymbol{c}$. The form (29) introduced by Borman *et al.* simplifies the analysis of the adsorbate layer [11,12,16]. Here, we assume that $\tau_{\rm ph}$ has the same length scale of variation as the potential W and is a function of the scaled normal coordinate ζ, i.e.,

$$\tau_{\rm ph}(z) = \tau_{\rm ph,s}(z/\delta) = \tau_{\rm ph,s}(\zeta). \tag{30}$$

Since there is no interaction between molecules and phonons far from the surface, we make the natural assumption $\lim_{z\to\infty} \tau_{\rm ph}(z) = \lim_{\zeta\to\infty} \tau_{\rm ph,s}(\zeta) = \infty$.

In order to nondimensionalize Eq. (29), we need to introduce additional dimensionless quantities $\hat{n}$, $\hat{\tau}_{\rm ph}$, and $\hat{\rm M}$ defined by

$$\hat{n} = n/n^\star, \;\; \hat{\rm M} = {\rm M}v^{\star 3}, \;\; \hat{\tau}_{\rm ph}(\zeta) = \tau_{\rm ph}(z)/\tau^\star_{\rm ph} = \tau_{\rm ph,s}(\zeta)/\tau^\star_{\rm ph}. \tag{31}$$

Then, because of Eqs. (18) and (19), Eq. (29) is expressed as

$$J_{\rm ph}(f) = \frac{n^\star}{\tau^\star_{\rm fr} v^{\star 3}} \frac{1}{\epsilon} \hat{J}_{\rm ph}(\hat{f}), \;\; \hat{J}_{\rm ph}(\hat{f}) = -\frac{1}{\hat{\tau}_{\rm ph}(\zeta)} (\hat{f} - \hat{n}\hat{\rm M}), \tag{32}$$

where

$$\hat{n} = \int \hat{f} \, d\hat{\boldsymbol{c}}, \tag{33a}$$

$$\hat{\rm M} = (2\pi)^{-3/2} \exp\bigl(-|\hat{\boldsymbol{c}}|^2/2\bigr). \tag{33b}$$

IV. INNER LAYER AND BOUNDARY CONDITION FOR THE BOLTZMANN EQUATION

In this section, we discuss the relation between the inner adsorbate layer and the boundary condition for the Boltzmann equation.

A. Inner layer problem

First, we formulate the inner layer problem. In what follows, the superscript $\langle 0\rangle$ of $\mathsf{f}^{\langle 0\rangle}$ and $\hat{f}_{\rm g}^{\langle 0\rangle}$ is omitted, since only the zeroth-order quantities will be considered. Then, the inner layer kinetic equation (26) with the simplified phonon collision operator (29) or (32) reads

$$\hat{c}_z \frac{\partial \mathsf{f}}{\partial \zeta} - \frac{d\hat{\rm w}(\zeta)}{d\zeta} \frac{\partial \mathsf{f}}{\partial \hat{c}_z} = -\frac{1}{\hat{\tau}_{\rm ph}(\zeta)} \bigl(\mathsf{f} - \hat{\mathsf{n}}\hat{\rm M}\bigr), \;\; (0 < \zeta < \infty), \tag{34}$$

with $\hat{\rm M}$ given by Eq. (33b) and $\hat{\mathsf{n}}$ given by

$$\hat{\mathsf{n}} = \int \mathsf{f} \, d\hat{\boldsymbol{c}}. \tag{35}$$

Note that $\hat{\mathsf{n}}$ is the zeroth-order number density in the inner layer. In addition, the connection condition (28) becomes

$$\mathsf{f}(\zeta \to \infty, \, \hat{c}_z) = \hat{f}_{\rm g}(\hat{z} = 0, \, \hat{c}_z). \tag{36}$$

Here and in what follows, the arguments $\hat{t}$, $\hat{\boldsymbol{x}}_\parallel$, and $\hat{\boldsymbol{c}}_\parallel$, which are just the parameters in Eq. (34), are not shown explicitly unless confusion may arise. Integrating both sides of Eq. (34) with respect to $\hat{\boldsymbol{c}}$ over $\mathbb{R}^3$ and considering the fact that $\mathsf{f} \to 0$ as $|\hat{c}_z| \to \infty$, we have

$$\frac{\partial}{\partial \zeta} \int \hat{c}_z \mathsf{f} d\hat{\boldsymbol{c}} = 0. \tag{37}$$

Since there is no molecule when ζ approaches zero, we have

$$\int \hat{c}_z \mathsf{f} d\hat{\boldsymbol{c}} = 0. \tag{38}$$

As $\zeta \to \infty$, $\partial \mathsf{f}/\partial\zeta$ as well as $d\hat{\rm w}(\zeta)/d\zeta$ vanishes, since we consider f bounded at infinity. If $\hat{\tau}_{\rm ph}$ remains finite as $\zeta \to \infty$, then Eq. (34) gives $\mathsf{f} = \hat{\mathsf{n}}\hat{\rm M}$ at infinity. This situation corresponds to usual half-space problems of the Boltzmann equation in which Maxwellian distributions are assumed at infinity. In contrast, because $1/\hat{\tau}_{\rm ph}$ vanishes as $\zeta \to \infty$, Eq. (34) imposes no condition on f at infinity. Since the gas molecules undergo more or less free transport in the far field, we may impose f arbitrarily but only for $\hat{c}_z < 0$ at infinity in analogy with free-molecular flows, that is,

$$\mathsf{f}(\zeta, \, \hat{c}_z) \to \mathsf{f}_\infty(\hat{c}_z), \;\; \text{as} \;\; \zeta \to \infty, \;\; \text{for} \;\; \hat{c}_z < 0, \tag{39}$$

where f_∞ is an arbitrary function of $\hat{c}_z$ (and $\hat{t}$, $\hat{\boldsymbol{x}}_\parallel$, and $\hat{\boldsymbol{c}}_\parallel$). Figure 2 shows the schematic view of the characteristic lines $\hat{c}_z^2/2 + \hat{\rm w}(\zeta) = \text{const}$ of Eq. (34) in the $(\zeta, \, \hat{c}_z)$ plane, where the direction of the lines is also shown. Because of the properties of the potential $\hat{\rm w}$, the characteristic lines starting from infinity do not touch the wall and go back to infinity. Therefore, we expect that the solution of Eq. (34) is determined uniquely just by imposing the condition (39) as will also be shown numerically later. If it is the case, Eq. (34) with Eq. (39) determines the solution f and thus f for $\hat{c}_z > 0$ at infinity. In other words, the solution defines the operator Λ that maps $\mathsf{f}(\zeta \to \infty, \, \hat{c}_z < 0)$ to $\mathsf{f}(\zeta \to \infty, \, \hat{c}_z > 0)$, i.e.,

$$\mathsf{f}(\zeta \to \infty, \, \hat{c}_z > 0) = \Lambda \, \mathsf{f}(\zeta \to \infty, \, \hat{c}_z < 0), \tag{40}$$

or equivalently

$$\hat{f}_{\rm g}(\hat{z} = 0, \, \hat{c}_z > 0) = \Lambda \, \hat{f}_{\rm g}(\hat{z} = 0, \, \hat{c}_z < 0), \tag{41}$$

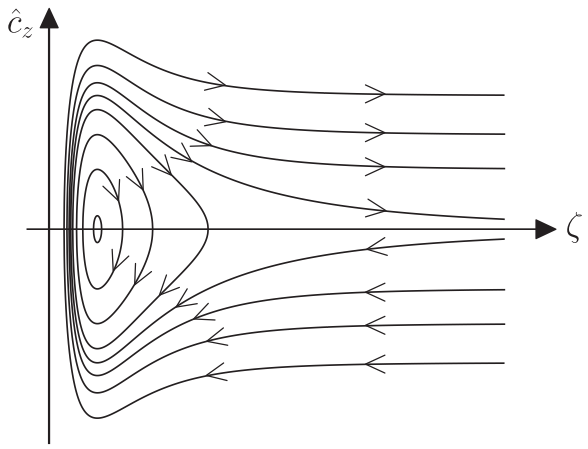

FIG. 2. Schematic view of the characteristic lines $(1/2)\hat{c}_z^2 + \hat{\rm w}(\zeta) = \text{const}$ of Eq. (34) in the $(\zeta, \, \hat{c}_z)$ plane. The direction of the lines is shown by the arrows.

because of Eq. (36). The operator Λ could be termed an adsorbate-layer albedo operator.

Equation (41) indicates that the operator Λ provides the boundary condition on the wall $\hat{z} = 0$ for $\hat{f}_g$, that is, for the Boltzmann equation. We try to solve the inner layer problem, Eqs. (34), (35), and (39), approximately in Sec. V and numerically in Sec. VI to establish the operator Λ.

B. Change of variables

Now, we let

$$\varepsilon = \tfrac{1}{2}\hat{c}_z^2 + \hat{\mathrm{W}}(\zeta). \tag{42}$$

Then, for each $\varepsilon \in [\hat{\mathrm{W}}_{\min}, \infty)$, where $\hat{\mathrm{W}}_{\min} = \mathrm{W}_{\min}/k_{\mathrm{B}}T_{\mathrm{w}}$, the range of ζ is as follows:

$$\begin{cases} [\zeta_a(\varepsilon), \infty) & \text{for } \varepsilon \geqslant 0, \\ [\zeta_a(\varepsilon), \zeta_b(\varepsilon)] & \text{for } \hat{\mathrm{W}}_{\min} \leqslant \varepsilon < 0, \end{cases} \tag{43}$$

where $\zeta_a(\varepsilon)$ is the solution of $\varepsilon = \hat{\mathrm{W}}(\zeta)$ for $\varepsilon \geqslant 0$, and $\zeta_a(\varepsilon)$ and $\zeta_b(\varepsilon)$ are the two solutions of the same equation satisfying $\zeta_a(\varepsilon) \leqslant \zeta_{\min} \leqslant \zeta_b(\varepsilon)$ for $\hat{\mathrm{W}}_{\min} \leqslant \varepsilon < 0$.

Here, we transform the independent variables from $(\zeta, \hat{c}_z)$ to (ζ, ε) and define

$$\mathsf{f}_{\pm}(\zeta, \varepsilon) = \mathsf{f}\big(\zeta, \pm\sqrt{2}\sqrt{\varepsilon - \hat{\mathrm{W}}(\zeta)}\big). \tag{44}$$

Recall that the arguments $(\hat{t}, \hat{\boldsymbol{x}}_{\parallel}, \hat{\boldsymbol{c}}_{\parallel})$, common to both sides, are omitted, and note that f_+ corresponds to $\hat{c}_z > 0$, and f_- to $\hat{c}_z < 0$. Then, Eqs. (34) and (35) are transformed to

$$\pm\sqrt{2}\sqrt{\varepsilon - \hat{\mathrm{W}}(\zeta)}\,\frac{\partial \mathsf{f}_{\pm}}{\partial \zeta} = -\frac{1}{\hat{\tau}_{\mathrm{ph}}(\zeta)}[\mathsf{f}_{\pm} - \hat{\mathsf{n}}\hat{\mathrm{M}}(\zeta, \varepsilon)], \tag{45a}$$

$$\hat{\mathrm{M}}(\zeta, \varepsilon) = (2\pi)^{-3/2}\exp(-|\hat{\boldsymbol{c}}_{\parallel}|^2/2 - \varepsilon + \hat{\mathrm{W}}(\zeta)), \tag{45b}$$

$$\hat{\mathsf{n}} = \frac{1}{\sqrt{2}}\int_{\hat{\mathrm{W}}(\zeta)}^{\infty}\left[\iint_{-\infty}^{\infty}(\mathsf{f}_- + \mathsf{f}_+)d\hat{c}_x d\hat{c}_y\right]\frac{1}{\sqrt{\varepsilon - \hat{\mathrm{W}}(\zeta)}}d\varepsilon, \tag{45c}$$

where $\hat{\mathrm{M}}(\zeta, \varepsilon)$ is the expression of $\hat{\mathrm{M}}$ in Eq. (33b) in terms of ζ and ε, and the number density $\hat{\mathsf{n}}$ is a function of $\hat{t}, \hat{\boldsymbol{x}}_{\parallel}$, and ζ. In addition, the boundary condition (39) becomes

$$\mathsf{f}_- \to \mathsf{f}_{\infty}(-\sqrt{2\varepsilon}), \quad \text{as } \zeta \to \infty, \quad \text{for } \varepsilon > 0. \tag{46}$$

Since the molecules with energy ε stop their motion in the ζ direction and are then reflected when they reach $\zeta_a(\varepsilon)$ and $\zeta_b(\varepsilon)$, it is natural to assume the following additional boundary conditions:

$$\mathsf{f}_+(\zeta_a(\varepsilon), \varepsilon) = \mathsf{f}_-(\zeta_a(\varepsilon), \varepsilon), \quad \text{for } \varepsilon > \hat{\mathrm{W}}_{\min}, \tag{47a}$$

$$\mathsf{f}_-(\zeta_b(\varepsilon), \varepsilon) = \mathsf{f}_+(\zeta_b(\varepsilon), \varepsilon), \quad \text{for } \hat{\mathrm{W}}_{\min} < \varepsilon < 0. \tag{47b}$$

The mass conservation (38) is transformed to

$$\int_{\hat{\mathrm{W}}(\zeta)}^{\infty}\iint_{-\infty}^{\infty}(\mathsf{f}_+ - \mathsf{f}_-)d\hat{c}_x d\hat{c}_y d\varepsilon = 0. \tag{48}$$

C. Integral equation

Let us solve Eq. (45) formally to express $\mathsf{f}_{\pm}$ in terms of $\hat{\mathsf{n}}$, supposing that $\hat{\mathsf{n}}$ is known and regarding Eq. (45) as the ordinary differential equations (ODEs) for $\mathsf{f}_{\pm}$. To be more specific, we integrate Eq. (45a), regarded as an ODE, for f_- from ∞ to ζ for $\varepsilon > 0$ under the boundary condition (46) and from $\zeta_b(\varepsilon)$ to ζ for $\hat{\mathrm{W}}_{\min} < \varepsilon < 0$ under the boundary condition (47b). Similarly, we integrate Eq. (45a) for f_+ from $\zeta_a(\varepsilon)$ to ζ for $\hat{\mathrm{W}}_{\min} < \varepsilon$ under the boundary condition (47a). Then, we have the following expressions:

$$\mathsf{f}_-(\zeta, \varepsilon) = \begin{cases} \theta(\zeta, \infty; \varepsilon)\Big[\mathsf{f}_{\infty}(-\sqrt{2\varepsilon}) + \frac{1}{\sqrt{2}}\int_{\zeta}^{\infty}\theta(\infty, s; \varepsilon)\frac{\hat{\mathsf{n}}(s)\hat{\mathrm{M}}(s, \varepsilon)}{\hat{\tau}_{\mathrm{ph}}(s)\sqrt{\varepsilon - \hat{\mathrm{W}}(s)}}ds\Big], & (\varepsilon > 0), \\ \theta(\zeta, \zeta_b(\varepsilon); \varepsilon)\Big[\mathsf{f}_+(\zeta_b(\varepsilon), \varepsilon) + \frac{1}{\sqrt{2}}\int_{\zeta}^{\zeta_b(\varepsilon)}\theta(\zeta_b(\varepsilon), s; \varepsilon)\frac{\hat{\mathsf{n}}(s)\hat{\mathrm{M}}(s, \varepsilon)}{\hat{\tau}_{\mathrm{ph}}(s)\sqrt{\varepsilon - \hat{\mathrm{W}}(s)}}ds\Big], \\ \qquad\qquad (\hat{\mathrm{W}}_{\min} < \varepsilon < 0), \end{cases} \tag{49a}$$

$$\mathsf{f}_+(\zeta, \varepsilon) = \theta(\zeta_a(\varepsilon), \zeta; \varepsilon)\left[\mathsf{f}_-(\zeta_a(\varepsilon), \varepsilon) + \frac{1}{\sqrt{2}}\int_{\zeta_a(\varepsilon)}^{\zeta}\theta(s, \zeta_a(\varepsilon); \varepsilon)\frac{\hat{\mathsf{n}}(s)\hat{\mathrm{M}}(s, \varepsilon)}{\hat{\tau}_{\mathrm{ph}}(s)\sqrt{\varepsilon - \hat{\mathrm{W}}(s)}}ds\right], \tag{49b}$$

$$\theta(a, b; \varepsilon) = \exp\left(-\frac{1}{\sqrt{2}}\int_a^b \frac{d\xi}{\hat{\tau}_{\mathrm{ph}}(\xi)\sqrt{\varepsilon - \hat{\mathrm{W}}(\xi)}}\right). \tag{49c}$$

Combined with Eq. (45c), Eq. (49) can be regarded as the integral equations for $\mathsf{f}_\pm$. If Eq. (49) is used in Eq. (45c), the latter can be regarded as the integral equation for $\hat{\mathsf{n}}$. Equation (49) will be used occasionally in our discussions though it will not be used for the numerical analysis. For $\varepsilon > 0$, Eqs. (49a) and (49b) give the following expression of f_+ as $\zeta \to \infty$:

$$\begin{aligned}\mathsf{f}_+(\infty,\,\varepsilon) &= [\theta(\zeta_a(\varepsilon),\,\infty;\,\varepsilon)]^2\mathsf{f}_\infty(-\sqrt{2\varepsilon}) \\ &+ \frac{\theta(\zeta_a(\varepsilon),\,\infty;\,\varepsilon)}{\sqrt{2}} \\ &\times \int_{\zeta_a(\varepsilon)}^{\infty}[\theta(\zeta_a(\varepsilon),\,s;\,\varepsilon)+\theta(s,\,\zeta_a(\varepsilon);\,\varepsilon)] \\ &\times \frac{\hat{\mathsf{n}}(s)\hat{\mathrm{M}}(s,\,\varepsilon)}{\hat{\tau}_{\mathrm{ph}}(s)\sqrt{\varepsilon-\hat{\mathrm{w}}(s)}}ds. \end{aligned} \tag{50}$$

V. APPROXIMATE SOLUTION

In order to establish the boundary condition (41) for the Boltzmann equation, we have to solve the half-space problem, Eqs. (45)–(47). It can be solved numerically, as we will do in the next section. However, the numerical solution does not give an explicit analytical form of the boundary operator Λ in Eq. (41). In this section, therefore, we try to obtain approximate iterative solutions to the half-space problem to deduce explicit approximations of the operator Λ.

A. Iteration scheme and first approximation

On the basis of Eqs. (45c) and (49), we can construct the following iteration scheme for $\mathsf{f}_\pm$:

$$\hat{\mathsf{n}}^{(n)}(\zeta) = \frac{1}{\sqrt{2}}\int_{\hat{\mathrm{w}}(\zeta)}^{\infty}\left\{\iint_{-\infty}^{\infty}[\mathsf{f}_-^{(n)}(\zeta,\,\varepsilon)+\mathsf{f}_+^{(n)}(\zeta,\,\varepsilon)]d\hat{c}_x d\hat{c}_y\right\}\frac{1}{\sqrt{\varepsilon-\hat{\mathrm{w}}(\zeta)}}d\varepsilon, \tag{51a}$$

$$\mathsf{f}_-^{(n+1)}(\zeta,\,\varepsilon) = \begin{cases}\theta(\zeta,\,\infty;\,\varepsilon)\left[\mathsf{f}_\infty(-\sqrt{2\varepsilon})+\frac{1}{\sqrt{2}}\int_\zeta^\infty\theta(\infty,\,s;\,\varepsilon)\frac{\hat{\mathsf{n}}^{(n)}(s)\hat{\mathrm{M}}(s,\,\varepsilon)}{\hat{\tau}_{\mathrm{ph}}(s)\sqrt{\varepsilon-\hat{\mathrm{w}}(s)}}ds\right], & (\varepsilon>0), \\ \theta(\zeta,\,\zeta_b(\varepsilon);\,\varepsilon)\left[\mathsf{f}_+^{(n+1)}(\zeta_b(\varepsilon),\,\varepsilon)+\frac{1}{\sqrt{2}}\int_\zeta^{\zeta_b(\varepsilon)}\theta(\zeta_b(\varepsilon),\,s;\,\varepsilon)\frac{\hat{\mathsf{n}}^{(n)}(s)\hat{\mathrm{M}}(s,\,\varepsilon)}{\hat{\tau}_{\mathrm{ph}}(s)\sqrt{\varepsilon-\hat{\mathrm{w}}(s)}}ds\right], & (\hat{\mathrm{w}}_{\min}<\varepsilon<0),\end{cases} \tag{51b}$$

$$\mathsf{f}_+^{(n+1)}(\zeta,\,\varepsilon) = \theta(\zeta_a(\varepsilon),\,\zeta;\,\varepsilon)\left[\mathsf{f}_-^{(n+1)}(\zeta_a(\varepsilon),\,\varepsilon)+\frac{1}{\sqrt{2}}\int_{\zeta_a(\varepsilon)}^{\zeta}\theta(s,\,\zeta_a(\varepsilon);\,\varepsilon)\frac{\hat{\mathsf{n}}^{(n)}(s)\hat{\mathrm{M}}(s,\,\varepsilon)}{\hat{\tau}_{\mathrm{ph}}(s)\sqrt{\varepsilon-\hat{\mathrm{w}}(s)}}ds\right], \tag{51c}$$

where $\mathsf{f}_\pm^{(n)}$ denotes the nth iteration of $\mathsf{f}_\pm$ and $\hat{\mathsf{n}}^{(n)}$ denotes the nth iteration of $\hat{\mathsf{n}}$. It should be recalled that the arguments $\hat{t}$, $\hat{\boldsymbol{x}}_\parallel$, and $\hat{\boldsymbol{c}}_\parallel$ are omitted in $\mathsf{f}_\pm^{(n+1)}$, and $\hat{t}$ and $\hat{\boldsymbol{x}}_\parallel$ are omitted in $\hat{\mathsf{n}}^{(n)}$.

Now, we consider the first iteration $\mathsf{f}_\pm^{(1)}$ starting from the following zeroth guess $\mathsf{f}_\pm^{(0)}$:

$$\mathsf{f}_+^{(0)} = \mathsf{f}_-^{(0)} = \hat{\beta}\,\hat{\mathsf{m}}(\varepsilon), \tag{52}$$

where

$$\hat{\mathsf{m}}(\varepsilon) = (2\pi)^{-3/2}\exp(-|\hat{\boldsymbol{c}}_\parallel|^2/2-\varepsilon), \tag{53}$$

which is the expression of $\hat{\mathsf{m}}$ in Eq. (21c) in terms of ε, and $\hat{\beta}$ is a constant to be determined later. Note that Eq. (52) is an exact solution of Eq. (45). Then, Eq. (51a) gives

$$\hat{\mathsf{n}}^{(0)}(\zeta) = \hat{\beta}\exp(-\hat{\mathrm{w}}(\zeta)). \tag{54}$$

It should be remarked that this density is the same as that obtained at the zeroth order in ϵ, with a fluid scaling, for the physisorbed molecules [see Eq. (70) in [25]]. With Eq. (54), the integrals in Eqs. (51b) and (51c) can be calculated explicitly.

Let us first consider the case where $\varepsilon > 0$. Since $\hat{\mathsf{n}}^{(0)}(s)\hat{\mathrm{M}}(s,\,\varepsilon) = \hat{\beta}\hat{\mathsf{m}}(\varepsilon)$, the integral in the first line of Eq. (51b) is reduced as follows:

$$\frac{1}{\sqrt{2}}\int_\zeta^\infty\theta(\infty,\,s;\,\varepsilon)\frac{\hat{\mathsf{n}}^{(0)}(s)\hat{\mathrm{M}}(s,\,\varepsilon)}{\hat{\tau}_{\mathrm{ph}}(s)\sqrt{\varepsilon-\hat{\mathrm{w}}(s)}}ds = -\hat{\beta}\hat{\mathsf{m}}(\varepsilon)\int_\zeta^\infty\frac{\partial}{\partial s}\theta(\infty,\,s;\,\varepsilon)ds = \hat{\beta}\hat{\mathsf{m}}(\varepsilon)[\theta(\infty,\,\zeta;\,\varepsilon)-1]. \tag{55}$$

The integral in Eq. (51c) can be calculated in the same way. As the result, $\mathsf{f}_\pm^{(1)}$ for $\varepsilon > 0$ are obtained as follows:

$$\mathsf{f}_-^{(1)}(\zeta,\,\varepsilon) = \theta(\zeta,\,\infty;\,\varepsilon)\mathsf{f}_\infty(-\sqrt{2\varepsilon})+[1-\theta(\zeta,\,\infty;\,\varepsilon)]\hat{\beta}\hat{\mathsf{m}}(\varepsilon), \tag{56a}$$

$$\mathsf{f}_+^{(1)}(\zeta,\,\varepsilon) = \theta(\zeta_a(\varepsilon),\,\zeta;\,\varepsilon)\mathsf{f}_-^{(1)}(\zeta_a(\varepsilon),\,\varepsilon)+[1-\theta(\zeta_a(\varepsilon),\,\zeta;\,\varepsilon)]\hat{\beta}\hat{\mathsf{m}}(\varepsilon). \tag{56b}$$

From Eq. (56), it follows that

$$\begin{aligned}\mathsf{f}_+^{(1)}(\infty,\,\varepsilon) &= \theta(\zeta_a(\varepsilon),\,\infty;\,\varepsilon)\mathsf{f}_-^{(1)}(\zeta_a(\varepsilon),\,\varepsilon)+[1-\theta(\zeta_a(\varepsilon),\,\infty;\,\varepsilon)]\hat{\beta}\,\hat{\mathsf{m}}(\varepsilon) \\ &= [\theta(\zeta_a(\varepsilon),\,\infty;\,\varepsilon)]^2\,\mathsf{f}_-^{(1)}(\infty,\,\varepsilon)+\{1-[\theta(\zeta_a(\varepsilon),\,\infty;\,\varepsilon)]^2\}\hat{\beta}\,\hat{\mathsf{m}}(\varepsilon)\end{aligned} \tag{57}$$

where $\mathsf{f}_\infty(-\sqrt{2\varepsilon})$ in Eq. (56a) has been replaced with the equivalent $\mathsf{f}_-^{(1)}(\infty,\ \varepsilon)$ for later convenience.

Now, we go back from the $(\zeta,\ \varepsilon)$ representation to the original $(\zeta,\ \hat{c}_z)$ representation. We omit the superscript (1) of $\mathsf{f}_\pm^{(1)}$, supposing that $\mathsf{f}_\pm^{(1)}$ is an approximation of $\mathsf{f}_\pm$, and note that

$$\mathsf{f}_+(\zeta,\ \varepsilon) = \mathsf{f}(\zeta,\ \hat{c}_z) \quad \text{for} \quad \hat{c}_z > 0, \tag{58a}$$

$$\mathsf{f}_-(\zeta,\ \varepsilon) = \mathsf{f}(\zeta,\ \hat{c}_z) \quad \text{for} \quad \hat{c}_z < 0, \tag{58b}$$

$$\varepsilon = \hat{c}_z^2/2 \quad \text{at} \quad \zeta = \infty. \tag{58c}$$

Then, Eq. (57) leads to the following expression:

$$\mathsf{f}(\infty,\ \hat{c}_z) = [1 - \hat{\alpha}(\hat{c}_z^2)]\,\mathsf{f}(\infty,\ -\hat{c}_z) + \hat{\alpha}(\hat{c}_z^2)\,\hat{\beta}\,\hat{\mathrm{M}}(\hat{\boldsymbol{c}}), \quad \text{for} \quad \hat{c}_z > 0, \tag{59}$$

where

$$\hat{\alpha}(\hat{c}_z^2) = 1 - \left[\theta\left(\zeta_a(\hat{c}_z^2/2),\ \infty;\ \hat{c}_z^2/2\right)\right]^2 = 1 - \exp\left(-\sqrt{2}\int_{\zeta_a(\hat{c}_z^2/2)}^\infty \frac{d\xi}{\hat{\tau}_{\mathrm{ph}}(\xi)\sqrt{\hat{c}_z^2/2 - \hat{\mathrm{w}}(\xi)}}\right), \tag{60}$$

and $\hat{\mathrm{M}}(\hat{\boldsymbol{c}})$ is given by Eq. (33b). Recall that $\zeta_a(\hat{c}_z^2/2)$ is the solution of $\hat{\mathrm{w}}(\zeta) = \hat{c}_z^2/2$ and note that $0 < \hat{\alpha}(\hat{c}_z^2) < 1$ holds.

It should be noted here that the mass is not generally conserved for $\mathsf{f}_\pm^{(1)}$. Therefore, $\hat{\beta}$ in Eq. (59) is chosen in such a way that the mass conservation (38) is satisfied at $\zeta = \infty$. As the result, $\hat{\beta}$ is obtained as follows:

$$\hat{\beta} = -\sqrt{2\pi}\left[\int_0^\infty \hat{c}_z\hat{\alpha}(\hat{c}_z^2)\exp\left(-\hat{c}_z^2/2\right)d\hat{c}_z\right]^{-1}\int_{\hat{c}_z<0}\hat{c}_z\hat{\alpha}(\hat{c}_z^2)\mathsf{f}(\infty,\ \hat{c}_z)d\hat{\boldsymbol{c}}. \tag{61}$$

Equation (59) with Eqs. (60) and (61) provides an approximation of the operator Λ in Eq. (40), and thus in Eq. (41).

In order to complete $\mathsf{f}_\pm^{(1)}$, we need to consider the case where $\hat{\mathrm{w}}_{\min} < \varepsilon < 0$. In this case, the second line of Eq. (51b) and Eq. (51c) give

$$\mathsf{f}_-^{(1)}(\zeta,\ \varepsilon) = \theta(\zeta,\ \zeta_b(\varepsilon);\ \varepsilon)\mathsf{f}_+^{(1)}(\zeta_b(\varepsilon),\ \varepsilon) + [1 - \theta(\zeta,\ \zeta_b(\varepsilon);\ \varepsilon)]\hat{\beta}\hat{\mathfrak{m}}(\varepsilon), \tag{62a}$$

$$\mathsf{f}_+^{(1)}(\zeta,\ \varepsilon) = \theta(\zeta_a(\varepsilon),\ \zeta;\ \varepsilon)\mathsf{f}_-^{(1)}(\zeta_a(\varepsilon),\ \varepsilon) + [1 - \theta(\zeta_a(\varepsilon),\ \zeta;\ \varepsilon)]\hat{\beta}\hat{\mathfrak{m}}(\varepsilon), \tag{62b}$$

from which it follows immediately that

$$\mathsf{f}_+^{(1)} = \mathsf{f}_-^{(1)} = \hat{\beta}\,\hat{\mathfrak{m}}(\varepsilon),\ \ \hat{\mathrm{w}}_{\min} < \varepsilon < 0. \tag{63}$$

With Eqs. (56) and (63), we can obtain the second iteration $\mathsf{f}_\pm^{(2)}$ from Eq. (51) with $n = 1$. In particular, $\mathsf{f}_\pm^{(2)}(\infty,\ \varepsilon)$ can be obtained as [see Eq. (50)]

$$\mathsf{f}_+^{(2)}(\infty,\ \varepsilon) = [\theta(\zeta_a(\varepsilon),\ \infty;\ \varepsilon)]^2\mathsf{f}_\infty(-\sqrt{2\varepsilon}) + \frac{\theta(\zeta_a(\varepsilon),\ \infty;\ \varepsilon)}{\sqrt{2}}\int_{\zeta_a(\varepsilon)}^\infty [\theta(\zeta_a(\varepsilon),\ s;\ \varepsilon) + \theta(s,\ \zeta_a(\varepsilon);\ \varepsilon)]\frac{\hat{\mathsf{n}}^{(1)}(s)\hat{\mathrm{M}}(s,\ \varepsilon)}{\hat{\tau}_{\mathrm{ph}}(s)\sqrt{\varepsilon - \hat{\mathrm{w}}(s)}}ds, \tag{64}$$

where $\varepsilon > 0$. The explicit form of $\hat{\mathsf{n}}^{(1)}$ is given in Appendix B. We note that $\hat{\beta}$ contained in $\hat{\mathsf{n}}^{(1)}$ is an adjustable parameter to satisfy the mass conservation for $\mathsf{f}_\pm^{(2)}$. Equation (64) provides the second approximation of the operator Λ in the boundary condition (41) for the Boltzmann equation.

B. Summary of the first approximation boundary condition

In the previous subsection, we have constructed approximate forms of the operator Λ in Eq. (41), which is the boundary condition for the Boltzmann equation on the wall, in the dimensionless setting. It is straightforward to transform the results to their dimensional forms. In this subsection, restricting ourselves to the first approximation, we will summarize the result.

The dimensional version of the first approximation of Eq. (41) is expressed as follows:

$$f_{\mathrm{g}}(t,\ \boldsymbol{x},\ \boldsymbol{c}_\parallel,\ c_z) = \left[1 - \alpha(c_z^2)\right]f_{\mathrm{g}}(t,\ \boldsymbol{x},\ \boldsymbol{c}_\parallel,\ -c_z) + \alpha(c_z^2)\,\beta\,\mathrm{M}(\boldsymbol{c}), \quad \text{at} \quad z = 0 \quad \text{for} \quad c_z > 0, \tag{65}$$

where

$$\mathrm{M}(\boldsymbol{c}) = \left(\frac{m}{2\pi k_{\mathrm{B}}T_{\mathrm{w}}}\right)^{3/2}\exp\left(-\frac{m|\boldsymbol{c}|^2}{2k_{\mathrm{B}}T_{\mathrm{w}}}\right), \tag{66a}$$

$$\alpha(c_z^2) = 1 - \exp\left(-\sqrt{2m}\int_{z_a(mc_z^2/2)}^\infty \frac{dz}{\tau_{\mathrm{ph}}(z)\sqrt{mc_z^2/2 - \mathrm{w}(z)}}\right) = 1 - \exp\left(-\sqrt{2m}\,\delta\int_{\zeta_a(mc_z^2/2k_{\mathrm{B}}T_{\mathrm{w}})}^\infty \frac{d\zeta}{\tau_{\mathrm{ph,s}}(\zeta)\sqrt{mc_z^2/2 - \mathrm{w}_{\mathrm{s}}(\zeta)}}\right), \tag{66b}$$

$$\beta = -\left(\frac{2\pi k_{\mathrm{B}}T_{\mathrm{w}}}{m}\right)^{1/2}\left[\int_0^\infty c_z\alpha(c_z^2)\exp\left(-\frac{mc_z^2}{2k_{\mathrm{B}}T_{\mathrm{w}}}\right)dc_z\right]^{-1}\int_{c_z<0}c_z\alpha(c_z^2)f_{\mathrm{g}}(t,\ \boldsymbol{x},\ \boldsymbol{c}_\parallel,\ c_z)d\boldsymbol{c}. \tag{66c}$$

Here, $z_a(mc_z^2/2) = \delta\,\zeta_a(mc_z^2/2k_{\rm B}T_{\rm w})$, i.e., $z = z_a$ is the solution of $\mathrm{W}(z) = mc_z^2/2$. In Eq. (66b), the middle is the expression in terms of the dimensional normal coordinate z, and the rightmost is that in terms of the dimensionless rescaled normal coordinate $\zeta = z/\delta$.

Equation (65) with Eq. (66) provides an explicit form of the operator Λ in Eq. (41) and is of the form of the so-called Maxwell type condition with c_z-dependent accommodation coefficient $\alpha(c_z^2)$. When $1/\tau_{\rm ph}(z)$ is sufficiently small, $\alpha(c_z^2) \approx 0$, so that Eq. (65) reduces to the specular reflection; when $1/\tau_{\rm ph}(z)$ is sufficiently large, $\alpha(c_z^2) \approx 1$, so that it reduces to the diffuse reflection. It should be emphasized that the accommodation coefficient $\alpha(c_z^2)$ is explicitly expressed in terms of the phonon characteristic time $\tau_{\rm ph}(z)$ and the potential $\mathrm{W}(z)$. In summary, Eqs. (65) and (66) give a model of the gas-surface interaction explicitly expressed in terms of the surface properties. This boundary condition will be compared with the numerical result obtained by solving the original half-space problem in the next section.

Under quite general assumptions, the boundary condition for the Boltzmann equation in the present geometry can be written in the following general form:

$$c_z f_{\rm g}(t,\,\boldsymbol{x},\,\boldsymbol{c}) = \int_{c_{*z}<0} |c_{*z}| f_{\rm g}(t,\,\boldsymbol{x},\,\boldsymbol{c}_*)\mathcal{R}(t,\,\boldsymbol{x}_\parallel;\,\boldsymbol{c},\,\boldsymbol{c}_*)d\boldsymbol{c}_*, \quad \text{at } z = 0 \text{ for } c_z > 0, \tag{67}$$

where $\mathcal{R}(t,\,\boldsymbol{x}_\parallel;\,\boldsymbol{c},\,\boldsymbol{c}_*)d\boldsymbol{c}$ indicates the probability that a molecule incident on the boundary with velocity $\boldsymbol{c}_*$ is reflected with the velocity contained in the neighborhood $d\boldsymbol{c}$ around $\boldsymbol{c}$ at time t and position $(\boldsymbol{x}_\parallel,\,0)$ [1,33]. The probability density $\mathcal{R}(\boldsymbol{c},\,\boldsymbol{c}_*)$, where t and $\boldsymbol{x}_\parallel$ are not shown explicitly, should satisfy the following conditions: (i) $\mathcal{R}(\boldsymbol{c},\,\boldsymbol{c}_*) \geqslant 0$ for $c_z > 0$ and $c_{*z} < 0$ (non-negativity); (ii) $\int_{c_z>0} \mathcal{R}(\boldsymbol{c},\,\boldsymbol{c}_*)d\boldsymbol{c} = 1$ for $c_{*z} < 0$ (normalization); and (iii) the wall Maxwellian $\mathrm{M}(\boldsymbol{c})$ [Eq. (3)] is the only Maxwellian satisfying Eq. (67) up to an arbitrary multiplication factor that is a function of t and $\boldsymbol{x}_\parallel$. For our model (65), it follows that

$$\begin{aligned}\mathcal{R}(\boldsymbol{c},\,\boldsymbol{c}_*) &= \left[1-\alpha\left(c_z^2\right)\right]\delta(c_{*x}-c_x)\delta(c_{*y}-c_y)\delta(c_{*z}+c_z) \\ &\quad + \left(\frac{2\pi k_{\rm B}T_{\rm w}}{m}\right)^{1/2}\left[\int_0^\infty c_z\alpha\left(c_z^2\right)\exp\left(-\frac{mc_z^2}{2k_{\rm B}T_{\rm w}}\right)dc_z\right]^{-1} \\ &\quad \times c_z\alpha\left(c_z^2\right)\alpha\left(c_{*z}^2\right)\mathrm{M}(\boldsymbol{c}),\end{aligned} \tag{68}$$

where $\delta(\,\cdot\,)$ indicates the Dirac delta function. It is easily seen that this $\mathcal{R}(\boldsymbol{c},\,\boldsymbol{c}_*)$ satisfies the three conditions (i), (ii), and (iii) (assuming that the Dirac delta function is non-negative). This is partially due to the fact that we adopted Eq. (52) as the initial guess and determined β by mass conservation. However, the boundary condition based on the numerical solution of the half-space problem, Eqs. (34) and (39), enjoys the properties (i)–(iii). It should be emphasized that Eq. (68) is one of few examples of an explicit and physics-based scattering kernel.

In the present paper, we have assumed for simplicity that the wall is planar, the potential W as well as the phonon relaxation time $\tau_{\rm ph}$ is the function of the normal coordinate z only, and the wall temperature $T_{\rm w}$ is uniform and constant. However, some generalizations can be made straightforwardly. If W, $\tau_{\rm ph}$, and $T_{\rm w}$ depend also on the time t and the tangential coordinates $\boldsymbol{x}_\parallel$ with the scales of variation $\tau_{\rm fr}^\star$ for t and $\lambda^\star$ for $\boldsymbol{x}_\parallel$, then one can generalize Eqs. (65) and (66) to this case just by the replacement

$$\begin{aligned}&\mathrm{W}(z) \to \mathrm{W}(t,\,\boldsymbol{x}_\parallel,\,z) \quad \text{or} \quad \mathrm{W}_{\rm s}(\zeta) \to \mathrm{W}_{\rm s}(t,\,\boldsymbol{x}_\parallel,\,\zeta), \\ &\tau_{\rm ph}(z) \to \tau_{\rm ph}(t,\,\boldsymbol{x}_\parallel,\,z) \quad \text{or} \quad \tau_{\rm ph,s}(\zeta) \to \tau_{\rm ph,s}(t,\,\boldsymbol{x}_\parallel,\,\zeta), \\ &z_a\left(mc_z^2/2\right) \to z_a\left(t,\,\boldsymbol{x}_\parallel;\,mc_z^2/2\right) \quad \text{or} \\ &\zeta_a\left(mc_z^2/2k_{\rm B}T_{\rm w}\right) \to \zeta_a\left(t,\,\boldsymbol{x}_\parallel;\,mc_z^2/2k_{\rm B}T_{\rm w}\right), \\ &T_{\rm w} \to T_{\rm w}(t,\,\boldsymbol{x}_\parallel),\end{aligned} \tag{69}$$

where $z = z_a(t,\,\boldsymbol{x}_\parallel;\,mc_z^2/2)$ is the solution of $\mathrm{W}(t,\,\boldsymbol{x}_\parallel,\,z) = mc_z^2/2$, and $\zeta_a(t,\,\boldsymbol{x}_\parallel;\,mc_z^2/2k_{\rm B}T_{\rm w}) = z_a(t,\,\boldsymbol{x}_\parallel;\,mc_z^2/2)/\delta$. Then, α and β naturally depend on t and $\boldsymbol{x}_\parallel$. When the wall is not planar but curved, and if the principal radii of curvature are of the order of $\lambda^\star$, the generalization (69) is also valid if $\boldsymbol{x}_\parallel$ is interpreted as the tangential coordinates on the surface. The generalization to the case where the wall is moving is also straightforward.

It should be remarked that Brull *et al.* [17] considered a model of the physisorbate layer similar to ours to deduce the kinetic boundary conditions. However, their model of the physisorbate layer has a finite thickness, so that the matching between the layer and the outer gas region is made at a finite distance from the wall. In contrast, we considered the confinement potentials, as well as the interaction with surface phonons, extending to infinity and vanishing there. Therefore, the matching between the inner physisorbate layer and the outer gas region is only asymptotic as the distance from the wall goes to infinity ($\zeta \to \infty$). Since there is no natural finite distance for such a matching, our model seems to be more natural. It should be mentioned that the approximate kinetic boundary condition derived in [17] corresponds to our first approximation of the iterative procedure, that is, Eqs. (65) and (66). Therefore, Eqs. (65) and (66) should be recovered from the result in [17] by letting the thickness of the surface layer be infinitely large under appropriate assumptions on the surface potential and the phonon relaxation time though it is not discussed there.

In the present approach via the half-space problem, Eqs. (34) and (39), including the approximate formula (65) with Eq. (66), the effect of surface roughness in the molecular scale is not taken into account. It should be mentioned that in [17,18] the effect is considered by using a confinement potential varying also in the tangential direction with the length scale of δ.

C. Some remarks on classical models

As mentioned at the beginning of Sec. I, most of the classical and conventional models [1–6] of the boundary conditions for the Boltzmann equation are of mathematical or empirical nature. In contrast, our model (65) [with Eq. (66)], based on the first iteration, has been derived systematically from the kinetic model based on microscopic information near the solid surface. Therefore, their nature is quite different. Nevertheless, it would be of interest to discuss the difference between

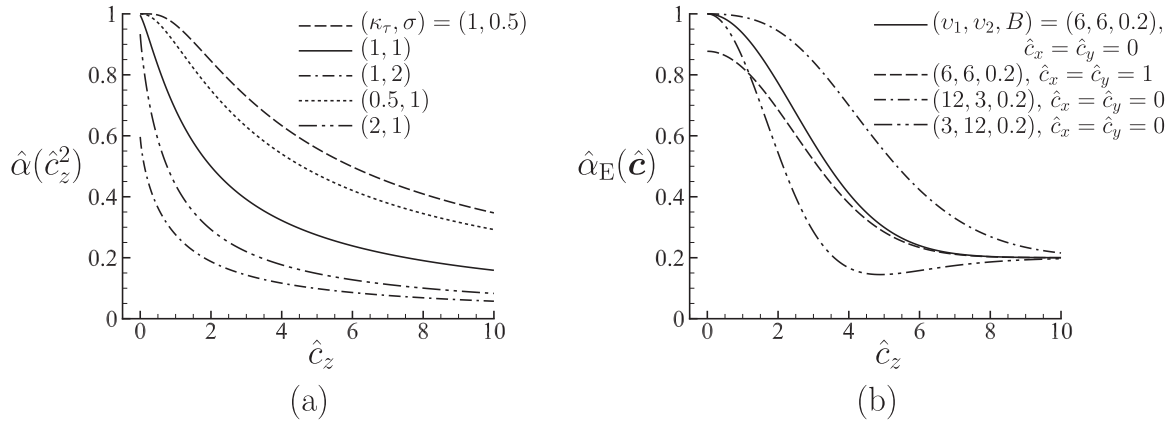

FIG. 3. $\hat{\alpha}(\hat{c}_z^2)$ and $\hat{\alpha}_{\mathrm{E}}(\hat{\boldsymbol{c}})$. (a) $\hat{\alpha}(\hat{c}_z^2)$ vs $\hat{c}_z$ for the Lennard-Jones (9, 3) potential (88) and the algebraic-type relaxation time (91) in the case of $\kappa = 1$, $n = 4$, and $(\kappa_\tau, \sigma) = (1, 0.5)$, $(1, 1)$, $(1, 2)$, $(0.5, 1)$, and $(2, 1)$. (b) $\hat{\alpha}_{\mathrm{E}}(\hat{\boldsymbol{c}})$ vs $\hat{c}_z$ for $(\upsilon_1, \upsilon_2, B) = (6, 6, 0.2)$, $(12, 3, 0.2)$, and $(3, 12, 0.2)$ at $\hat{c}_x = \hat{c}_y = 0$ and for $(6, 6, 0.2)$ at $\hat{c}_x = \hat{c}_y = 1$.

our model and the conventional models. Here, we consider the Epstein model [2] and the Cercignani-Lampis model [1,4].

The Epstein model is of the same form as our Eq. (65), but the function $\alpha(c_z^2)$ should be replaced with the following $\alpha_{\mathrm{E}}(\boldsymbol{c})$:

$$\alpha_{\mathrm{E}}(\boldsymbol{c}) = \exp\left(-\frac{m|\boldsymbol{c}|^2}{2k_{\mathrm{B}}T_{\mathrm{w}}\upsilon_1}\right) + B\left[1 - \exp\left(-\frac{m|\boldsymbol{c}|^2}{2k_{\mathrm{B}}T_{\mathrm{w}}\upsilon_2}\right)\right], \tag{70}$$

where υ_1, υ_2, and B are the adjustable parameters to be determined empirically. If we denote by $\hat{\alpha}_{\mathrm{E}}(\hat{\boldsymbol{c}})$ its equivalent in terms of the dimensionless molecular velocity $\hat{\boldsymbol{c}}$, then

$$\hat{\alpha}_{\mathrm{E}}(\hat{\boldsymbol{c}}) = \exp(-|\hat{\boldsymbol{c}}|^2/2\upsilon_1) + B[1 - \exp(-|\hat{\boldsymbol{c}}|^2/2\upsilon_2)]. \tag{71}$$

The $\alpha_{\mathrm{E}}(\boldsymbol{c})$ was introduced as the probability that the incident velocity $\boldsymbol{c}$ and the reflected velocity of an incident molecule are uncorrelated, and the form of Eq. (65) [with $\alpha(c_z^2) \to \alpha_{\mathrm{E}}(\boldsymbol{c})$] was deduced with the help of the conditions (i), (ii), and (iii) in Sec. V B. The form of Eq. (70) is assumed heuristically. Therefore, the origin and background of the Epstein model are quite different from those of Eqs. (65) and (66) though the form (65) is common to both models.

Nevertheless, we compare the behavior of our $\alpha(c_z^2)$ and $\alpha_{\mathrm{E}}(\boldsymbol{c})$ of the Epstein model numerically. We consider their equivalents $\hat{\alpha}(\hat{c}_z^2)$ [Eq. (60)] and $\hat{\alpha}_{\mathrm{E}}(\hat{\boldsymbol{c}})$ [Eq. (71)] in terms of the dimensionless variables for convenience. Figure 3(a) shows $\hat{\alpha}(\hat{c}_z^2)$ versus $\hat{c}_z$ in the case where the potential $\hat{\mathrm{w}}$ and the relaxation time $\hat{\tau}_{\mathrm{ph}}$ are, respectively, assumed to be the Lennard-Jones (9, 3) potential appearing later in Eq. (88) and the algebraic-type relaxation time appearing later in Eq. (91). The parameters in Eqs. (88) and (91) are chosen as $\kappa = 1$, $n = 4$, $(\kappa_\tau, \sigma) = (1, 0.5)$, $(1, 1)$, $(1, 2)$, $(0.5, 1)$, and $(2, 1)$. Figure 3(b) shows $\hat{\alpha}_{\mathrm{E}}(\hat{\boldsymbol{c}})$ versus $\hat{c}_z$ for $(\upsilon_1, \upsilon_2, B) = (6, 6, 0.2)$, $(12, 3, 0.2)$, and $(3, 12, 0.2)$ at $\hat{c}_x = \hat{c}_y = 0$ and for $(6, 6, 0.2)$ at $\hat{c}_x = \hat{c}_y = 1$. Although the direct comparison between Figs. 3(a) and 3(b) does not make sense, one can see the overall tendency of the functions $\hat{\alpha}(\hat{c}_z^2)$ and $\hat{\alpha}_{\mathrm{E}}(\hat{\boldsymbol{c}})$.

The Cercignani-Lampis model, which has widely been used in numerical simulation of rarefied gas flows in recent years, is a mathematical model constructed heuristically in such a way that the probability density $\mathcal{R}(\boldsymbol{c}, \boldsymbol{c}_*)$ satisfies the conditions (i)–(iii) in Sec. V B. Since its explicit form is shown in [1,4], it is omitted here. One of the advantages of this model is that it can reproduce the leaflike (or plumelike) velocity distribution of the reflected molecules observed experimentally when a molecular beam is incident on the surface.

The models of the form (65), including our model and Epstein's model, are not able to describe the leaflike distribution because the velocity distribution of the reflected molecules is a superposition of the reflected beam and an isotropic distribution when a molecular beam is injected on the surface. However, this drawback of our model is not important. It is constructed for the purpose of application in general rarefied gas flows, and special situations such as molecular-beam injection are beyond the aim of the model. Although the Cercignani-Lampis model was originally proposed as a purely mathematical model, the dynamics underlying the model has been investigated recently in [19].

VI. BOUNDARY CONDITION FOR THE BOLTZMANN EQUATION: NUMERICAL APPROACH

In this section, we analyze the inner layer problem formulated in Secs. IV A and IV B numerically to obtain numerical information on the boundary condition (41) for the Boltzmann equation. Then, we compare the results with those obtained by the approximate formula (65) constructed in Sec. V B.

A. Preliminaries

Let us define the marginal distribution functions $\phi_\pm$ of $\mathsf{f}_\pm$ by

$$\phi_\pm(\hat{t}, \hat{\boldsymbol{x}}_\parallel, \zeta, \varepsilon) = \iint_{-\infty}^{\infty} \mathsf{f}_\pm(\hat{t}, \hat{\boldsymbol{x}}_\parallel, \zeta, \hat{\boldsymbol{c}}_\parallel, \varepsilon) d\hat{c}_x d\hat{c}_y, \tag{72}$$

where all the arguments are shown for clarity. By integrating Eq. (45a) with respect to $\hat{c}_x$ and $\hat{c}_y$ over $\mathbb{R}^2$, we obtain the

following equations for $\phi_\pm$:

$$\pm\sqrt{2}\sqrt{\varepsilon-\hat{\mathrm{w}}(\zeta)}\,\frac{\partial\phi_\pm}{\partial\zeta}=-\frac{1}{\hat{\tau}_{\mathrm{ph}}(\zeta)}[\phi_\pm-\hat{\mathsf{n}}\hat{\mathrm{M}}_{\mathrm{m}}(\zeta,\,\varepsilon)], \tag{73a}$$

$$\hat{\mathrm{M}}_{\mathrm{m}}(\zeta,\,\varepsilon)=(2\pi)^{-1/2}\exp(-\varepsilon+\hat{\mathrm{w}}(\zeta)), \tag{73b}$$

$$\hat{\mathsf{n}}=\frac{1}{\sqrt{2}}\int_{\hat{\mathrm{w}}(\zeta)}^{\infty}(\phi_-+\phi_+)\frac{1}{\sqrt{\varepsilon-\hat{\mathrm{w}}(\zeta)}}d\varepsilon. \tag{73c}$$

The boundary conditions for Eq. (73) are obtained from Eqs. (46) and (47) by the same procedure, that is,

$$\phi_-\to\phi_\infty(-\sqrt{2\varepsilon}),\ \text{as}\ \ \zeta\to\infty,\ \text{for}\ \ \varepsilon>0, \tag{74a}$$

$$\phi_+(\zeta_a(\varepsilon),\,\varepsilon)=\phi_-(\zeta_a(\varepsilon),\,\varepsilon),\ \ \text{for}\ \ \varepsilon>\hat{\mathrm{w}}_{\mathrm{min}}, \tag{74b}$$

$$\phi_-(\zeta_b(\varepsilon),\,\varepsilon)=\phi_+(\zeta_b(\varepsilon),\,\varepsilon),\ \ \text{for}\ \ \hat{\mathrm{w}}_{\mathrm{min}}<\varepsilon<0, \tag{74c}$$

where $\phi_\infty(-\sqrt{2\varepsilon})=\iint_{-\infty}^{\infty}\mathsf{f}_\infty(-\sqrt{2\varepsilon})d\hat{c}_x d\hat{c}_y$. Corresponding to Eq. (48), we have

$$\int_{\hat{\mathrm{w}}(\zeta)}^{\infty}(\phi_+-\phi_-)d\varepsilon=0. \tag{75}$$

Once the solution $\phi_\pm$ is obtained from Eqs. (73) and (74), the number density $\hat{\mathsf{n}}$ is known. Therefore, Eq. (45a) reduces to an ODE, which can be solved immediately for any $\hat{t}$, $\hat{\boldsymbol{x}}_\parallel$, and $\hat{\boldsymbol{c}}_\parallel$ under the boundary conditions (46) and (47). In this way, the full distributions $\mathsf{f}_\pm$ can be reconstructed from the marginals $\phi_\pm$.

Next, we try to reduce the half-space problem, Eqs. (73) and (74), to a problem in a finite range. For this purpose, we choose ζ in the admissible range (43) for each ε and define η by

$$\eta=\int_{\zeta_a(\varepsilon)}^{\zeta}\frac{1}{\hat{\tau}_{\mathrm{ph}}(s)}ds \tag{76}$$

assuming that the integral is finite as $\zeta\to\infty$ for $\varepsilon>0$. Since the correspondence between η and ζ is one to one for each ε, Eq. (76) determines $\eta=\eta(\zeta,\,\varepsilon)$ and its inverse $\zeta=\zeta(\eta,\,\varepsilon)$ uniquely. The range of η is $\eta\in[0,\,\eta_b(\varepsilon)]$, and $\eta_b(\varepsilon)$ is given by

$$\eta_b(\varepsilon)=\begin{cases}\displaystyle\int_{\zeta_a(\varepsilon)}^{\infty}\frac{1}{\hat{\tau}_{\mathrm{ph}}(s)}ds & (\varepsilon\geqslant 0),\\ \displaystyle\int_{\zeta_a(\varepsilon)}^{\zeta_b(\varepsilon)}\frac{1}{\hat{\tau}_{\mathrm{ph}}(s)}ds & (\hat{\mathrm{w}}_{\mathrm{min}}\leqslant\varepsilon<0).\end{cases} \tag{77}$$

Now, using Eq. (76), we change the independent variables from $(\zeta,\,\varepsilon)$ to $(\eta,\,\varepsilon)$ and define

$$\widetilde{\phi}_\pm(\eta,\,\varepsilon)=\phi_\pm(\zeta(\eta,\,\varepsilon),\,\varepsilon). \tag{78}$$

Then, Eq. (73) is transformed to

$$\pm\sqrt{2}\sqrt{\varepsilon-\widetilde{\mathrm{w}}(\eta,\,\varepsilon)}\,\frac{\partial\widetilde{\phi}_\pm}{\partial\eta}=-[\widetilde{\phi}_\pm-\widetilde{\mathsf{n}}(\eta,\,\varepsilon)\widetilde{\mathrm{M}}_{\mathrm{m}}(\eta,\,\varepsilon)], \tag{79a}$$

$$\widetilde{\mathrm{w}}(\eta,\,\varepsilon)=\hat{\mathrm{w}}(\zeta(\eta,\,\varepsilon)), \tag{79b}$$

$$\widetilde{\mathrm{M}}_{\mathrm{m}}(\eta,\,\varepsilon)=\hat{\mathrm{M}}_{\mathrm{m}}(\zeta(\eta,\,\varepsilon),\,\varepsilon)=(2\pi)^{-1/2}\exp(-\varepsilon+\widetilde{\mathrm{w}}(\eta,\,\varepsilon)), \tag{79c}$$

$$\widetilde{\mathsf{n}}(\eta,\,\varepsilon)=\hat{\mathsf{n}}(\zeta(\eta,\,\varepsilon))=\frac{1}{\sqrt{2}}\int_{\widetilde{\mathrm{w}}(\eta,\,\varepsilon)}^{\infty}[\phi_-(\zeta(\eta,\,\varepsilon),\,\mathcal{E})+\phi_+(\zeta(\eta,\,\varepsilon),\,\mathcal{E})]\frac{1}{\sqrt{\mathcal{E}-\widetilde{\mathrm{w}}(\eta,\,\varepsilon)}}d\mathcal{E}, \tag{79d}$$

and the boundary condition (74) becomes

$$\widetilde{\phi}_+(0,\,\varepsilon)=\widetilde{\phi}_-(0,\,\varepsilon),\quad \widetilde{\phi}_-(\eta_b(\varepsilon),\,\varepsilon)=\phi_\infty(-\sqrt{2\varepsilon}),\quad \text{for}\ \ \varepsilon>0, \tag{80a}$$

$$\widetilde{\phi}_+(0,\,\varepsilon)=\widetilde{\phi}_-(0,\,\varepsilon),\quad \widetilde{\phi}_-(\eta_b(\varepsilon),\,\varepsilon)=\widetilde{\phi}_+(\eta_b(\varepsilon),\,\varepsilon),\quad \text{for}\ \ \hat{\mathrm{w}}_{\mathrm{min}}<\varepsilon<0, \tag{80b}$$

because $\zeta(0,\,\varepsilon)=\zeta_a(\varepsilon)$ for $\varepsilon>\hat{\mathrm{w}}_{\mathrm{min}}$, $\zeta(\eta_b(\varepsilon),\,\varepsilon)=\infty$ for $\varepsilon>0$, and $\zeta(\eta_b(\varepsilon),\,\varepsilon)=\zeta_b(\varepsilon)$ for $\hat{\mathrm{w}}_{\mathrm{min}}<\varepsilon<0$. In this way, the problem has seemingly been reduced to that in the finite domain $0\leqslant\eta\leqslant\eta_b(\varepsilon)$. However, since the integration of $\phi_\pm$ in Eq. (79d) is only with respect to the second argument $\mathcal{E}$, the integrands $\phi_\pm$ cannot be expressed in terms of $\widetilde{\phi}_\pm$. Therefore, precisely speaking, Eqs. (79) and (80) do not form a closed system for $\widetilde{\phi}_\pm$. Nevertheless, they are useful for numerical analysis because we can handle the finite range $0\leqslant\eta\leqslant\eta_b(\varepsilon)$.

If we integrate Eq. (50) with respect to $\hat{c}_x$ and $\hat{c}_y$ over $\mathbb{R}^2$ and make use of ϕ_+ and $\phi_\infty(-\sqrt{2\varepsilon})$, we obtain the following expression for $\varepsilon>0$:

$$\phi_+(\infty,\,\varepsilon)=[\theta(\zeta_a(\varepsilon),\,\infty;\,\varepsilon)]^2\phi_\infty(-\sqrt{2\varepsilon})+\frac{\theta(\zeta_a(\varepsilon),\,\infty;\,\varepsilon)}{\sqrt{2}}\times\int_{\zeta_a(\varepsilon)}^{\infty}[\theta(\zeta_a(\varepsilon),\,s;\,\varepsilon)+\theta(s,\,\zeta_a(\varepsilon);\,\varepsilon)]\times\frac{\hat{\mathsf{n}}(s)\hat{\mathrm{M}}_{\mathrm{m}}(s,\,\varepsilon)}{\hat{\tau}_{\mathrm{ph}}(s)\sqrt{\varepsilon-\hat{\mathrm{w}}(s)}}ds, \tag{81}$$

where $\phi_+(\infty,\,\varepsilon)$ indicates $\phi_+(\hat{t},\,\hat{\boldsymbol{x}}_\parallel,\,\infty,\,\varepsilon)$. Then, Eq. (50) is recast as

$$\mathsf{f}_+(\infty,\,\varepsilon)=[\theta(\zeta_a(\varepsilon),\,\infty;\,\varepsilon)]^2\mathsf{f}_\infty(-\sqrt{2\varepsilon})+\{\phi_+(\infty,\,\varepsilon)-[\theta(\zeta_a(\varepsilon),\,\infty;\,\varepsilon)]^2\phi_\infty(-\sqrt{2\varepsilon})\}\times(2\pi)^{-1}\exp(-|\hat{\boldsymbol{c}}_\parallel|^2/2), \tag{82}$$

where $\varepsilon>0$. For given $\mathsf{f}_\infty(-\sqrt{2\varepsilon})$ [and thus $\phi_\infty(-\sqrt{2\varepsilon})$], $\mathsf{f}_+(\infty,\,\varepsilon)$ can be established immediately once $\phi_+(\infty,\,\varepsilon)$ is obtained by solving Eqs. (73) and (74). If the independent variables are changed back from $(\zeta,\,\varepsilon)$ to $(\zeta,\,\hat{c}_z)$, Eq. (82)

is transformed to the following form:

$$\begin{aligned}\mathsf{f}(\infty,\hat{c}_z) &= \left[1-\hat{\alpha}\left(\hat{c}_z^2\right)\right]\mathsf{f}(\infty,\,-\hat{c}_z)\\ &\quad+\left\{\phi_+(\infty,\hat{c}_z^2/2)-\left[1-\hat{\alpha}\left(\hat{c}_z^2\right)\right]\phi_\infty(-\hat{c}_z)\right\}\\ &\quad\times(2\pi)^{-1}\exp(-|\hat{\boldsymbol{c}}_\parallel|^2/2),\ \ (\hat{c}_z>0),\end{aligned}\tag{83}$$

where $\hat{\alpha}(\hat{c}_z^2)$ is defined by Eq. (60), and $\mathsf{f}_\infty(-\hat{c}_z)$ has been replaced with the equivalent $\mathsf{f}(\infty,\,-\hat{c}_z)$ [see Eq. (39)]. Recall that in Eqs. (82) and (83) the arguments $\hat{t}$, $\hat{\boldsymbol{x}}_\parallel$, and $\hat{\boldsymbol{c}}_\parallel$ are omitted in f_+, f, and f_∞, and $\hat{t}$ and $\hat{\boldsymbol{x}}_\parallel$ are omitted in ϕ_+ and ϕ_∞.

B. Interaction potential and phonon relaxation time

For the numerical analysis of Eqs. (79) and (80), the interaction potential w and the phonon relaxation time τ_{ph} should be specified explicitly.

1. Interaction potential

We consider two different Lennard-Jones potentials, to be more specific, the standard (12, 6) potential and the (9, 3) potential. The latter may be more realistic as a potential of interaction between a gas molecule and a solid surface [37–39].

(a) For the Lennard-Jones (12, 6) potential, the potential $\mathrm{w}(z)$ is defined by

$$\mathrm{w}(z)=4\bar{\kappa}\left[\left(\frac{\delta}{z}\right)^{12}-\left(\frac{\delta}{z}\right)^{6}\right],\tag{84}$$

where $\bar{\kappa}$ (>0) is a parameter, and the characteristic range δ of the interaction potential is chosen in such a way that $\mathrm{w}(z)$ vanishes at $z=\delta$. If we let $\kappa=\bar{\kappa}/k_{\mathrm{B}}T_{\mathrm{w}}$, the dimensionless potential $\hat{\mathrm{w}}(\zeta)$ is expressed as

$$\hat{\mathrm{w}}(\zeta)=4\kappa\left(\frac{1}{\zeta^{12}}-\frac{1}{\zeta^{6}}\right),\tag{85}$$

where we should recall $\zeta=z/\delta=\hat{z}/\epsilon$. Thus, $\hat{\mathrm{w}}(1)=0$, and $\hat{\mathrm{w}}(\zeta)$ takes the minimum $-\kappa$ at $\zeta=\zeta_{\min}=2^{1/6}$, i.e., $\hat{\mathrm{w}}(\zeta_{\min})=-\kappa$ $(\equiv\hat{\mathrm{w}}_{\min})$. The solutions $\zeta_a(\varepsilon)$ and $\zeta_b(\varepsilon)$ of $\varepsilon=\hat{\mathrm{w}}(\zeta)$ (see Sec. IV B) are given by

$$\zeta_a(\varepsilon)=\left[\frac{2\kappa}{\varepsilon}\left(\sqrt{1+\frac{\varepsilon}{\kappa}}-1\right)\right]^{1/6}\quad(\varepsilon\geqslant-\kappa),\tag{86a}$$

$$\zeta_b(\varepsilon)=\left[\frac{2\kappa}{-\varepsilon}\left(\sqrt{1+\frac{\varepsilon}{\kappa}}+1\right)\right]^{1/6}\quad(-\kappa\leqslant\varepsilon<0).\tag{86b}$$

Note that $\zeta_a(\varepsilon)=1$ for $\varepsilon=0$.

(b) For the Lennard-Jones (9, 3) potential, let us define the potential $\mathrm{w}(z)$ by

$$\mathrm{w}(z)=\frac{3\sqrt{3}}{2}\bar{\kappa}\left[\left(\frac{\delta}{z}\right)^{9}-\left(\frac{\delta}{z}\right)^{3}\right].\tag{87}$$

The meanings of $\bar{\kappa}$ and δ are the same as Eq. (84). Then, with $\kappa=\bar{\kappa}/k_{\mathrm{B}}T_{\mathrm{w}}$, the dimensionless potential $\hat{\mathrm{w}}(\zeta)$ is given by

$$\hat{\mathrm{w}}(\zeta)=\frac{3\sqrt{3}}{2}\kappa\left(\frac{1}{\zeta^{9}}-\frac{1}{\zeta^{3}}\right).\tag{88}$$

Thus, $\hat{\mathrm{w}}(1)=0$, and $\hat{\mathrm{w}}(\zeta)$ takes the minimum $-\kappa$ at $\zeta=\zeta_{\min}=3^{1/6}$, i.e., $\hat{\mathrm{w}}(\zeta_{\min})=-\kappa$ $(\equiv\hat{\mathrm{w}}_{\min})$. The solutions $\zeta_a(\varepsilon)$ and $\zeta_b(\varepsilon)$ of $\varepsilon=\hat{\mathrm{w}}(\zeta)$ (see Sec. IV B) are obtained, after some algebra, as follows:

$$\zeta_a(\varepsilon)=\begin{cases}\left[\frac{\sqrt{3}\kappa}{2\varepsilon}(-1+u+u^{-1})\right]^{1/3} & (\varepsilon\geqslant\kappa),\\ \left[\frac{\sqrt{3}\kappa}{2\varepsilon}\left(-1+2\cos\frac{\vartheta}{3}\right)\right]^{1/3} & (0<\varepsilon<\kappa),\\ 1\ (\varepsilon=0),\\ \left\{\frac{\sqrt{3}\kappa}{2|\varepsilon|}\left[1+2\cos\left(\frac{\vartheta}{3}+\frac{\pi}{3}\right)\right]\right\}^{1/3} & (-\kappa\leqslant\varepsilon<0),\end{cases}\tag{89a}$$

$$\zeta_b(\varepsilon)=\left\{\frac{\sqrt{3}\kappa}{2|\varepsilon|}\left[1+2\cos\left(\frac{\vartheta}{3}-\frac{\pi}{3}\right)\right]\right\}^{1/3}\quad(-\kappa\leqslant\varepsilon<0),\tag{89b}$$

where, with $a=\varepsilon/\kappa$ $(\geqslant-1)$, u and ϑ are defined by

$$u=\left(2a^2-1+2a\sqrt{a^2-1}\right)^{1/3}\quad\text{for}\ \ a\geqslant1\ \ (\text{or}\ \ \varepsilon\geqslant\kappa),$$

$$\vartheta=\arccos\left(2a^2-1\right)\quad(0\leqslant\vartheta\leqslant\pi)$$

$$\text{for}\quad-1\leqslant a<1\quad(\text{or}\quad-\kappa\leqslant\varepsilon<\kappa).$$

The Lennard-Jones (9, 3) potential (88) with $\kappa=1$, 5, and 10 is shown in Fig. 4(a), the (12, 6) potential (85) with $\kappa=5$ is shown in Fig. 4(b) together with the (9, 3) potential with $\kappa=5$ for comparison, and the characteristic lines $\hat{c}_z^2/2+\hat{\mathrm{w}}(\zeta)=\varepsilon$ with $\varepsilon=-0.99,\,-0.9,\,-0.8,\ldots,-0.1,\,0,\,0.1,\ldots,0.9,$ and 1 are shown for the (9, 3) potential (88) with $\kappa=1$ in Fig. 4(c).

2. Phonon relaxation time

For the phonon relaxation time $\tau_{\mathrm{ph}}(z)$, we consider two different types: one is an algebraic function of z that increases slowly as $z\to\infty$, and the other is an exponential function that increases rapidly as $z\to\infty$.

(a) For the algebraic type, we define the relaxation time $\tau_{\mathrm{ph}}(z)$ by

$$\tau_{\mathrm{ph}}(z)=\bar{\kappa}_\tau\left(1+\sigma\frac{z}{n\delta}\right)^{n},\tag{90}$$

where σ (>0), $\bar{\kappa}_\tau$ (>0), and n (>1) are constants. With $\kappa_\tau=\bar{\kappa}_\tau/\tau_{\mathrm{ph}}^\star$, its dimensionless counterpart $\hat{\tau}_{\mathrm{ph}}$ is given by

$$\hat{\tau}_{\mathrm{ph}}(\zeta)=\kappa_\tau\left(1+\frac{\sigma}{n}\zeta\right)^{n}.\tag{91}$$

Then, $\eta(\zeta,\,\varepsilon)$, determined by Eq. (76), is obtained as

$$\begin{aligned}\eta(\zeta,\,\varepsilon)=\frac{n}{(n-1)\kappa_\tau\sigma}\Bigg[&\left(1+\frac{\sigma}{n}\zeta_a(\varepsilon)\right)^{-(n-1)}\\ &-\left(1+\frac{\sigma}{n}\zeta\right)^{-(n-1)}\Bigg].\end{aligned}\tag{92}$$

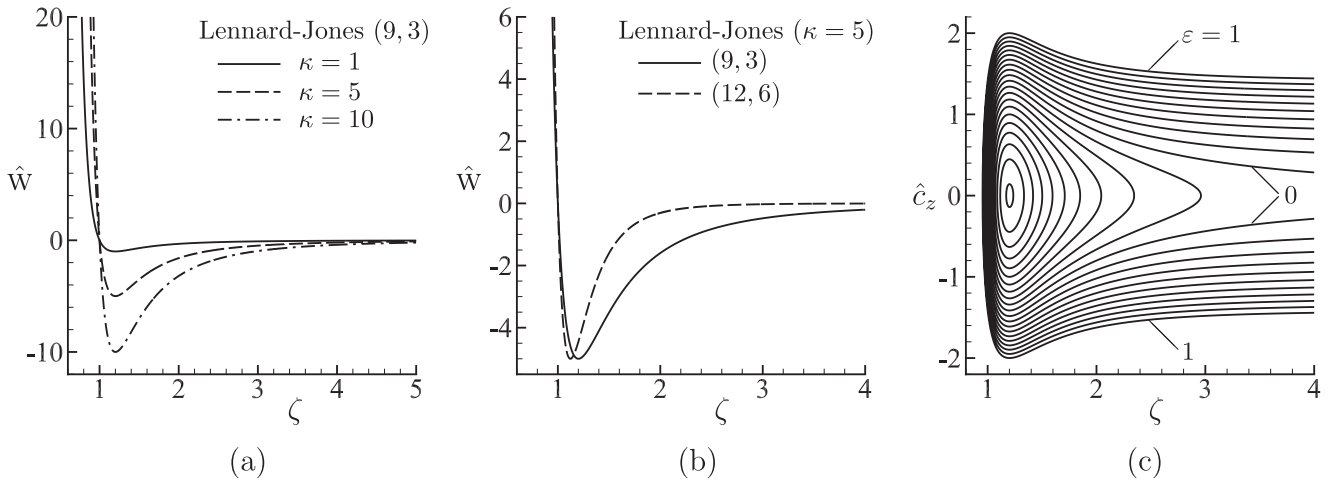

FIG. 4. Lennard-Jones potentials: (a) the (9, 3) potential with $\kappa = 1$, 5, and 10; (b) the (12, 6) and (9, 3) potentials with $\kappa = 5$; and (c) characteristic lines $(1/2)\hat{c}_z^2 + \hat{\mathrm{W}}(\zeta) = \varepsilon$ with $\varepsilon = -0.99, -0.9, -0.8, \ldots, -0.1, 0, 0.1, \ldots, 0.9$, and 1 for the (9, 3) potential with $\kappa = 1$.

Therefore, the end point $\eta_b(\varepsilon)$ defined by Eq. (77) and the inverse function $\zeta(\eta,\ \varepsilon)$ of Eq. (92) are, respectively, obtained as follows:

$$\eta_b(\varepsilon) = \begin{cases} \dfrac{n}{(n-1)\kappa_\tau\sigma}\Big(1+\dfrac{\sigma}{n}\zeta_a(\varepsilon)\Big)^{-(n-1)} & (\varepsilon \geqslant 0), \\ \dfrac{n}{(n-1)\kappa_\tau\sigma}\Big[\Big(1+\dfrac{\sigma}{n}\zeta_a(\varepsilon)\Big)^{-(n-1)} - \Big(1+\dfrac{\sigma}{n}\zeta_b(\varepsilon)\Big)^{-(n-1)}\Big] & (-\kappa \leqslant \varepsilon < 0), \end{cases} \tag{93a}$$

$$\zeta(\eta,\ \varepsilon) = \frac{n}{\sigma}\left[\Big(1+\frac{\sigma}{n}\zeta_a(\varepsilon)\Big)^{-(n-1)} - \frac{(n-1)\kappa_\tau\sigma}{n}\eta\right]^{-1/(n-1)} - \frac{n}{\sigma}. \tag{93b}$$

In particular, for $\varepsilon \geqslant 0$, Eq. (93b) can be expressed as

$$\zeta(\eta,\ \varepsilon) = \frac{n}{\sigma}\left[\frac{n-1}{n}\kappa_\tau\sigma\big(\eta_b(\varepsilon) - \eta\big)\right]^{-1/(n-1)} - \frac{n}{\sigma}. \tag{94}$$

(b) For the exponential type, let us define $\tau_{\mathrm{ph}}(z)$ by

$$\tau_{\mathrm{ph}}(z) = \bar{\kappa}_\tau \exp(\sigma z/\delta), \tag{95}$$

where σ (> 0) and $\bar{\kappa}_\tau$ (> 0) are constants. With $\kappa_\tau = \bar{\kappa}_\tau/\tau^\star_{\mathrm{ph}}$, its dimensionless form is given by

$$\hat{\tau}_{\mathrm{ph}}(\zeta) = \kappa_\tau \exp(\sigma\zeta). \tag{96}$$

Then, Eq. (76) gives

$$\eta(\zeta,\ \varepsilon) = \frac{1}{\kappa_\tau\sigma}[\exp(-\sigma\zeta_a(\varepsilon)) - \exp(-\sigma\zeta)]. \tag{97}$$

Therefore, we obtain the following $\eta_b(\varepsilon)$ and the inverse function $\zeta(\eta,\ \varepsilon)$:

$$\eta_b(\varepsilon) = \begin{cases} \dfrac{1}{\kappa_\tau\sigma}\exp(-\sigma\zeta_a(\varepsilon)) & (\varepsilon \geqslant 0), \\ \dfrac{1}{\kappa_\tau\sigma}[\exp(-\sigma\zeta_a(\varepsilon)) - \exp(-\sigma\zeta_b(\varepsilon))] & (-\kappa \leqslant \varepsilon < 0), \end{cases} \tag{98a}$$

$$\zeta(\eta,\ \varepsilon) = -\tfrac{1}{\sigma}\ln(\exp(-\sigma\zeta_a(\varepsilon)) - \kappa_\tau\sigma\eta). \tag{98b}$$

For $\varepsilon \geqslant 0$, Eq. (98b) can be expressed as

$$\zeta(\eta,\ \varepsilon) = -\frac{1}{\sigma}\ln(\kappa_\tau\sigma(\eta_b(\varepsilon) - \eta)). \tag{99}$$

C. Numerical results

1. Velocity distribution for reflected molecules

In Sec. VI C 1, we show some numerical results of the velocity distribution $\mathsf{f}(\infty, \hat{c}_z)$ for $\hat{c}_z > 0$ (the output distribution), in response to $\mathsf{f}(\infty, \hat{c}_z)$ for $\hat{c}_z < 0$ (the input distribution), obtained by Eq. (40) with the albedo operator Λ constructed by the numerical solution $\phi_\pm$ to Eqs. (73) and (74). We also compare the numerical results with the results obtained by the approximate formula (59). The outline of the numerical procedure is given in Appendix C.

In order to give a clear representation, we will concentrate on the molecular velocity components $\hat{c}_x$ and $\hat{c}_z$. For this purpose, we consider the following marginal h_∞:

$$\mathsf{h}_\infty(\hat{t}, \hat{\boldsymbol{x}}_\parallel, \hat{c}_x, \hat{c}_z) = \int_{-\infty}^{\infty} \mathsf{f}(\hat{t}, \hat{\boldsymbol{x}}_\parallel, \infty, \hat{\boldsymbol{c}}_\parallel, \hat{c}_z) d\hat{c}_y. \tag{100}$$

In the following, the arguments $\hat{t}$ and $\hat{\boldsymbol{x}}_\parallel$ will be omitted as in the preceding sections.

Integration of Eq. (83) with respect to $\hat{c}_y$ from $-\infty$ to ∞ gives

$$\begin{aligned}\mathsf{h}_\infty(\hat{c}_x, \hat{c}_z) = {} & \big[1 - \hat{\alpha}\big(\hat{c}_z^2\big)\big]\, \mathsf{h}_\infty(\hat{c}_x, -\hat{c}_z) \\ & + \big\{\phi_+\big(\infty, \hat{c}_z^2/2\big) - \big[1 - \hat{\alpha}\big(\hat{c}_z^2\big)\big]\, \phi_\infty(-\hat{c}_z)\big\} \\ & \times (2\pi)^{-1/2} \exp\big(-\hat{c}_x^2/2\big), \quad (\hat{c}_z > 0). \end{aligned} \tag{101}$$

Similarly, the approximate formula (59), based on the first iteration, leads to the following expression:

$$\begin{aligned}\mathsf{h}_\infty(\hat{c}_x, \hat{c}_z) = {} & [1 - \hat{\alpha}(\hat{c}_z^2)]\, \mathsf{h}_\infty(\hat{c}_x, -\hat{c}_z) + \hat{\alpha}(\hat{c}_z^2)\, \frac{\hat{\beta}}{2\pi} \\ & \times \exp\left(-\frac{\hat{c}_x^2 + \hat{c}_z^2}{2}\right), \quad \text{for} \quad \hat{c}_z > 0, \end{aligned} \tag{102}$$

where

$$\begin{aligned}\hat{\beta} = {} & -\sqrt{2\pi}\left[\int_0^\infty \hat{c}_z \hat{\alpha}(\hat{c}_z^2) \exp\big(-\hat{c}_z^2/2\big) d\hat{c}_z\right]^{-1} \\ & \times \int_{\hat{c}_z < 0} \hat{c}_z \hat{\alpha}(\hat{c}_z^2) \mathsf{h}_\infty(\hat{c}_x, \hat{c}_z) d\hat{c}_x d\hat{c}_z. \end{aligned} \tag{103}$$

In the following computation, we assume the marginal Maxwellian of the form

$$\mathsf{h}_\infty(\hat{c}_x, \hat{c}_z) = \frac{1}{2\pi \hat{T}_\infty} \exp\left(-\frac{(\hat{c}_x - \hat{v}_{x\infty})^2 + (\hat{c}_z - \hat{v}_{z\infty})^2}{2\hat{T}_\infty}\right), \quad (\hat{c}_z < 0), \tag{104}$$

for the molecules incident from infinity, where $\hat{v}_{x\infty}$, $\hat{v}_{z\infty}$, and $\hat{T}_\infty$ are the parameters to be specified. Correspondingly, we have

$$\phi_\infty(\hat{c}_z) = \frac{1}{(2\pi \hat{T}_\infty)^{1/2}} \exp\left(-\frac{(\hat{c}_z - \hat{v}_{z\infty})^2}{2\hat{T}_\infty}\right), \quad (\hat{c}_z < 0). \tag{105}$$

In addition, the parameters κ, κ_τ, and σ contained in the potentials (85) and (88) and the phonon relaxation times (91) and (96) are set as

$$(\kappa, \kappa_\tau, \sigma) = (1, 1, 1). \tag{106}$$

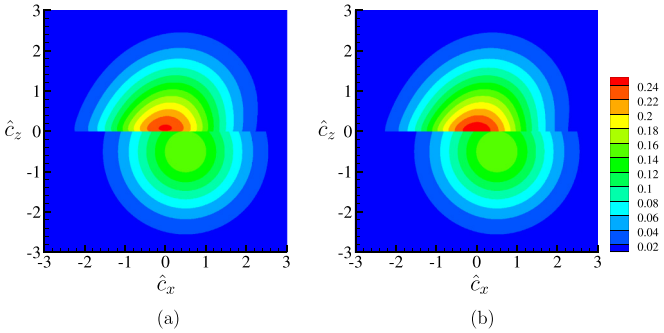

FIG. 5. Contour lines of $\mathsf{h}_\infty(\hat{c}_x, \hat{c}_z)$ for the Lennard-Jones (12, 6) potential (85) and the relaxation time of algebraic type (91) ($n = 7$) in the $(\hat{c}_x, \hat{c}_z)$ plane in the case of $(\hat{T}_\infty, \hat{v}_{z\infty}, \hat{v}_{x\infty}) = (1, -0.5, 0.5)$ and $(\kappa, \kappa_\tau, \sigma) = (1, 1, 1)$. (a) Numerical solution. (b) Approximate formula (102). The function $\mathsf{h}_\infty(\hat{c}_x, \hat{c}_z)$ with $\hat{c}_z < 0$ indicates the input, i.e., Eq. (104), and $\mathsf{h}_\infty(\hat{c}_x, \hat{c}_z)$ with $\hat{c}_z > 0$ indicates the output.

Figures 5–8 show the contour lines of the input h_∞ ($\hat{c}_z < 0$), i.e., Eq. (104), and the output h_∞ ($\hat{c}_z > 0$) in the $(\hat{c}_x, \hat{c}_z)$ plane for different potentials and phonon relaxation times in the case of $(\hat{T}_\infty, \hat{v}_{z\infty}, \hat{v}_{x\infty}) = (1, -0.5, 0.5)$. More specifically, Fig. 5 is for the LJ (12, 6) potential (85) and the relaxation time of algebraic type (91) ($n = 7$); Fig. 6 is for the LJ (12, 6) potential and the relaxation time of exponential type (96); Fig. 7 is for the LJ (9, 3) potential (88) and the relaxation time of algebraic type (91) ($n = 4$); and Fig. 8 is for the LJ (9, 3) potential and the relaxation time of exponential type (96). In each figure, panel (a) indicates the result based on the numerical solution, i.e., Eq. (101), and panel (b) indicates that based on the approximate formula (102). The lower half ($\hat{c}_z < 0$) of each figure, which indicates the input, is common.

Figures 9–12 show the profiles of $\mathsf{h}_\infty(\hat{c}_x, \hat{c}_z)$ at $\hat{c}_z = \text{const}$ and at $\hat{c}_x = \text{const}$ in the case of Figs. 5–8, respectively. In each figure, panel (a) shows the profiles at $\hat{c}_z = 0\pm$, ± 0.520, ± 0.972, ± 1.510, and ± 2.132; panel (b) shows those at

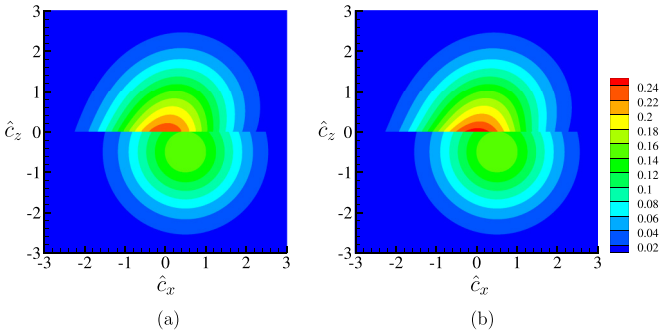

FIG. 6. Contour lines of $\mathsf{h}_\infty(\hat{c}_x, \hat{c}_z)$ for the Lennard-Jones (12, 6) potential (85) and the relaxation time of exponential type (96) in the $(\hat{c}_x, \hat{c}_z)$ plane in the case of $(\hat{T}_\infty, \hat{v}_{z\infty}, \hat{v}_{x\infty}) = (1, -0.5, 0.5)$ and $(\kappa, \kappa_\tau, \sigma) = (1, 1, 1)$. (a) Numerical solution. (b) Approximate formula (102). See the caption of Fig. 5.

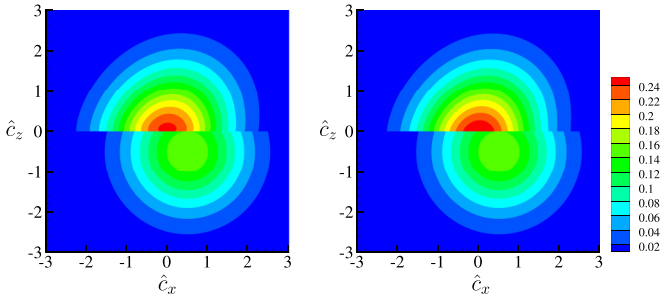

FIG. 7. Contour lines of $\mathsf{h}_\infty(\hat{c}_x,\ \hat{c}_z)$ for the Lennard-Jones (9, 3) potential (88) and the relaxation time of algebraic type (91) ($n = 4$) in the $(\hat{c}_x,\ \hat{c}_z)$ plane in the case of $(\hat{T}_\infty,\ \hat{v}_{z\infty},\ \hat{v}_{x\infty}) = (1,\ -0.5,\ 0.5)$ and $(\kappa,\ \kappa_\tau,\ \sigma) = (1,\ 1,\ 1)$. (a) Numerical solution. (b) Approximate formula (102). See the caption of Fig. 5.

$\hat{c}_x = 0$, 0.515, 1.008, 1.600, and 2.185; and panel (c) shows those at $\hat{c}_x = 0$, -0.515, -1.008, -1.600, and -2.185. In the figures, the green (light gray in grayscale) lines indicate the input distribution $\mathsf{h}_\infty(\hat{c}_x,\ \hat{c}_z)$ $(\hat{c}_z < 0)$, the (thick) red lines indicate the output distribution $\mathsf{h}_\infty(\hat{c}_x,\ \hat{c}_z)$ $(\hat{c}_z > 0)$ based on the numerical solution [see panels (a) in Figs. 5–8], and the (thin) black lines indicate that based on the approximate formula (102) [see panels (b) in Figs. 5–8]. The same types of lines are used for different positions; for example, the dashed line shows the profiles at $\hat{c}_z = \pm 0.520$ and ± 1.510 in panels (a) in Figs. 9–12; however, no confusion is expected.

It is seen from Figs. 5–12 that the approximate formula (102) is sufficiently accurate on the whole. It predicts slightly higher values for $|\hat{c}_x| \lesssim 1$ and $|\hat{c}_z| \lesssim 0.2$. The numerical solution [the (thick) red curves] in panels (b) and (c) in Figs. 9 and 11 (the relaxation time of algebraic type) exhibits a peak at small $\hat{c}_z$ (> 0), which is not reproduced by the approximate formula.

Since the input distribution h_∞ with $\hat{c}_z < 0$ is centered at $(\hat{c}_x,\ \hat{c}_z) = (0.5,\ -0.5)$, there are many high-speed molecules. The interaction of these molecules with the surface phonons slows them down and produces slow molecules. As the result, the output distribution h_∞ with $\hat{c}_z > 0$ contains many slow molecules, i.e., the molecules with small $|\hat{c}_x|$ and small $\hat{c}_z$ (> 0). This interaction takes place over a longer distance for the phonon relaxation time of algebraic type than for that of exponential type. Therefore, the curves of h_∞ with $\hat{c}_z > 0$ in Fig. 9 are slightly higher than those in Fig. 10 for slow molecules. The difference is more eminent between Figs. 11 and 12.

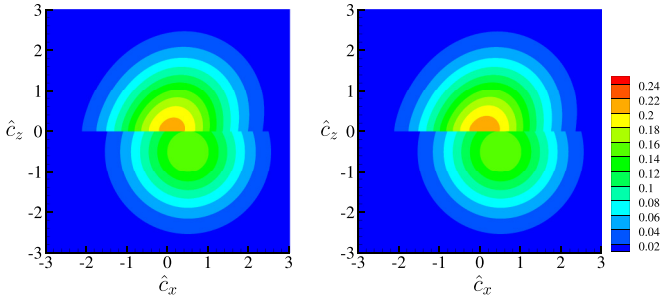

FIG. 8. Contour lines of $\mathsf{h}_\infty(\hat{c}_x,\ \hat{c}_z)$ for the Lennard-Jones (9, 3) potential (88) and the relaxation time of exponential type (96) in the $(\hat{c}_x,\ \hat{c}_z)$ plane in the case of $(\hat{T}_\infty,\ \hat{v}_{z\infty},\ \hat{v}_{x\infty}) = (1,\ -0.5,\ 0.5)$ and $(\kappa,\ \kappa_\tau,\ \sigma) = (1,\ 1,\ 1)$. (a) Numerical solution. (b) Approximate formula (102). See the caption of Fig. 5.

Restricting ourselves to the LJ (9, 3) potential (88) and the phonon relaxation time of algebraic type (91) ($n = 4$) [recall Eq. (106)], we will show some more results. In Figs. 13–15, we show the contour lines of the input h_∞ $(\hat{c}_z < 0)$ [Eq. (104)] and the output h_∞ $(\hat{c}_z > 0)$ in the $(\hat{c}_x,\ \hat{c}_z)$ plane: Fig. 13 is for $(\hat{T}_\infty,\ \hat{v}_{z\infty},\ \hat{v}_{x\infty}) = (1,\ 0.5,\ 0.5)$, Fig. 14 is for $(\hat{T}_\infty,\ \hat{v}_{z\infty},\ \hat{v}_{x\infty}) = (0.6,\ 0,\ 0.5)$, and Fig. 15 is for $(\hat{T}_\infty,\ \hat{v}_{z\infty},\ \hat{v}_{x\infty}) = (0.6,\ -0.5,\ 0.5)$. In each figure, panel (a) indicates the result based on the numerical solution, i.e., Eq. (101), and panel (b) indicates that based on the approximate formula (102).

Figures 16–18 show the profiles of $\mathsf{h}_\infty(\hat{c}_x,\ \hat{c}_z)$ at $\hat{c}_z =$ const and at $\hat{c}_x =$ const in the case of Figs. 13–15, respectively. In each figure, panel (a) shows the profiles at $\hat{c}_z = 0\pm$, ± 0.520, ± 0.972, ± 1.510, and ± 2.132; panel (b) shows those at $\hat{c}_x = 0$, 0.515, 1.008, 1.600, and 2.185; and panel (c) shows those at $\hat{c}_x = 0$, -0.515, -1.008, -1.600, and -2.185. As in Figs. 9–12, the green (light gray in grayscale) lines indicate the input distribution $\mathsf{h}_\infty(\hat{c}_x,\ \hat{c}_z)$ $(\hat{c}_z < 0)$, the (thick) red lines indicate the output distribution $\mathsf{h}_\infty(\hat{c}_x,\ \hat{c}_z)$ $(\hat{c}_z > 0)$ based on the numerical solution [see panels (a) in Figs. 13–15], and the (thin) black lines indicate that based on the approximate formula (102) [see panels (b) in Figs. 13–15]. Note that, as in Figs. 9–12, the same types of lines are used for different positions.

The input distribution in Figs. 15 and 18 is slightly narrower and centered at $(\hat{c}_x,\ \hat{c}_z) = (0.5,\ -0.5)$, so that it has a beamlike nature. However, the output distribution is more or less centered at $(\hat{c}_x,\ \hat{c}_z) = (0,\ 0)$ because the interaction with the phonons tends to equilibrate the molecules to the wall Maxwellian.

The approximate formula (102) gives sufficiently good results also in Figs. 13–18. Therefore, we may expect that the original three-dimensional version, Eq. (59), and its dimensional counterpart, Eq. (65), provide a reasonably good model as the boundary condition for the Boltzmann equation.

2. Density distribution in the adsorbate layer

So far, we have shown the velocity distribution for the reflected molecules skipping the details of the inner adsorbate layer. Leaving the behavior of the velocity distribution function in the layer to Sec. VII, we briefly show the behavior of the number density there. Figure 19 shows the dimensionless number density $\hat{\mathsf{n}}$ versus the scaled normal coordinate ζ $(= z/\delta)$ in the case of Figs. 7 and 13–15 obtained from the numerical solution $\phi_\pm$ to Eqs. (73) and (74). Note that $\hat{\mathsf{n}}$ is equal to $n/n^\star$ at the level of the zeroth approximation in ϵ. As ζ increases from zero to ∞, each curve increases from zero to the peak, then decreases, and finally approaches a constant. The high-density zone, which corresponds to the adsorbate layer, appears because of the trapped molecules in the potential wall.

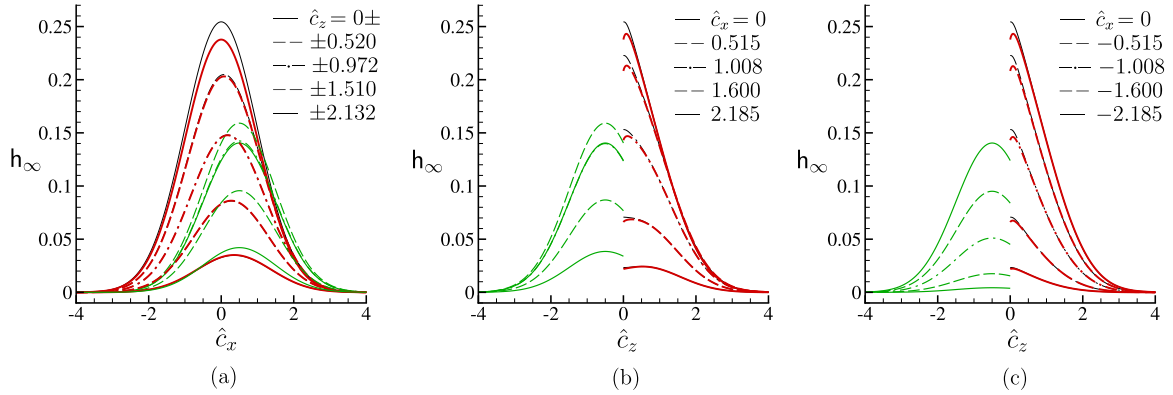

FIG. 9. Profiles of h_∞ ($\hat{c}_z < 0$ and $\hat{c}_z > 0$) at $\hat{c}_z = \text{const}$ and $\hat{c}_x = \text{const}$ in the case of Fig. 5: (a) profiles at $\hat{c}_z = \text{const}$, (b) those at $\hat{c}_x = \text{const} > 0$, and (c) those at $\hat{c}_x = \text{const} < 0$. The green (light gray in grayscale) lines indicate the input distribution h_∞ ($\hat{c}_z < 0$), the (thick) red lines indicate the output distribution h_∞ ($\hat{c}_z > 0$) based on the numerical solution, and the (thin) black lines indicate that based on the approximate formula (102).

VII. VELOCITY DISTRIBUTION FUNCTION INSIDE THE ADSORBATE LAYER

In the preceding section, we have solved numerically the inner layer problem, which has been reduced to Eq. (73), to establish the boundary condition (40) or (41) for the Boltzmann equation. Although the problem (73) is seemingly simple, it contains some nontrivial features that may attract mathematical interest. Therefore, we choose the case of Figs. 8 and 12 as an example and show the detailed behavior of the solution. To be more specific, we assume the Lennard-Jones (9, 3) potential (88) with $\kappa = 1$ and the phonon relaxation time of exponential type (96) with $\kappa_\tau = \sigma = 1$ and consider the input distribution (105) with $\hat{T}_\infty = 1$ and $\hat{v}_{z\infty} = -0.5$. The choice of Eq. (96) for the relaxation time *enhances* the singular nature of the problem (73).

In accordance with the figures in Sec. VI C, the result will be shown in terms of the molecular velocity $\hat{c}_z$ rather than the energy variable ε. Therefore, we introduce the following ϕ corresponding to $\phi_\pm$:

$$\phi(\hat{t},\, \hat{\boldsymbol{x}}_\parallel,\, \zeta,\, \hat{c}_z) = \iint_{-\infty}^{\infty} \mathsf{f}(\hat{t},\, \hat{\boldsymbol{x}}_\parallel,\, \zeta,\, \hat{\boldsymbol{c}}_\parallel,\, \hat{c}_z) d\hat{c}_x d\hat{c}_y. \quad (107)$$

In fact, ϕ is related to $\phi_\pm$ as

$$\phi(\hat{t},\, \hat{\boldsymbol{x}}_\parallel,\, \zeta,\, \hat{c}_z) = \begin{cases} \phi_-\big(\hat{t},\, \hat{\boldsymbol{x}}_\parallel,\, \zeta,\, \hat{c}_z^2/2 + \hat{\mathrm{w}}(\zeta)\big), & (\hat{c}_z < 0), \\ \phi_+\big(\hat{t},\, \hat{\boldsymbol{x}}_\parallel,\, \zeta,\, \hat{c}_z^2/2 + \hat{\mathrm{w}}(\zeta)\big), & (\hat{c}_z > 0). \end{cases} \quad (108)$$

Since the input distribution (105) with $\hat{T}_\infty = 1$ and $\hat{v}_{z\infty} = -0.5$ is independent of $\hat{t}$ and $\hat{\boldsymbol{x}}_\parallel$, ϕ is the function of ζ and $\hat{c}_z$ only.

In Fig. 20, the marginal velocity distribution $\phi(\zeta,\, \hat{c}_z)$ is shown versus $\hat{c}_z$ at various positions ζ. Figure 20(a) shows the result for the far field, Figs. 20(b) and 20(c) show that for the substantial part of ζ with $\hat{\mathrm{w}}(\zeta) < 0$, and Fig. 20(d) shows that for the part with $\hat{\mathrm{w}}(\zeta) > 0$ near the wall [see Fig. 4(b)].

Because the interaction with phonons vanishes at infinity, the gas molecules make free transport there. Therefore, the distribution of the incident molecules ($\hat{c}_z < 0$) and that of the outgoing molecules ($\hat{c}_z > 0$) do not interact there and thus exhibit a discontinuity at $\hat{c}_z = 0$ [Fig. 20(a)]. It is seen from Figs. 20(a)–(c) that ϕ for $1 < \zeta < \infty$ has two discontinuities at the positions symmetric with respect to $\hat{c}_z = 0$. The two discontinuities move outward as ζ changes from ∞ to 1.201 [Figs. 20(a) and 20(b)], move inward as ζ changes from 1.201 to 1 [Fig. 20(c)], and merge into a single line at $\zeta = 1$. In

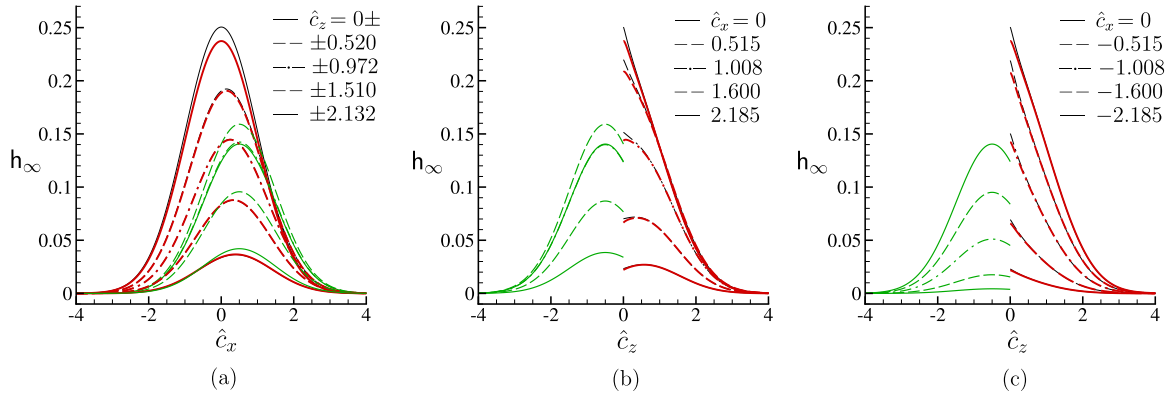

FIG. 10. Profiles of h_∞ ($\hat{c}_z < 0$ and $\hat{c}_z > 0$) at $\hat{c}_z = \text{const}$ and $\hat{c}_x = \text{const}$ in the case of Fig. 6: (a) profiles at $\hat{c}_z = \text{const}$, (b) those at $\hat{c}_x = \text{const} > 0$, and (c) those at $\hat{c}_x = \text{const} < 0$. See the caption of Fig. 9 about the color and thickness of the lines.

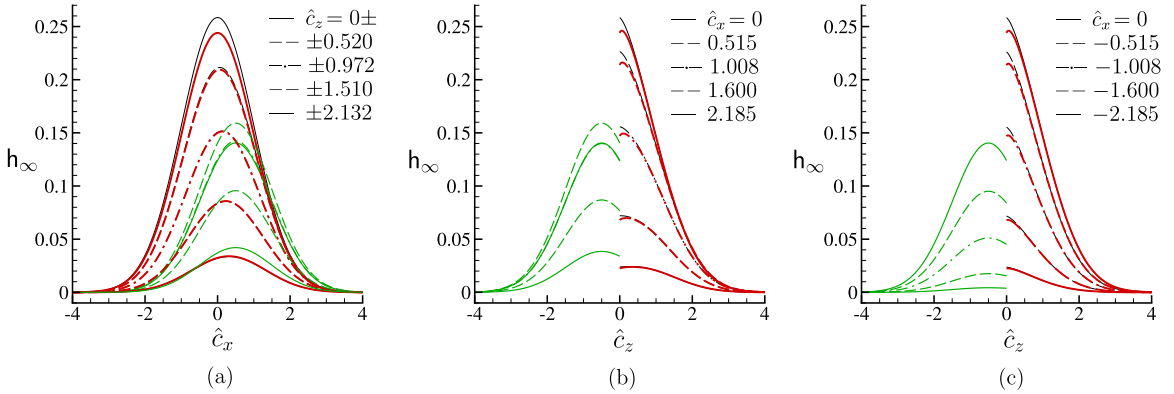

FIG. 11. Profiles of h_∞ ($\hat{c}_z < 0$ and $\hat{c}_z > 0$) at $\hat{c}_z = \text{const}$ and $\hat{c}_x = \text{const}$ in the case of Fig. 7: (a) profiles at $\hat{c}_z = \text{const}$, (b) those at $\hat{c}_x = \text{const} > 0$, and (c) those at $\hat{c}_x = \text{const} < 0$. See the caption of Fig. 9 about the color and thickness of the lines.

order to see the details of the behavior of the discontinuities, we show some magnified figures around the discontinuities in Fig. 21. It turns out that the two discontinuities are located on the characteristic line $\hat{c}_z^2/2 + \hat{\mathrm{w}}(\zeta) = 0$. Figures 21(c) and 21(d) show that the gradient $\partial\phi/\partial\hat{c}_z$ is steep on the outer side of the discontinuity. The formal differentiation, with respect to ζ, of the equation for $\phi_\pm$ corresponding to Eqs. (49a) and (49b) suggests that $\partial\phi/\partial\hat{c}_z$ diverges on the outer side of the discontinuity for the present choices of the potential and the phonon relaxation time.

Let us consider the characteristic line $\varepsilon = \hat{c}_z^2/2 + \hat{\mathrm{w}}(\zeta) = 0$ with $\hat{c}_z < 0$ [see Fig. 4(c)], along which the molecules are moving toward the wall. The line with $\varepsilon = 0+$ extends to infinity, and the value of ϕ on this line at infinity is given by the boundary condition, i.e., $\phi_\infty(0-)$. On the other hand, the line with $\varepsilon = 0-$, which also extends to infinity, is a part of a loop line and is connected to the line $\varepsilon = 0-$ with $\hat{c}_z > 0$ at infinity. Therefore, the value of ϕ on the line $\varepsilon = 0-$ at infinity is given by the boundary condition (74c) with $\varepsilon = 0-$ or equivalently $\phi(\infty, 0-) = \phi(\infty, 0+)$. For this reason, the value of ϕ is discontinuous, having different values on $\varepsilon = 0+$ and $0-$, at infinity. This discontinuity is expressed by the vertical dashed line, spanning $0.35 \lesssim \phi \lesssim 0.63$, at $\hat{c}_z = 0$ in Fig. 21(a). The discontinuity propagates toward the wall along the characteristic line $\varepsilon = 0$ decaying because of the interaction through the phonon collision term. However, the decay is very slow in the present case, and the discontinuity reaches the turning point $\zeta = 1$. Then, it starts to propagate toward infinity along the line $\varepsilon = 0$ with $\hat{c}_z > 0$. The discontinuity continues to decay very slowly and has a finite size even when it reaches infinity, as indicated by the vertical dashed line spanning $0.53 \lesssim \phi \lesssim 0.63$ at $\hat{c}_z = 0$ in Fig. 21(a). If the potential is weaker and the interaction with phonons is stronger in the far field, such as in the case of the Lennard-Jones (12, 6) potential with the phonon relaxation time of algebraic type, the discontinuity decays faster and cannot be seen in the near field.

VIII. CONCLUDING REMARKS

In the present paper, we proposed a kinetic model for gas-surface interaction that takes into account physisorbed molecules interacting with a surface potential and with surface phonons (Sec. II). The surface potential, consisting of the repulsive and attractive parts, as well as the interaction with surface phonons, was assumed to vanish away from the surface. Under the assumption that the interaction (or physisorbate) layer is thinner than the mean free path of the molecules, we derived the kinetic equation for the interaction layer, which forms a half-space problem with respect to the length scale of the potential (Sec. III). This kinetic equation has such a structure that its solution is determined by

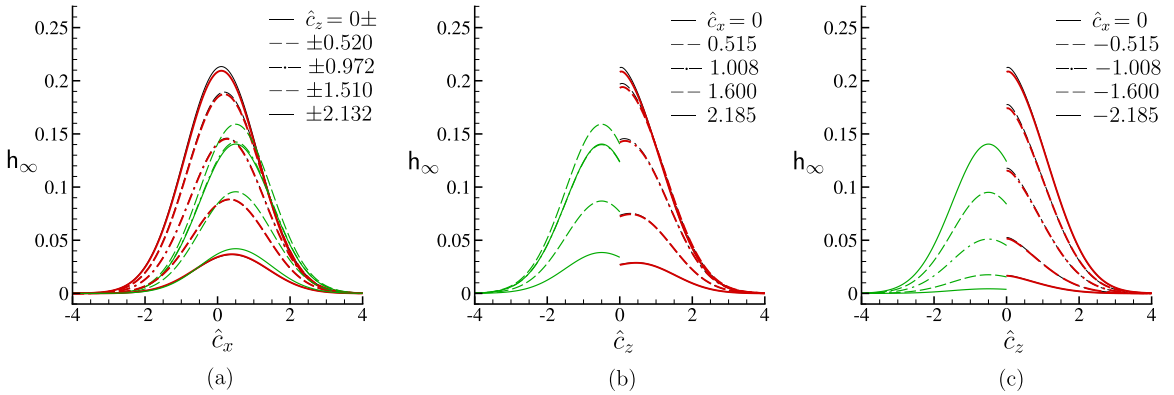

FIG. 12. Profiles of h_∞ ($\hat{c}_z < 0$ and $\hat{c}_z > 0$) at $\hat{c}_z = \text{const}$ and $\hat{c}_x = \text{const}$ in the case of Fig. 8: (a) profiles at $\hat{c}_z = \text{const}$, (b) those at $\hat{c}_x = \text{const} > 0$, and (c) those at $\hat{c}_x = \text{const} < 0$. See the caption of Fig. 9 about the color and thickness of the lines.

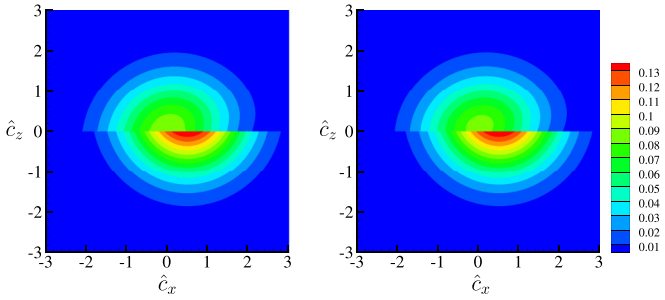

FIG. 13. Contour lines of $\mathsf{h}_\infty(\hat{c}_x, \hat{c}_z)$ for the Lennard-Jones (9, 3) potential (88) and the relaxation time of algebraic type (91) ($n = 4$) in the $(\hat{c}_x, \hat{c}_z)$ plane in the case of $(\hat{T}_\infty, \hat{v}_{z\infty}, \hat{v}_{x\infty}) = (1, 0.5, 0.5)$ and $(\kappa, \kappa_\tau, \sigma) = (1, 1, 1)$. (a) Numerical solution. (b) Approximate formula (102). See the caption of Fig. 5.

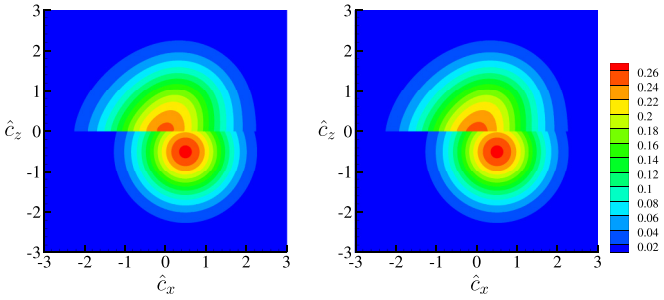

FIG. 15. Contour lines of $\mathsf{h}_\infty(\hat{c}_x, \hat{c}_z)$ for the Lennard-Jones (9, 3) potential (88) and the relaxation time of algebraic type (91) ($n = 4$) in the $(\hat{c}_x, \hat{c}_z)$ plane in the case of $(\hat{T}_\infty, \hat{v}_{z\infty}, \hat{v}_{x\infty}) = (0.6, -0.5, 0.5)$ and $(\kappa, \kappa_\tau, \sigma) = (1, 1, 1)$. (a) Numerical solution. (b) Approximate formula (102). See the caption of Fig. 5.

specifying the velocity distribution for the incident molecules, i.e., the molecules toward the surface, at infinity. This means that the solution determines the velocity distribution for the outgoing molecules, i.e., the molecules toward infinity, at infinity in response to that for the incident molecules there. In other words, the solution of the kinetic equation for the interaction layer provides the boundary condition for the Boltzmann equation that is assumed to hold outside the interaction layer (Sec. IV).

We first derived a model of the boundary condition for the Boltzmann equation by obtaining an approximate solution, based on the first iteration of an iteration scheme, of the half-space problem for the interaction layer. It is of the form of Maxwell's diffuse-specular reflection condition with an accommodation coefficient depending on the normal component of the molecular velocity (Sec. V). Then, we solved the inner layer problem numerically, for several sets of values of the parameters, to observe the velocity distribution of the outgoing molecules for a given velocity distribution of the incoming molecules at infinity. The comparison between the numerical result and the model based on the approximate solution shows good agreement on the whole though there are slight discrepancies for the outgoing molecules with low speed (Sec. VI). Therefore, it is concluded that the latter model gives a reasonable model of the boundary condition for the Boltzmann equation. The numerical solution also revealed some interesting properties of the inner layer half-space problem (Sec. VII).

Applications of the model to some fundamental problems of rarefied gas flows would be of high interest. The model is based only on the first iteration of the scheme. It would also be interesting to make an assessment of the second iteration that was mentioned in Sec. V A. Another limitation of the present approach is that the surface roughness in the molecular scale is neglected. It can be taken into account by considering a surface potential varying also in the tangential direction, for example, a potential periodic in that direction [17,18]. In this paper, we considered only physisorbed molecules. It would be of importance and of interest to consider also chemisorbed species [23–26]. This approach may give a possibility to derive the boundary condition for the Boltzmann equation that takes into account chemical reactions on the surface.

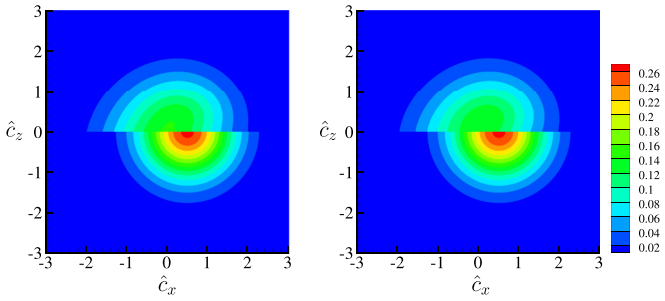

FIG. 14. Contour lines of $\mathsf{h}_\infty(\hat{c}_x, \hat{c}_z)$ for the Lennard-Jones (9, 3) potential (88) and the relaxation time of algebraic type (91) ($n = 4$) in the $(\hat{c}_x, \hat{c}_z)$ plane in the case of $(\hat{T}_\infty, \hat{v}_{z\infty}, \hat{v}_{x\infty}) = (0.6, 0, 0.5)$ and $(\kappa, \kappa_\tau, \sigma) = (1, 1, 1)$. (a) Numerical solution. (b) Approximate formula (102). See the caption of Fig. 5.

APPENDIX A: PHONON COLLISION OPERATORS

The collision term $J_{\rm ph}$ between molecules and phonons involves operators in the general form [11,20–22]

$$J_{\rm ph} = \int \{[f_{\rm ph}(\boldsymbol{q}) + 1] f(\boldsymbol{c}') - f_{\rm ph}(\boldsymbol{q}) f(\boldsymbol{c})\} \overline{\mathsf{W}}_{\rm ph}\, d\boldsymbol{c}' d\boldsymbol{q}, \quad \text{(A1)}$$

where $f_{\rm ph}(\boldsymbol{q})$ denotes the phonon distribution function, $\boldsymbol{q}$ denotes the phonon wave vector or quasimomentum, $\boldsymbol{c}$ and $\boldsymbol{c}'$ denote the molecular velocities before and after the interaction, and $\overline{\mathsf{W}}_{\rm ph}$ denotes the transition probability. The dilute approximation has been used for f in deriving the simplified form (A1), and the appearance of the additional factor 1 in the gain term is a typical quantum effect [11,20–22]. The operator (A1) corresponds to collisions such that $m\boldsymbol{c} + \boldsymbol{q} = m\boldsymbol{c}' + \boldsymbol{b}$ where $\boldsymbol{b}$ is a vector of the reciprocal crystal lattice. There is another operator associated with collisions such that $m\boldsymbol{c} = m\boldsymbol{c}' + \boldsymbol{q} + \boldsymbol{b}$ that leads to the same type of simplified source term and the corresponding details are omitted.

The equilibrium relation between distribution functions corresponding to Eq. (A1) reads $[f^{\rm e}_{\rm ph}(\boldsymbol{q}) + 1] f^{\rm e}(\boldsymbol{c}') = f^{\rm e}_{\rm ph}(\boldsymbol{q}) f^{\rm e}(\boldsymbol{c})$ where the superscript e stands for *physical equilibrium*. The equilibrium distribution for the phonons $f^{\rm e}_{\rm ph}$ is the Bose-Einstein distribution, $f^{\rm e}$ is the wall Maxwellian and

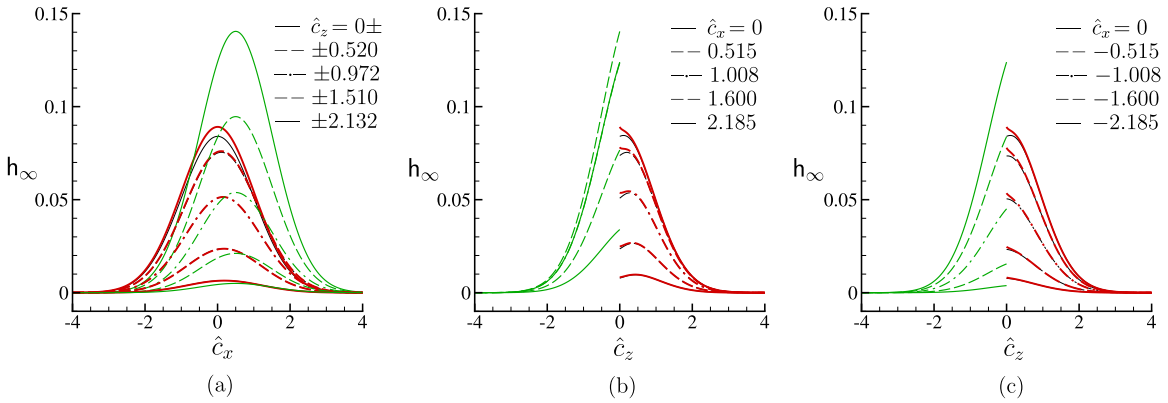

FIG. 16. Profiles of h_∞ ($\hat{c}_z < 0$ and $\hat{c}_z > 0$) at $\hat{c}_z = \text{const}$ and $\hat{c}_x = \text{const}$ in the case of Fig. 13: (a) profiles at $\hat{c}_z = \text{const}$, (b) those at $\hat{c}_x = \text{const} > 0$, and (c) those at $\hat{c}_x = \text{const} < 0$. See the caption of Fig. 9 about the color and thickness of the lines.

the equilibrium relation may be rewritten for convenience in the form $[f^{\mathrm{e}}_{\mathrm{ph}}(\boldsymbol{q}) + 1]\mathrm{m}(\boldsymbol{c}') = f^{\mathrm{e}}_{\mathrm{ph}}(\boldsymbol{q})\mathrm{m}(\boldsymbol{c})$. Dividing then the integrands in the collision term (A1) by the factor $[f^{\mathrm{e}}_{\mathrm{ph}}(\boldsymbol{q}) + 1]\mathrm{m}(\boldsymbol{c}') = f^{\mathrm{e}}_{\mathrm{ph}}(\boldsymbol{q})\mathrm{m}(\boldsymbol{c})$ and further *assuming that phonons are at equilibrium* $f^{\mathrm{e}}_{\mathrm{ph}} = f_{\mathrm{ph}}$, it is obtained that

$$J_{\mathrm{ph}}(f) = \int \left[\frac{f(\boldsymbol{c}')}{\mathrm{m}(\boldsymbol{c}')} - \frac{f(\boldsymbol{c})}{\mathrm{m}(\boldsymbol{c})}\right] \mathsf{W}_{\mathrm{ph}} d\boldsymbol{c}', \tag{A2}$$

where $\mathsf{W}_{\mathrm{ph}} = \mathrm{m}(\boldsymbol{c}) \int f^{\mathrm{e}}_{\mathrm{ph}}(\boldsymbol{q}) \overline{\mathsf{W}}_{\mathrm{ph}} d\boldsymbol{q}$ denotes the resulting transition probability. This assumption of phonons at equilibrium is frequently introduced in the literature and eliminates the phonon distribution function f_{ph} that is governed by kinetic equations [12]. The transition probability W_{ph} satisfies the reciprocity relation $\mathsf{W}_{\mathrm{ph}}(\boldsymbol{c}, \boldsymbol{c}') = \mathsf{W}_{\mathrm{ph}}(\boldsymbol{c}', \boldsymbol{c})$ and is nonzero only in the neighborhood of the surface [11,12]. This term J_{ph} may further be simplified as $-(f - n\mathrm{M})/\tau_{\mathrm{ph}}$ where τ_{ph} denotes a relaxation time independent of $\boldsymbol{c}$ [12].

APPENDIX B: EXPLICIT FORM OF $\hat{\mathsf{n}}^{(1)}$ IN EQ. (64)

The number density $\hat{\mathsf{n}}^{(1)}(\zeta)$ included in Eq. (64) can be obtained by using Eqs. (56) and (63) in Eq. (51a) with $n = 1$. To complete the second iteration (64), we summarize the resulting $\hat{\mathsf{n}}^{(1)}(\zeta)$ below.

Let us put

$$\begin{aligned}\Theta(\zeta,\, \varepsilon) &= \theta(\zeta,\, \infty;\, \varepsilon) + \theta(\zeta_a(\varepsilon),\, \zeta;\, \varepsilon)\,\theta(\zeta_a(\varepsilon),\, \infty;\, \varepsilon) \\ &= \theta(\zeta,\, \infty;\, \varepsilon)\{1 + [\theta(\zeta_a(\varepsilon),\, \zeta;\, \varepsilon)]^2\},\end{aligned} \tag{B1}$$

where the function θ is defined by Eq. (49c). Then, $\hat{\mathsf{n}}^{(1)}(\zeta)$ is obtained as follows.

(a) For $0 < \zeta \leqslant 1$, where $\hat{\mathrm{w}}(\zeta) \geqslant 0$,

$$\begin{aligned}\hat{\mathsf{n}}^{(1)}(\zeta) = \frac{1}{\sqrt{2}} \int_{\hat{\mathrm{w}}(\zeta)}^{\infty} \Bigg\{ \Theta(\zeta,\, \varepsilon) \iint_{-\infty}^{\infty} \mathsf{f}_\infty(-\sqrt{2\varepsilon}) d\hat{c}_x d\hat{c}_y \\ + \frac{1}{\sqrt{2\pi}} \hat{\beta}[2 - \Theta(\zeta,\, \varepsilon)] e^{-\varepsilon} \Bigg\} \frac{d\varepsilon}{\sqrt{\varepsilon - \hat{\mathrm{w}}(\zeta)}}.\end{aligned} \tag{B2}$$

(b) For $\zeta > 1$, where $\hat{\mathrm{w}}(\zeta) < 0$,

$$\begin{aligned}\hat{\mathsf{n}}^{(1)}(\zeta) = \frac{1}{\sqrt{2}} \int_{0}^{\infty} \Bigg\{ \Theta(\zeta,\, \varepsilon) \iint_{-\infty}^{\infty} \mathsf{f}_\infty(-\sqrt{2\varepsilon}) d\hat{c}_x d\hat{c}_y \\ + \frac{1}{\sqrt{2\pi}} \hat{\beta}[2 - \Theta(\zeta,\, \varepsilon)] e^{-\varepsilon} \Bigg\} \frac{d\varepsilon}{\sqrt{\varepsilon - \hat{\mathrm{w}}(\zeta)}} \\ + \hat{\beta} e^{-\hat{\mathrm{w}}(\zeta)} \mathrm{erf}\Big(\sqrt{-\hat{\mathrm{w}}(\zeta)}\Big),\end{aligned} \tag{B3}$$

where $\mathrm{erf}(x)$ is the error function, i.e.,

$$\mathrm{erf}(x) = \frac{2}{\sqrt{\pi}} \int_0^x e^{-t^2} dt.$$

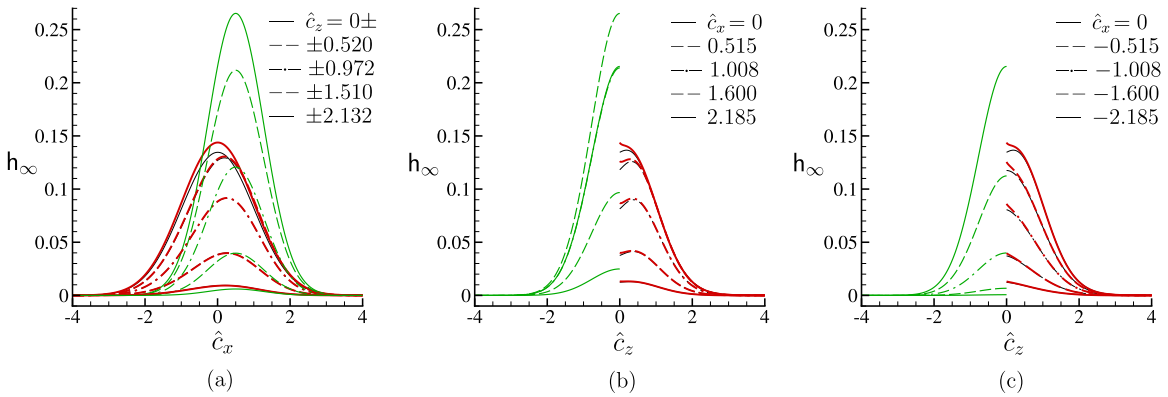

FIG. 17. Profiles of h_∞ ($\hat{c}_z < 0$ and $\hat{c}_z > 0$) at $\hat{c}_z = \text{const}$ and $\hat{c}_x = \text{const}$ in the case of Fig. 14: (a) profiles at $\hat{c}_z = \text{const}$, (b) those at $\hat{c}_x = \text{const} > 0$, and (c) those at $\hat{c}_x = \text{const} < 0$. See the caption of Fig. 9 about the color and thickness of the lines.

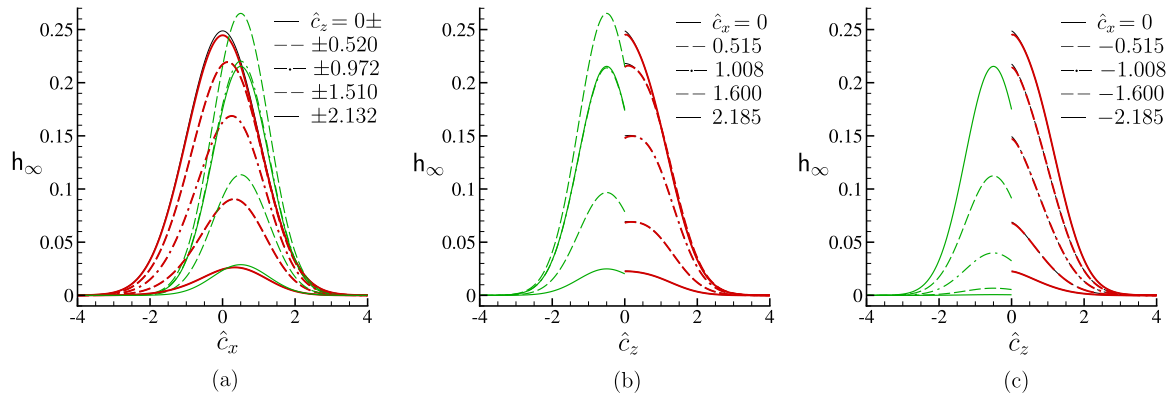

FIG. 18. Profiles of h_∞ ($\hat{c}_z < 0$ and $\hat{c}_z > 0$) at $\hat{c}_z = \text{const}$ and $\hat{c}_x = \text{const}$ in the case of Fig. 15: (a) profiles at $\hat{c}_z = \text{const}$, (b) those at $\hat{c}_x = \text{const} > 0$, and (c) those at $\hat{c}_x = \text{const} < 0$. See the caption of Fig. 9 about the color and thickness of the lines.

APPENDIX C: OUTLINE OF THE NUMERICAL METHOD

In this Appendix, we summarize the numerical procedure that has been used in Secs. VI C and VII. In order to simplify the description, we restrict ourselves to the case of Lennard-Jones (9, 3) potential (88) and the algebraic phonon relaxation time (91) here.

1. Grid systems

For the computation of the number density $\hat{\mathsf{n}}$, we use Eq. (73c) in the (ζ, ε) system. Therefore, we first define the grid points in the (ζ, ε) plane.

Let us choose sufficiently large E and E_0, where $1 \ll E_0 \ll E$, in such a way that

$$|\exp(-E_0)| \ll 1, \quad |\zeta_a(E) - \zeta_a(E + E_0)| \ll 1.$$

This is possible because of the behavior of the potential for $\zeta \ll 1$. The reason why the two large numbers E and E_0 are necessary will become clear soon. Restricting the range of

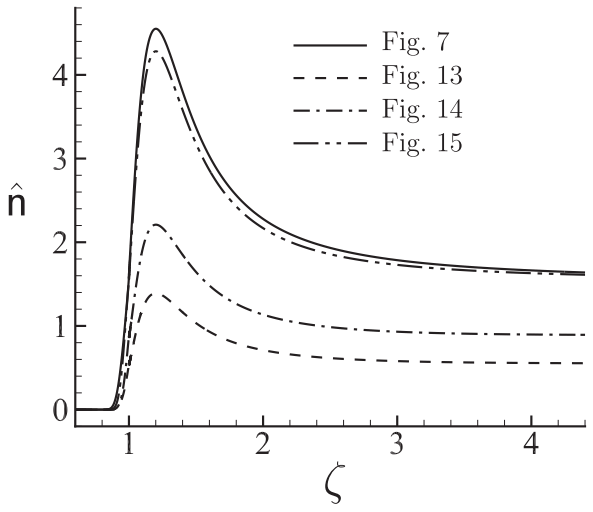

FIG. 19. Dimensionless number density $\hat{\mathsf{n}}$ vs the scaled normal coordinate ζ ($= z/\delta$) in the case of Figs. 7 and 13–15 obtained by the numerical solution (see the captions of Figs. 7 and 13–15).

ε to $\hat{\mathrm{W}}_{\min} \leqslant \varepsilon \leqslant E + E_0$, we define the grid points $\varepsilon^{(j)}$ ($j = -N_0, -N_0 + 1, \ldots, 0, \ldots, N_1, \ldots, N_2$) in ε as (see Fig. 22)

$$\varepsilon^{(-N_0)} = \hat{\mathrm{W}}_{\min} < \varepsilon^{(-N_0+1)} < \cdots < \varepsilon^{(0)} = 0 < \cdots < \varepsilon^{(N_1)} = E < \cdots < \varepsilon^{(N_2)} = E + E_0.$$

Then, the grid points $\zeta^{(i)}$ ($i = -N_2, -N_2 + 1, \ldots, 0, \ldots, 2N_0 - 1$) are defined by the use of $\varepsilon^{(j)}$ as follows (see Fig. 22):

$$\zeta^{(i)} = \begin{cases} \zeta_a(\varepsilon^{(-i)}) & (i = -N_2, -N_2 + 1, \ldots, N_0), \\ \zeta_b(\varepsilon^{(i-2N_0)}) & (i = N_0 + 1, N_0 + 2, \ldots, 2N_0 - 1). \end{cases}$$

We also let $\zeta^{(2N_0)} = \infty$. Thus, the following relation holds:

$$\zeta^{(-N_2)} = \zeta_a(E + E_0) < \zeta^{(-N_2+1)} < \cdots < \zeta^{(-N_1)} = \zeta_a(E) < \cdots < \zeta^{(0)} = 1 < \cdots < \zeta^{(N_0)} = \zeta_{\min} < \cdots < \zeta^{(2N_0-1)} = \zeta_b(\varepsilon^{(-1)}) \equiv Z,$$

where $\varepsilon^{(-1)}$ is chosen to be close to zero in such a manner that Z [i.e., $\zeta_b(\varepsilon^{(-1)})$] is sufficiently large and satisfies

$$\left| \eta_b(\varepsilon) - \int_{\zeta_a(\varepsilon)}^{Z} \frac{1}{\hat{\tau}_{\mathrm{ph}}(s)} ds \right| = \left| \int_{Z}^{\infty} \frac{1}{\hat{\tau}_{\mathrm{ph}}(s)} ds \right| \ll 1, \quad (\varepsilon \geqslant 0).$$

The range of ε at $\zeta = \zeta^{(i)}$ ($i = -N_2, -N_2 + 1, \ldots, 2N_0 - 1$) is $\hat{\mathrm{w}}(\zeta^{(i)})$ [$= \varepsilon^{(\max\{-i, i-2N_0\})}$] $\leqslant \varepsilon \leqslant E + E_0$ [$= \varepsilon^{(N_2)}$]. The range of ζ at $\varepsilon = \varepsilon^{(j)} < 0$ ($j = -N_0, -N_0 + 1, \ldots, -1$) is $\zeta_a(\varepsilon^{(j)})$ [$= \zeta^{(-j)}$] $\leqslant \zeta \leqslant \zeta_b(\varepsilon^{(j)})$ [$= \zeta^{(2N_0+j)}$], while that at $\varepsilon = \varepsilon^{(j)} \geqslant 0$ ($j = 0, 1, \ldots, N_2$) is $\zeta_a(\varepsilon^{(j)})$ [$= \zeta^{(-j)}$] $\leqslant \zeta \leqslant Z$ [$= \zeta^{(2N_0-1)}$]. The number density $\hat{\mathsf{n}}(\zeta)$ is computed down to $\zeta = \zeta^{(-N_1)}$, at which the integration range in Eq. (73c) becomes $\hat{\mathrm{w}}(\zeta^{(-N_1)}) = E < \varepsilon < \infty$. This range is approximated by $E < \varepsilon < E + E_0$ with sufficiently large E_0. This is the reason why we need the grid points also in the range $E < \varepsilon < E + E_0$.

In order to solve Eq. (79a) numerically, we need to set the grid points $\eta^{(i,j)}$ in η on the basis of $(\zeta^{(i)}, \varepsilon^{(j)})$ constructed above. Let us define the following $\eta^{(i,j)}$ and

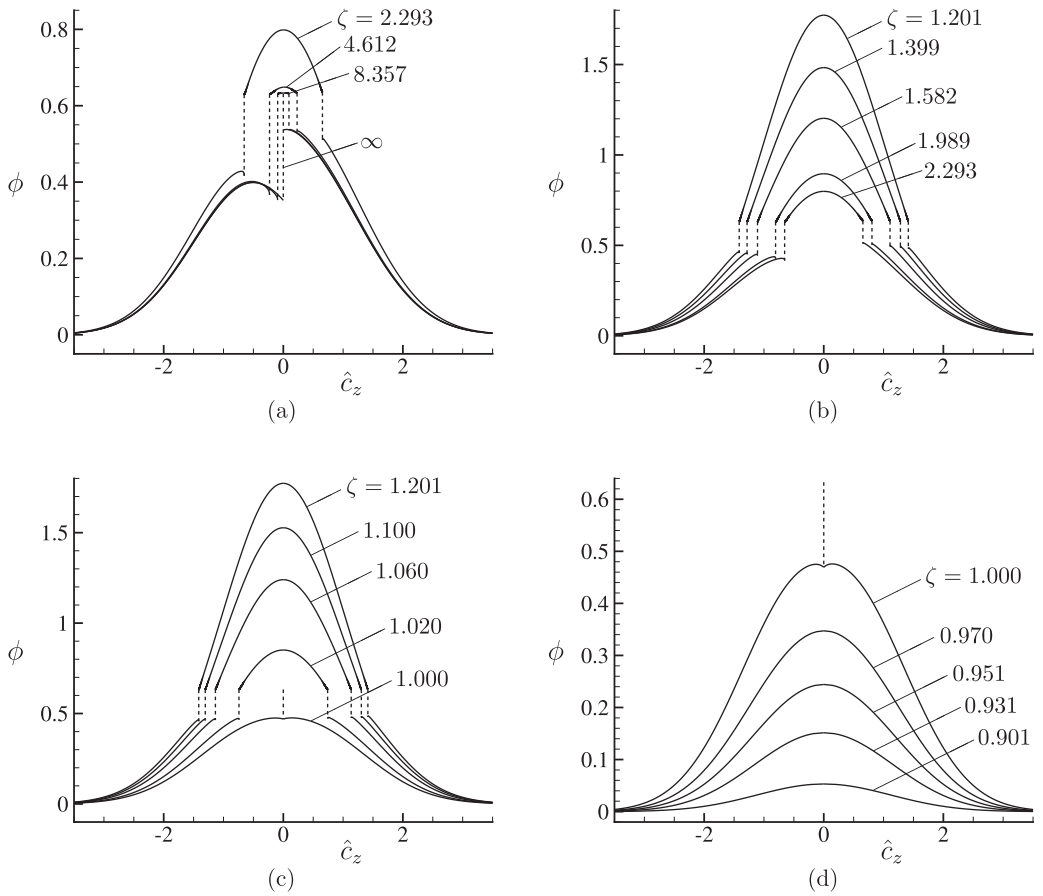

FIG. 20. Profiles of $\phi(\zeta,\ \hat{c}_z)$ ($\hat{c}_z < 0$ and $\hat{c}_z > 0$) at various positions ζ in the case of Fig. 8: (a) profiles for $2.293 \leqslant \zeta \leqslant \infty$, (b) for $1.201 \leqslant \zeta \leqslant 2.293$, (c) for $1 \leqslant \zeta \leqslant 1.201$, and (d) for $0.901 \leqslant \zeta \leqslant 1$. The dashed line indicates the jump between the values at $\varepsilon = 0-$ and $0+$.

$\Delta\eta^{(i)}$:

$$\eta^{(i,j)} = \int_{\zeta_a(\varepsilon^{(j)})}^{\zeta^{(i)}} \frac{1}{\hat{\tau}_{\rm ph}(s)} ds,$$

$$\Delta\eta^{(i)} = \eta^{(i,j)} - \eta^{(i-1,j)} = \int_{\zeta^{(i-1)}}^{\zeta^{(i)}} \frac{1}{\hat{\tau}_{\rm ph}(s)} ds.$$

Then, $\eta^{(i,j)} = \eta(\zeta^{(i)},\ \varepsilon^{(j)})$ and $\zeta^{(i)} = \zeta(\eta^{(i,j)},\ \varepsilon^{(j)})$ hold.

2. Finite-difference scheme

a. Preliminaries

If we divide both sides of Eq. (79a) by $\sqrt{2}\sqrt{\varepsilon - \widetilde{\rm W}(\eta,\ \varepsilon)}$ and integrate the resulting equation with respect to η over a small interval $[\eta_0,\ \eta_1]$ ($\eta_0 < \eta_1$), we obtain

$$\pm[\widetilde{\phi}_\pm(\eta_1,\ \varepsilon) - \widetilde{\phi}_\pm(\eta_0,\ \varepsilon)] = \int_{\eta_0}^{\eta_1} \frac{\widetilde{\rm n}(\eta,\ \varepsilon)\widetilde{\rm M}_{\rm m}(\eta,\ \varepsilon) - \widetilde{\phi}_\pm(\eta,\ \varepsilon)}{\sqrt{2}\sqrt{\varepsilon - \widetilde{\rm W}(\eta,\ \varepsilon)}} d\eta. \tag{C1}$$

Let ζ_0 and ζ_1 correspond to η_0 and η_1, respectively, i.e., $\zeta_0 = \zeta(\eta_0,\ \varepsilon)$ and $\zeta_1 = \zeta(\eta_1,\ \varepsilon)$. If $\eta_0 = 0$, then $\zeta_0 = \zeta_a(\varepsilon)$, so that $\widetilde{\rm W}(0,\ \varepsilon) = \hat{\rm W}(\zeta_a(\varepsilon)) = \varepsilon$ holds. Similarly, if $\eta_1 = \eta_b(\varepsilon)$ ($\varepsilon < 0$), then $\widetilde{\rm W}(\eta_b(\varepsilon),\ \varepsilon) = \hat{\rm W}(\zeta_b(\varepsilon)) = \varepsilon$ holds. Therefore, the integral in the right-hand side (RHS) of Eq. (C1) becomes a singular integral. Keeping this in mind, we approximate the RHS as follows:

$$\text{RHS} \approx \begin{cases} [\widetilde{\rm n}(\eta_1,\ \varepsilon)\widetilde{\rm M}_{\rm m}(\eta_1,\ \varepsilon) - \widetilde{\phi}_\pm(\eta_1,\ \varepsilon)]I, & (\text{when } \eta_0 = 0), \\ [\widetilde{\rm n}(\eta_0,\ \varepsilon)\widetilde{\rm M}_{\rm m}(\eta_0,\ \varepsilon) - \widetilde{\phi}_\pm(\eta_0,\ \varepsilon)]J, & [\text{when } \eta_1 = \eta_b(\varepsilon)], \\ \dfrac{\eta_1 - \eta_0}{2\sqrt{2}}\left(\dfrac{\widetilde{\rm n}(\eta_1,\ \varepsilon)\widetilde{\rm M}_{\rm m}(\eta_1,\ \varepsilon) - \widetilde{\phi}_\pm(\eta_1,\ \varepsilon)}{\sqrt{\varepsilon - \widetilde{\rm W}(\eta_1,\ \varepsilon)}} + \dfrac{\widetilde{\rm n}(\eta_0,\ \varepsilon)\widetilde{\rm M}_{\rm m}(\eta_0,\ \varepsilon) - \widetilde{\phi}_\pm(\eta_0,\ \varepsilon)}{\sqrt{\varepsilon - \widetilde{\rm W}(\eta_0,\ \varepsilon)}}\right), & (\text{otherwise}), \end{cases} \tag{C2}$$

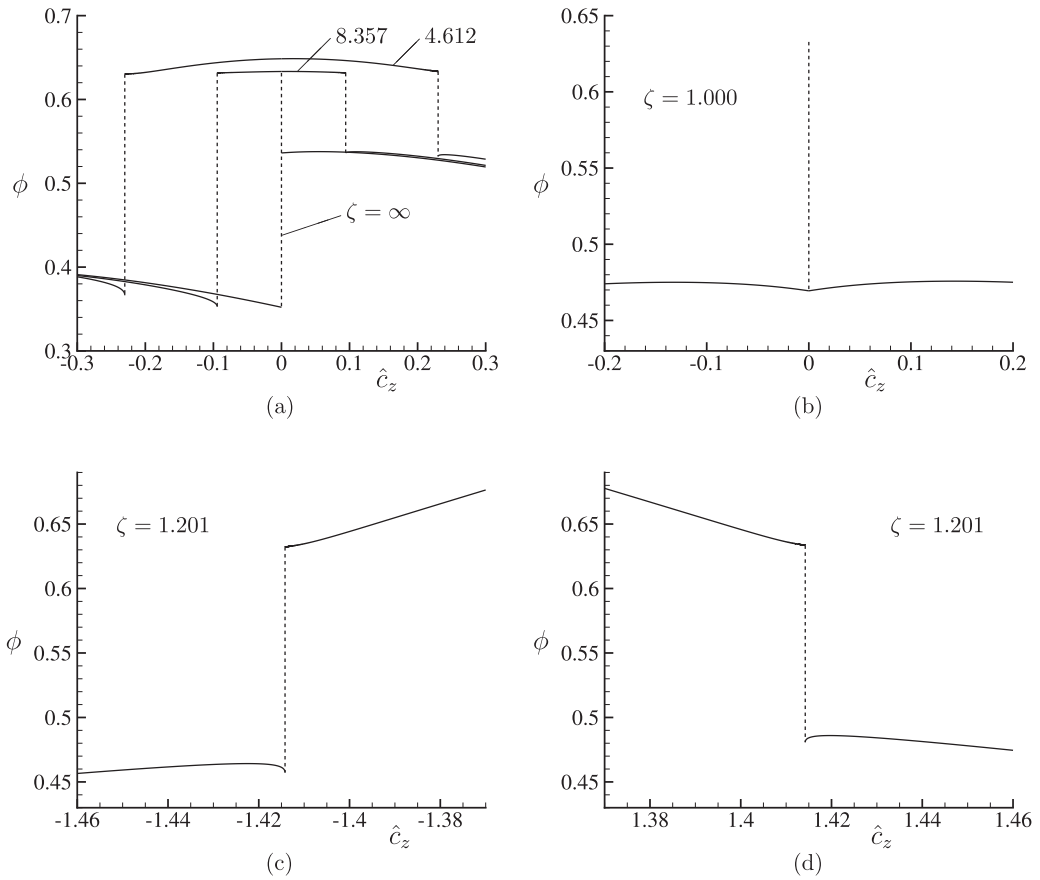

FIG. 21. Magnified figures of some of the profiles in Fig. 20 around the discontinuities. See the caption of Fig. 20.

where

$$I = \frac{1}{\sqrt{2}} \int_0^{\eta_1} \frac{d\eta}{\sqrt{\varepsilon - \widetilde{\mathrm{w}}(\eta,\, \varepsilon)}} = \frac{1}{\sqrt{2}} \int_{\zeta_a(\varepsilon)}^{\zeta_1} \frac{d\zeta}{\hat{\tau}_{\mathrm{ph}}(\zeta)\sqrt{\varepsilon - \hat{\mathrm{w}}(\zeta)}}, \tag{C3a}$$

$$J = \frac{1}{\sqrt{2}} \int_{\eta_0}^{\eta_b(\varepsilon)} \frac{d\eta}{\sqrt{\varepsilon - \widetilde{\mathrm{w}}(\eta,\, \varepsilon)}} = \frac{1}{\sqrt{2}} \int_{\zeta_0}^{\zeta_b(\varepsilon)} \frac{d\zeta}{\hat{\tau}_{\mathrm{ph}}(\zeta)\sqrt{\varepsilon - \hat{\mathrm{w}}(\zeta)}}. \tag{C3b}$$

In the last terms of Eq. (C3), the integration variable has been changed from η to ζ [see Eq. (76)]. Since ζ_1 and ζ_0 in Eq. (C3) should be sufficiently close to $\zeta_a(\varepsilon)$ and $\zeta_b(\varepsilon)$, respectively, I and J can be calculated approximately by using appropriate Taylor expansions of $\hat{\tau}_{\mathrm{ph}}(\zeta)$ and $\hat{\mathrm{w}}(\zeta)$. As the result, the following approximate formulas are obtained for Eqs. (88) and (91):

$$I \approx \frac{1}{\hat{\tau}_{\mathrm{ph}}(\zeta_a)} \sqrt{\frac{2\zeta_a}{A(\zeta_a)B(\zeta_a)}} \arctan\sqrt{A(\zeta_a)(\zeta_1 - \zeta_a)}, \tag{C4a}$$

$$J \approx \frac{1}{\hat{\tau}_{\mathrm{ph}}(\zeta_b)} \sqrt{\frac{\zeta_b}{2A(\zeta_b)B(\zeta_b)}} \log \frac{1 + \sqrt{A(\zeta_b)(\zeta_b - \zeta_0)}}{1 - \sqrt{A(\zeta_b)(\zeta_b - \zeta_0)}}, \tag{C4b}$$

$$A(\zeta) = \frac{n\sigma}{n + \sigma\zeta}, \quad B(\zeta) = \frac{3\sqrt{3}}{2}\kappa \left| \frac{9}{\zeta^9} - \frac{3}{\zeta^3} \right|, \tag{C4c}$$

where ζ_a and ζ_b indicate $\zeta_a(\varepsilon)$ and $\zeta_b(\varepsilon)$, respectively, and the explicit forms of Eqs. (88) and (91) have been used. For $\varepsilon = 0$, Eq. (C3b) reduces to

$$J = \frac{1}{\sqrt{2}} \int_{\eta_0}^{\eta_b(0)} \frac{d\eta}{\sqrt{-\widetilde{\mathrm{w}}(\eta,\, 0)}} = \frac{1}{\sqrt{2}} \int_{\zeta_0}^{\infty} \frac{d\zeta}{\hat{\tau}_{\mathrm{ph}}(\zeta)\sqrt{-\hat{\mathrm{w}}(\zeta)}}. \tag{C5}$$

This requires a special treatment, which is omitted here.

b. Difference scheme

Noting that $\zeta^{(i)} = \zeta(\eta^{(i,j)},\, \varepsilon^{(j)})$, we express the values of relevant functions at the grid points in the following way:

$$\phi^{[m]}_{\pm(i,j)} = \{\widetilde{\phi}_{\pm}(\eta^{(i,j)},\, \varepsilon^{(j)}) = \phi_{\pm}(\zeta^{(i)},\, \varepsilon^{(j)}) \text{ at the } m\text{th step of iteration}\},$$

$$\mathsf{n}^{[m]}_{(i)} = \{\widetilde{\mathsf{n}}(\eta^{(i,j)},\, \varepsilon^{(j)}) = \hat{\mathsf{n}}(\zeta^{(i)}) \text{ at the } m\text{th step of iteration}\},$$

$$\mathrm{M}_{(i,j)} = \widetilde{\mathrm{M}}_{\mathrm{m}}(\eta^{(i,j)},\ \varepsilon^{(j)}) = \hat{\mathrm{M}}_{\mathrm{m}}(\zeta^{(i)},\ \varepsilon^{(j)}) = \frac{1}{\sqrt{2\pi}}\exp(-\varepsilon^{(j)} + \hat{\mathrm{w}}(\zeta^{(i)})),$$

$$\mathrm{w}_{(i)} = \hat{\mathrm{w}}(\zeta^{(i)}) = \varepsilon^{(\max\{-i,\, i-2N_0\})},\quad \tau_{(i)} = \hat{\tau}_{\mathrm{ph}}(\zeta^{(i)}),$$
$$A_{(i)} = A(\zeta^{(i)}),\quad B_{(i)} = B(\zeta^{(i)}).$$

We solve Eqs. (C1) and (C2) with respect to $\widetilde{\phi}_{\pm}(\eta_0,\ \varepsilon)$ or $\widetilde{\phi}_{\pm}(\eta_1,\ \varepsilon)$, apply the results to the grid points suitably, and regard $\widetilde{\phi}_{\pm}$ and $\widetilde{\mathsf{n}}$ as the value at the $(m+1)$th step and that at the mth step, respectively. Then, we obtain the following equations for $\phi^{[m+1]}_{\pm(i,j)}$.

(a) For $\phi^{[m+1]}_{-(i,j)}$,

$$\phi^{[m+1]}_{-(i,j)} = \left(\mathsf{n}^{[m]}_{(i+1)}\mathrm{M}_{(i+1,j)} - \phi^{[m+1]}_{-(i+1,j)}\right)I_{(i)} + \phi^{[m+1]}_{-(i+1,j)},\quad (\varepsilon^{(j)} = \mathrm{w}_{(i)}), \tag{C6a}$$

$$\phi^{[m+1]}_{-(i,j)} = \left(\mathsf{n}^{[m]}_{(i)}\mathrm{M}_{(i,j)}J_{(i+1)} + \phi^{[m+1]}_{-(i+1,j)}\right)\Big/(J_{(i+1)}+1),\quad (\varepsilon^{(j)} = \mathrm{w}_{(i+1)}), \tag{C6b}$$

$$\phi^{[m+1]}_{-(i,j)} = \left[\frac{\Delta\eta^{(i+1)}}{2^{3/2}}\left(\sqrt{\varepsilon^{(j)} - \mathrm{w}_{(i)}}\,\frac{\mathsf{n}^{[m]}_{(i+1)}\mathrm{M}_{(i+1,j)} - \phi^{[m+1]}_{-(i+1,j)}}{\sqrt{\varepsilon^{(j)} - \mathrm{w}_{(i+1)}}} + \mathsf{n}^{[m]}_{(i)}\mathrm{M}_{(i,j)}\right) + \sqrt{\varepsilon^{(j)} - \mathrm{w}_{(i)}}\,\phi^{[m+1]}_{-(i+1,j)}\right]\Big/\left(\sqrt{\varepsilon^{(j)} - \mathrm{w}_{(i)}} + \frac{\Delta\eta^{(i+1)}}{2^{3/2}}\right),\quad \text{(otherwise)}. \tag{C6c}$$

(b) For $\phi^{[m+1]}_{+(i,j)}$,

$$\phi^{[m+1]}_{+(i,j)} = \left(\mathsf{n}^{[m]}_{(i)}\mathrm{M}_{(i,j)}I_{(i-1)} + \phi^{[m+1]}_{+(i-1,j)}\right)\Big/(I_{(i-1)}+1),\quad (\varepsilon^{(j)} = \mathrm{w}_{(i-1)}), \tag{C7a}$$

$$\phi^{[m+1]}_{+(i,j)} = \left(\mathsf{n}^{[m]}_{(i-1)}\mathrm{M}_{(i-1,j)} - \phi^{[m+1]}_{+(i-1,j)}\right)J_{(i)} + \phi^{[m+1]}_{+(i-1,j)},\quad (\varepsilon^{(j)} = \mathrm{w}_{(i)}), \tag{C7b}$$

$$\phi^{[m+1]}_{+(i,j)} = \left[\frac{\Delta\eta^{(i)}}{2^{3/2}}\left(\mathsf{n}^{[m]}_{(i)}\mathrm{M}_{(i,j)} + \sqrt{\varepsilon^{(j)} - \mathrm{w}_{(i)}}\,\frac{\mathsf{n}^{[m]}_{(i-1)}\mathrm{M}_{(i-1,j)} - \phi^{[m+1]}_{+(i-1,j)}}{\sqrt{\varepsilon^{(j)} - \mathrm{w}_{(i-1)}}}\right) + \sqrt{\varepsilon^{(j)} - \mathrm{w}_{(i)}}\,\phi^{[m+1]}_{+(i-1,j)}\right]\Big/\left(\sqrt{\varepsilon^{(j)} - \mathrm{w}_{(i)}} + \frac{\Delta\eta^{(i)}}{2^{3/2}}\right),\quad \text{(otherwise)}. \tag{C7c}$$

Here,

$$I_{(i)} = \frac{1}{\tau_{(i)}}\sqrt{\frac{2\zeta^{(i)}}{A_{(i)}B_{(i)}}}\arctan\sqrt{A_{(i)}(\zeta^{(i+1)} - \zeta^{(i)})},\quad (i = -N_1,\ -N_1+1,\ \ldots,\ N_0-1), \tag{C8a}$$

$$J_{(i)} = \frac{1}{\tau_{(i)}}\sqrt{\frac{\zeta^{(i)}}{2A_{(i)}B_{(i)}}}\log\frac{1+\sqrt{A_{(i)}(\zeta^{(i)} - \zeta^{(i-1)})}}{1-\sqrt{A_{(i)}(\zeta^{(i)} - \zeta^{(i-1)})}},\quad (i = N_0+1,\ N_0+2,\ \ldots,\ 2N_0-1), \tag{C8b}$$

$$J_{(2N_0)} = \frac{1}{\kappa_\tau\sigma^{5/2}}\frac{1}{\sqrt{3\sqrt{3}\kappa}}\frac{n^n}{(\sigma\zeta^{(2N_0-1)})^{n-5/2}}\left[\frac{2}{2n-5} - \frac{2n^2}{(2n-3)\sigma\zeta^{(2N_0-1)}} + \frac{n^3(n+1)}{(2n-1)(\sigma\zeta^{(2N_0-1)})^2}\right], \tag{C8c}$$

where $J_{(2N_0)}$ corresponds to the value of J at $\varepsilon = 0$ and has been obtained on the basis of Eq. (C5).

c. Process of computation

Let us assume that $\mathsf{n}^{[m]}_{(i)}$ $(i = -N_1,\ -N_1+1,\ \ldots,\ 2N_0)$ and $\phi^{[m]}_{+(i,i-2N_0)}$ $(i = N_0+1,\ N_0+2,\ \ldots,\ 2N_0-1)$, which are the values of ϕ at the grid points on the curve $\varepsilon = \hat{\mathrm{w}}(\zeta)$ in Fig. 22, at the mth step have been known. Here, $\mathsf{n}^{[m]}_{(2N_0)}$ indicates the value as $\zeta \to \infty$. In the following, we set

$$\Delta\eta^{(2N_0)} = \eta_b(\varepsilon^{(j)}) - \eta^{(2N_0-1,j)} = \int_{\zeta^{(2N_0-1)}}^{\infty}\frac{1}{\hat{\tau}_{\mathrm{ph}}(s)}ds,$$
$$(\varepsilon^{(j)} \geqslant 0), \tag{C9}$$

$\mathrm{M}_{(2N_0,j)} = (2\pi)^{-1/2}\exp(-\varepsilon^{(j)})$, and $\mathrm{w}_{(2N_0)} = 0$.

(i) From the boundary conditions, we let $\phi^{[m+1]}_{-(2N_0,j)} = \phi_\infty(-\sqrt{2\varepsilon^{(j)}})$ $(j = 0,\ 1,\ \ldots,\ N_2)$ and $\phi^{[m+1]}_{-(i,i-2N_0)} = \phi^{[m]}_{+(i,i-2N_0)}$ $(i = N_0+1,\ N_0+2,\ \ldots,\ 2N_0-1)$. In addition, we set $\phi^{[m+1]}_{-(N_0,-N_0)} = \mathsf{n}^{[m]}_{(N_0)}\mathrm{M}_{(N_0,-N_0)}$.

(iia) For the case of $\varepsilon^{(j)} < 0$, for each j of $j = -N_0+1,\ -N_0+2,\ \ldots,\ -1$, we obtain $\phi^{[m+1]}_{-(i,j)}$ with $i = 2N_0+j-1,\ 2N_0+j-2,\ \ldots,\ -j$ successively using Eq. (C6).

(iib) For the case of $0 \leqslant \varepsilon^{(j)} \leqslant E$, for each j of $j = 0,\ 1,\ \ldots,\ N_1$, we obtain $\phi^{[m+1]}_{-(i,j)}$ with $i = 2N_0-1,\ 2N_0-2,\ \ldots,\ -j$ successively using Eq. (C6).

(iic) For the case of $E < \varepsilon^{(j)} \leqslant E+E_0$, for each j of $j = N_1+1,\ N_1+2,\ \ldots,\ N_2$, we obtain $\phi^{[m+1]}_{-(i,j)}$ with $i = 2N_0-1,\ 2N_0-2,\ \ldots,\ -N_1$ successively using Eq. (C6). In

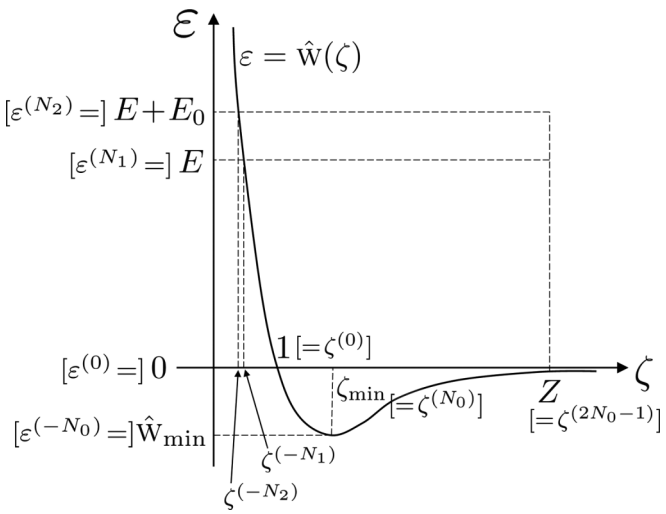

FIG. 22. Grid points $(\zeta^{(i)},\ \varepsilon^{(j)})$ in the $(\zeta,\ \varepsilon)$ plane.

addition, we determine $\phi^{[m+1]}_{-(-j,j)}$ by

$$\phi^{[m+1]}_{-(-j,j)} = \big(\mathsf{n}^{[m]}_{(-N_1)}\mathrm{M}_{(-N_1,j)} - \phi^{[m+1]}_{-(-N_1,j)}\big)\tilde{I}_{(-j)} + \phi^{[m+1]}_{-(-N_1,j)}, \tag{C10a}$$

$$\tilde{I}_{(-j)} = \frac{1}{\tau_{(-j)}}\sqrt{\frac{2\zeta^{(-j)}}{A_{(-j)}B_{(-j)}}}\arctan\sqrt{A_{(-j)}(\zeta^{(-N_1)} - \zeta^{(-j)})}. \tag{C10b}$$

(iii) From the boundary conditions, we let $\phi^{[m+1]}_{+(i,-i)} = \phi^{[m+1]}_{-(i,-i)}$ $(i = -N_2,\ -N_2+1,\ \ldots,\ N_0)$.

(iva) For the case of $\varepsilon^{(j)} < 0$, for each j of $j = -N_0+1,\ -N_0+2,\ \ldots,\ -1$, we obtain $\phi^{[m+1]}_{+(i,j)}$ with $i = -j+1,\ -j+2,\ \ldots,\ 2N_0+j$ successively using Eq. (C7).

(ivb) For the case of $0 \leqslant \varepsilon^{(j)} \leqslant E$, for each j of $j = 0,\ 1,\ \ldots,\ N_1$, we obtain $\phi^{[m+1]}_{+(i,j)}$ with $i = -j+1,\ -j+2,\ \ldots,\ 2N_0$ successively using Eq. (C7).

(ivc) For the case of $E < \varepsilon^{(j)} \leqslant E + E_0$, for each j of $j = N_1+1,\ N_1+2,\ \ldots,\ N_2$, we first obtain $\phi^{[m+1]}_{+(-N_1,j)}$ from

$$\phi^{[m+1]}_{+(-N_1,j)} = \big(\mathsf{n}^{[m]}_{(-N_1)}\mathrm{M}_{(-N_1,j)}\tilde{I}_{(-j)} + \phi^{[m+1]}_{+(-j,j)}\big)\Big/(\tilde{I}_{(-j)} + 1), \tag{C11}$$

and then $\phi^{[m+1]}_{+(i,j)}$ with $i = -N_1+1,\ -N_1+2,\ \ldots,\ 2N_0$ successively using Eq. (C7).

(v) We carry out the integration in Eq. (73c) by the Simpson rule to obtain $\mathsf{n}^{[m+1]}_{(i)}$ $(i = -N_1,\ -N_1+1,\ \ldots,\ 2N_0)$.

We repeat the processes (i)–(v) until

$$\max_{-N_1 \leqslant i \leqslant 2N_0} |\mathsf{n}^{[m+1]}_{(i)} - \mathsf{n}^{[m]}_{(i)}| < \delta_0 \tag{C12}$$

holds, where δ_0 is a sufficiently small positive number.

The $\phi^{[m+1]}_{\pm(i,0)}$ $(i = 0,\ 1,\ \ldots,\ 2N_0)$ obtained by the process described above originate from the boundary condition (74a) [or the second condition in Eq. (80a)]. Thus, they indicate the values at $\varepsilon = 0+$. Instead, if we let

$$\phi^{[m+1]}_{-(2N_0,0)} = \phi^{[m]}_{+(2N_0,0)},$$

following the boundary condition (74c) [or the second condition in Eq. (80b)], then the obtained $\phi^{[m+1]}_{\pm(i,0)}$ $(i = 0,\ 1,\ \ldots,\ 2N_0)$ indicate the values at $\varepsilon = 0-$. In the actual computation, we obtain the values both at $\varepsilon = 0+$ and $0-$. In this way, we are able to describe the discontinuity in $\phi_\pm$ propagating along the characteristic line $\varepsilon = 0$ in the $(\zeta,\ \varepsilon)$ plane or $\hat{c}_z^2/2 + \hat{\mathrm{W}}(\zeta) = 0$ in the $(\zeta,\ \hat{c}_z)$ plane, as shown in Figs. 20 and 21.

Because of the discontinuity in $\phi_\pm$ at $\varepsilon = 0$, care should be taken in the numerical integration of the integral in Eq. (73c) in the process (v). For $i = 1,\ 2,\ \ldots,\ 2N_0 - 1$, the integral is split into the part for $\varepsilon < 0$ and that for $\varepsilon > 0$, and the Simpson rule is applied to each part: the values at $\varepsilon = 0-$ are used in the former part, whereas those at $\varepsilon = 0+$ are used in the latter.

d. Data for actual computation

In the actual computation, the distributions of the grid points $\zeta^{(i)}$ and $\varepsilon^{(j)}$ are chosen *carefully* and tuned *manually*. Since its description is cumbersome, the details are omitted here. However, in order to give a rough idea, we will provide some pieces of information about the grid points in the case of Fig. 7.

The large numbers E_0, E, and Z are chosen as $E_0 = 25$, $E = 300$, and $Z = 6000$. Concerning the grid points $\varepsilon^{(j)}$, about 8400 nonuniformly distributed points are set in the interval $[\hat{\mathrm{W}}_{\min},\ 0) = [-1,\ 0)$ (the minimum interval is about 7.7×10^{-14} around $\varepsilon = 0-$, and the maximum is about 1.1×10^{-3} around $\varepsilon = -0.54$); about 800 nonuniformly distributed points are set in the interval $[0,\ E_0)$ (the minimum interval is about 6.3×10^{-6} around $\varepsilon = 0+$, and the maximum is about 0.1 around $\varepsilon = E_0$); and about 3000 uniformly distributed points are set in the interval $[E_0,\ E_0 + E]$ (the grid interval is about 0.1). As for the grid points $\zeta^{(i)}$, about 3800 nonuniformly distributed points are set in the interval $[\zeta_a(E_0 + E),\ 1) \approx [0.58,\ 1)$ (the minimum interval is about 4.0×10^{-7} around $\zeta = 1-$, and the maximum is about 4.0×10^{-4} around $\zeta = 0.90$); about 8400 nonuniformly distributed points are set in the interval $[1,\ \zeta_{\min}] \approx [1,\ 1.20]$ (the minimum interval is about 5.0×10^{-15} around $\zeta = 1+$ and the maximum is about 9.5×10^{-4} around $\zeta = \zeta_{\min}$); and about 8400 nonuniformly distributed points are set in the interval $[\zeta_{\min},\ Z] \approx [1.20,\ 6000]$ (the minimum interval is about 2.7×10^{-4} around $\zeta = 1.40$, and the maximum is about 12.8 around $\zeta = Z$). The accuracy is confirmed by poor resolution tests using a smaller number of grid points and smaller computational domains.

It is a good accuracy test to check if the vanishing of the molecular flux in the normal direction, i.e., Eq. (38), (48), or (75), is satisfied numerically. In the present case, the maximum of the numerical values of the left-hand side of Eq. (38) in the computational domain of ζ is less than 2.2×10^{-6}. Note that the incident flux at infinity, i.e., $|\int_{\hat{c}_z<0} \hat{c}_z \mathsf{f}_\infty(\hat{\boldsymbol{c}})d\hat{\boldsymbol{c}}|$, is equal to 0.6978 in this case. The accuracy of the same level has been confirmed for the cases in the other figures.

[1] C. Cercignani, *The Boltzmann Equation and its Applications*, Applied Mathematical Sciences (Springer-Verlag, Berlin, 1988) Vol. 67.

[2] M. Epstein, A model of the wall boundary condition in kinetic theory, AIAA J. **5**, 1797 (1967).

[3] I. Kuščer, Reciprocity in scattering of gas molecules by surfaces, Surf. Sci. **25**, 225 (1971).

[4] C. Cercignani and M. Lampis, Kinetic models for gas-surface interactions, Transp. Theory Stat. Phys. **1**, 101 (1971).

[5] R. G. Lord, Some extensions to the Cercignani-Lampis gas-surface scattering kernel, Phys. Fluids A **3**, 706 (1991).

[6] H. Struchtrup, Maxwell boundary condition and velocity dependent accommodation coefficient, Phys. Fluids **25**, 112001 (2013).

[7] H. Y. Wachman, I. Greber, and G. Kass, Molecular dynamics computations of scattering from a surface using a Lennard-Jones model of a solid, in *Rarefied Gas Dynamics: Experimental Techniques and Physical Systems*, Progress in Astronautics and Aeronautics, edited by B. D. Shizgal and D. P. Weaver (AIAA, Washington, DC, 1994), Vol. 158, pp. 479–493.

[8] J. Matsui and Y. Matsumoto, Study of scattering process in gas-surface interactions, in *Rarefied Gas Dynamics: Experimental Techniques and Physical Systems*, Progress in Astronautics and Aeronautics Vol. 158, edited by B. D. Shizgal and D. P. Weaver (AIAA, Washington, DC, 1994), pp. 515–524.

[9] K. Yamamoto, H. Takeuchi, and T. Hyakutake, Characteristics of reflected gas molecules at a solid surface, Phys. Fluids **18**, 046103 (2006).

[10] Z. Wang, C. Song, F. Qin, and X. Luo, Establishing a data-based scattering kernel model for gas-solid interaction by molecular dynamics simulation, J. Fluid Mech. **928**, A34 (2021).

[11] V. D. Borman, S. Yu. Krylov, A. V. Prosyanov, and A. M. Kharitonov, Theory of transport processes in a nonequilibrium gas-solid system, Sov. Phys. JETP **63**, 43 (1986).

[12] V. D. Borman, S. Yu. Krylov, and A. V. Prosyanov, Theory of nonequilibrium phenomena at a gas-solid interface, Sov. Phys. JETP **67**, 2110 (1988).

[13] J. J. M. Beenakker, V. D. Borman, and S. Yu. Krylov, Molecular transport in the nanometer regime, Phys. Rev. Lett. **72**, 514 (1994).

[14] A. V. Bogdanov, G. V. Dubrovskiy, M. P. Krutikov, D. V. Kulginov, and V. M. Strelchenya, *Interaction of Gases with Surfaces* (Springer-Verlag, Berlin, 1995).

[15] A. Frezzotti and L. Gibelli, A kinetic model for fluid-wall interaction, Proceedings of the Institution of Mechanical Engineers, Part C: Journal of Mechanical Engineering Science **222**, 787 (2008).

[16] K. Aoki, P. Charrier, and P. Degond, A hierarchy of models related to nanoflows and surface diffusion, Kin. Rel. Models **4**, 53 (2011).

[17] S. Brull, P. Charrier, and L. Mieussens, Gas-surface interaction and boundary conditions for the Boltzmann equation, Kin. Rel. Models **7**, 219 (2014).

[18] S. Brull, P. Charrier, and L. Mieussens, Nanoscale roughness effect on Maxwell-like boundary conditions for the Boltzmann equation, Phys. Fluids **28**, 082004 (2016).

[19] S. Takata, S. Akasobe, and M. Hattori, A revisit to the Cercignani-Lampis model: Langevin picture and its numerical simulation, in *Recent Advances in Kinetic Equations and Applications*, Springer INdAM Series Vol. 48, edited by F. Salvarani (Springer, New York, 2021), pp. 345–365.

[20] E. M. Lifshitz and L. P. Pitaevskii, *Physical Kinetics*, Landau and Lifshitz Course on Theoretical Physics Vol. 10 (Pergamon, Oxford, 1981).

[21] A. Rossani, Generalized kinetic theory of electrons and phonons, Physica A **305**, 323 (2002).

[22] M. Galler, *Multigroup Equations for the Description of the Particle Transport in Semiconductors* (World Scientific, Singapore, 2005).

[23] K. Aoki, V. Giovangigli, and M. Hattori, A kinetic model of adsorption on solid surfaces, in *30th International Symposium on Rarefied Gas*, AIP Conf. Proc. No. 1786 (AIP, Melville, NY, 2016), p. 100005.

[24] K. Aoki and V. Giovangigli, A kinetic model of reactive crystal surfaces, in *31st International Symposium on Rarefied Gas Dynamics*, AIP Conf. Proc. No. 2132 (AIP, Melville, NY, 2019), p. 130003.

[25] K. Aoki and V. Giovangigli, A kinetic model of adsorption on crystal surfaces, Phys. Rev. E **99**, 052137 (2019).

[26] K. Aoki and V. Giovangigli, Kinetic theory of chemical reactions on crystal surfaces, Physica A **565**, 125573 (2021).

[27] C. Bardos, R. E. Caflisch, and B. Nicolaenko, The Milne and Kramers problems for the Boltzmann equation of a hard sphere gas, Commun. Pure Appl. Math. **39**, 323 (1986).

[28] F. Golse and F. Poupaud, Stationary solutions of the linearized Boltzmann equation in a half-space, Math. Methods Appl. Sci. **11**, 483 (1989).

[29] C. Bardos, F. Golse, and Y. Sone, Half-space problems for the Boltzmann equation: A survey, J. Stat. Phys. **124**, 275 (2006).

[30] S. Chapman and T. G. Cowling, *The Mathematical Theory of Non-Uniform Gases* (Cambridge University, Cambridge, England, 1970).

[31] J. H. Ferziger and H. G. Kaper, *Mathematical Theory of Transport Processes in Gases* (North-Holland, Amsterdam, 1972).

[32] V. Giovangigli, *Multicomponent Flow Modeling* (Birkhäuser, Boston, 1999).

[33] E. Nagnibeda and E. Kustova, *Non-Equilibrium Reacting Gas Flows: Kinetic Theory of Transport and Relaxation Processes* (Springer-Verlag, Berlin, 2009).

[34] Y. Sone, *Molecular Gas Dynamics: Theory, Techniques, and Applications* (Birkhäuser, Boston, 2007).

[35] N. Masmoudi and M. L. Tayeb, Diffusion limit of a semiconductor Boltzmann-Poisson system, SIAM J. Math. Anal. **38**, 1788 (2007).

[36] A. Majorana and C. Milazzo, Space homogeneous solutions of the linear semiconductor Boltzmann equation, J. Math. Anal. Appl. **259**, 609 (2001).

[37] D. M. Ruthven, *Principles of Adsorption and Adsorption Processes* (Wiley, New York, 1984).

[38] G. D. Billing, *Dynamics of Molecule Surface Interactions* (Wiley, New York, 2000).

[39] R. Lalauze, *Physico-Chemistry of Solid-Gas Interfaces: Concepts and Methodology for Gas Sensor Development* (Wiley, New York, 2010).